Research Group of Climatology

Master Thesis

Relationships of precipitation and temperature extremes in Southern Africa (1981 - 2019)

Environmental Geography, Geographic Institute

Tzu-Yun Chiu

Matriculation Number: 1633890

in partial fulfilment of the requirements for the degree of

Master of Science (M.Sc.)

Bayreuth,

August 18th, 2021

submitted to: Faculty of Biology, Chemistry and Earth Science

1. Examiner: Prof. Dr. Cyrus Samimi

Research Group of Climatology

2. Examiner: Dr. rer. nat. Wolfgang Babel

Research Group of Micrometeorology

Statutory declaration

I hereby declare on oath that the present thesis entitled

Relationships of precipitation and temperature extremes in Southern Africa (1981 - 2019)

is independently authored by myself. I did not use any unnamed, illegitimate assistance from third parties, media or materials than the ones referred to in this thesis. I further declare that all direct and indirect sources quoted either verbatim or in substance from published or unpublished documents are marked as citations.

This thesis has not been submitted to any other examination institution, and not been published wholly or substantially.

Bayreuth, August 18th, 2021

                    _____

                    Tzu-Yun Chiu

Acknowledgement

Abstract

With global warming, more climatic extremes occur including intense precipitations and heat waves events. Especially in Southern Africa, supposed to be more vulnerable regions, since the water resources are the crucial issues. This study gives an overview of the trends of precipitation as well as maximum temperature, heat wave events and the relationships between these two variable extremes. Cluster analysis was conducted in order to regionalise precipitation patterns. Then pixel-wise trends analysis, detection of heat wave events and lag regression models were applied. The 10 sub-regions are established considering mean monthly precipitations from 1981 to 2019 in the whole study region. There are positive trends of annual precipitation in northern part and significant negative trends in southern part of Southern Africa, with the main contribution of monthly precipitations from December to April. Except for the west-central part of our research area, annual maximum temperatures show increasing trends with the higher monthly maximum temperature from August to November. There are one to 24 heat waves detected over the 39 years, but the frequency, duration and intensity are not significantly increasing. The mean durations, the mean intensities and the cumulative intensities are 5.0 ± 0.09 - 23.7 ± 7.97 days, 3.6 ± 0.30 - 11.7 ± 1.18 °C and 20.4 ± 6 - 143.4 ± 47.7 °C × day, respectively. In general, lag regression models exhibit the reduction of weekly rainfalls during heat wave events and the enhancement of weekly rainfalls after one to two weeks of the events. However, heterogeneous spatial patterns of these relationships exist for different heat wave events over the 39 years. The inter- and intra-annual variations of atmospheric circulations, sea surface temperatures, displacements of the ITCZ, movements of the oceanic as well as the continental highs and lows, cloud covers and topographic features might construct the complexity of relationships between precipitation and temperature extremes altogether. More environmental variables and the usage of long-term datasets should be taken into consideration for understanding more comprehensive concepts in future research.

Table of contents

List of figures

List of tables

1. Introduction

1.1. Climatology of Southern Africa

The climatological parameters (e.g. precipitation, temperature) in Southern Africa is complex and with large inter-annual variations. The most symbolic features of surface and near-surface pressure distribution over this region are the subtropical highs and the intervening equatorial trough (Mozambique Channel trough) (Buckle, 1996; Tyson and Preston-Whyte, 2000). Together with the influence of trade winds and jet streams, two oceanic subtropical highs - the South Atlantic High (St. Helena High) and the South Indian High as well as the two main continental pressures - the Botswana High and the Angola Low build up the seasonal changes of climatological patterns and regional circulations in Southern Africa (Figure 1) (Buckle, 1996; Endlicher, 2000; Hart et al., 2016; Driver and Reason, 2017; Munday and Washington, 2017). Extratropical cyclones moving through the Westerlies and summer convective storms are the main sources of rainfalls in Southern Africa (Buckle, 1996; Endlicher, 2000; Hart et al., 2016). Moisture sourced from the Southern Atlantic and Indian Oceans facilitated by the Easterlies also brings precipitation to land, although their effects diminish farther onto the continent (Aloysisu et al., 2015). Cold Benguela Current along the west coastal region and Warm Agulhas Current along the east coasts generate the difference of annual air temperature between two coasts, and the annual variation of their influences are caused by prevailing wind direction (Figure 1) (Buckle, 1996; Endlicher, 2000; Hart et al., 2016). In austral winter, due to the equator-wards movement of the subtropical highs, extratropical cyclones have space to influence the South tip of Africa with their cold fronts (Endlicher, 2000). The west wind drifts bring the moist maritime air masses, thus the Western cape is classified as Mediterranean climate, with winter rains from May to August (Dedekind et al., 2016; Tyson and Preston-Whyte, 2000). The importance of the relief such as Drakensberg and Manicaland mountains in the South-East, the western escarpment and the central plateau can be seen in the difference between climate regimes and a high complexity of seasonal and spatial repartition of rainfall (Fauchereau et al., 2003). Topographic features influence small-scale regional climatology since they can trigger convective instabilities (Buckle, 1996; Endlicher, 2000; Tyson and Preston-Whyte, 2000; Aloysius et al., 2015). As air crosses the upland, it causes cooling, condensation and cloud formation on the upper slopes, which enhances the precipitation processes. The amounts of precipitation decrease from east to west of Southern Africa (Dedekind et al., 2016). In general, the

additional friction of crossing barriers will increase the rainfall totals because the passage of the storm is slowed down (Buckle, 1996; Hart et al., 2016). Besides, temperatures in the atmosphere vary with altitude and are also impacted by aspect. For example, steep slopes contributing adiabatic descent in coastal locations of Southern Africa cause higher air pressures thus rising temperatures (Buckle, 1996).

Precipitation patterns in the tropics and subtropics are dominated by shifts when sea surface temperatures change (Trenberth, 2011; Aloysius et al., 2015). Sea surface temperatures (SSTs) are associated with larger-scale atmospheric circulation anomalies, for example, wind directions at near-surface levels, which might affect the local wind systems due to the movement of the Southern African Walker-style cells. They are related to the Southern Oscillation, and consequently enhance rainfalls in the South Atlantic Convergence Zone (Tyson and Preston-Whyte, 2000; Williams et al., 2011). During El Niño-Southern Oscillation (ENSO) episodes, the Southern Oscillation is in low phase (warm oceanic phase) with a weak Walker circulation, where SSTs are anomalously low over the Indonesian region and the pressure rises, whilst SSTs are anomalously high and the pressure falls over the Eastern Pacific Ocean (Tyson and Preston-Whyte, 2000). Under converse conditions, the Southern Oscillation in high phase is called a La Niña (non-ENSO) event. Overall, ENSO is associated with extreme rainfall events (Fauchereau et al., 2003; Munday and Washington, 2017; Driver and Reason, 2017). There are increased rainfalls in East Africa from March to May and decreased rainfalls in South-Central Africa (mainly in Zambia, Zimbabwe, Mozambique and Botswana) in December-February during ENSO events, whilst wetter in Southern as well as drier-than-normal conditions in equatorial East Africa during La Niña events (Tyson and Preston-Whyte, 2000; Kenyon and Hegerl, 2008; Lyon, 2009; Munday and Washington, 2017; Driver and Reason, 2017). SSTs variability influences the position of the maritime intertropical convergence Zone (ITCZ) as well. The ITCZ is located within the equatorial trough and is active when cloud clusters with low pressures form in this zone. Its position, length and width vary geographically and seasonally, and the mean position of it lies slightly north of the equator (Buckle, 1996). In Africa, the influential extension of the ITCZ covers mostly West Africa, while on the East of the continent, it moves northwards over Sudan in July and southwards over Zambia and Mozambique in January and thus is one important factor of the rainfall seasonality.
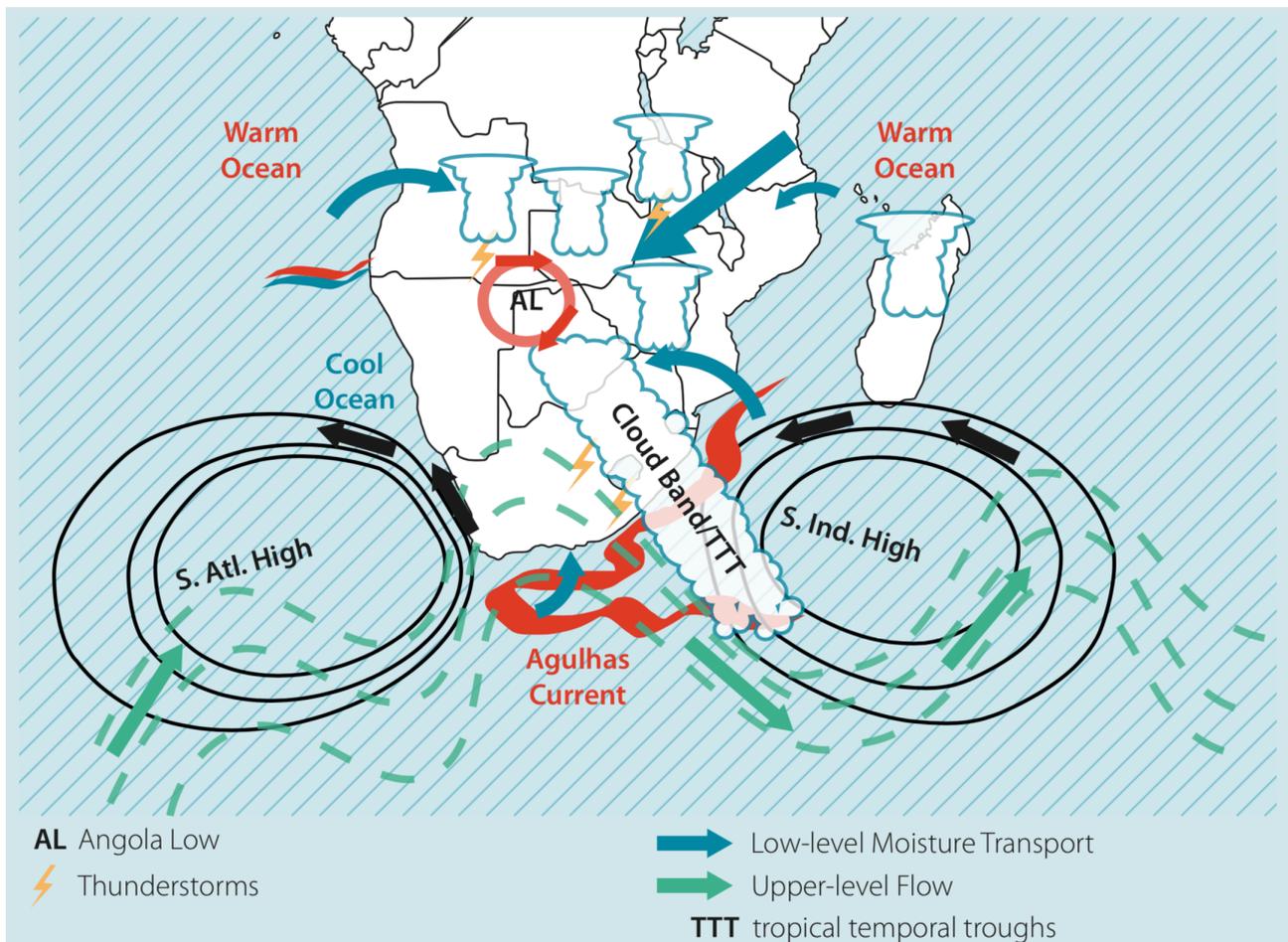
Figure 1-1. The schematic detailed key features of the Southern African climate system (Hart et al., 2016).

1.2. Extreme weathers in Southern Africa

The most critical issues in Southern Africa are water resources, basic infrastructures and agricultural tools and techniques as well as appropriate crop information (Fauchereau et al., 2003; Williams and Kniveton, 2011; Munday and Washington, 2017; Russo et al., 2016; Adisa et al., 2018). Recently, climate change especially global warming enlarges the magnitudes of extreme events and has worsened the issues in this region, which has been relatively less discussed. The atmospheric and surface energy budget (land-atmosphere feedbacks / couplings) play an important role in the hydrological cycle and extreme weather conditions. It is proved that in recent years with global warming and enhanced greenhouse gas concentrations, higher maximum temperatures are recorded

worldwide, which brings about more heat wave events (HWEs) with larger magnitude and increased duration (Ganguly et al., 2009; Perkins et al., 2012; Nicholson et al., 2013; Russo et al., 2014, 2016; Perkins, 2015; Donat et al., 2016; Barbier et al., 2018; Ilori and Ajayi, 2020). When the temperature rises, heating in the atmospheric system increases, the evaporation processes are more active, which leads to the surface drying out and causes higher intensity as well as longer duration of droughts. Drought conditions may have contributed to higher persistence of the heat wave because of the increasing surface net radiation (Perkins, 2015; Hulley et al., 2020). Frich et al. (2002) propose five climate indicators associated with temperature (Table 1-1), and mention that after the employment of these metrics, large areas such as Africa and South America are still not represented due to unavailability of high-density records. Nonetheless, the Heat Wave Duration Index (HWDI) is not representative well in places where day-to-day variability in temperature is small (e.g. tropical and sub-tropical regions) (Zhang et al., 2011). Therefore, other similar proposals related to the indicators for climate change are discussed many times in the joint meetings and workshops by the World Meteorological Organization (WMO), the Expert Team on Climate Change Detection, Monitoring and Indices (ETCCDI), the Intergovernmental Panel on Climate Change (IPCC), etc. with the purpose of establishing unified indices for robust detection of temperature extremes (Frich et al., 2002; Zhang et al., 2011; Perkins, 2015). Heat waves have enormous socio-economic impacts and are mostly observed by the measures of daily temperature extremes such as the Number of Hot Day (NHD), the Maximum Heat Wave Duration (HWD), in order to identify strength, duration and spatial extent of heat waves (Fisher et al., 2007). For example, the reduced surface moisture caused by one more intense dry season leads to the decrease in spring convection in monsoon regions (e.g. Western and Southern Africa), hence, a delay in onset of the precipitation season is found, which might influence the water supply for local people (Trenberth, 2011; James and Washington, 2013). Conversely, the amount of water vapour in the atmosphere rises and the moisture content is higher, for this reason, numbers of thunderstorm, extratropical rain, snow storms and tropical cyclone are also increasing. This contributes as intense precipitation events, though total precipitation amounts in an area might not increase but stay the same or decrease (Trenberth, 2011; James and Washington, 2013; Westra et al., 2014; Donat et al., 2016). The alterations in precipitation patterns such as intensity and amount may cause more frequent flooding or drought, which builds the large inter-annual precipitation variability and brings the issues of health (diseases), water, infrastructure damages, as well as agriculture (yield of the crops), and indirectly

influences migration and conflicts patterns in Southern Africa (Mason et al., 1999; Trenberth, 2011; Williams and Kniveton, 2011; James and Washington, 2013; Munday and Washingto, 2017; Ongoma and Chen, 2017; Adisa et al., 2018). Based on the suggestions that examinations for climate change should focus on changes in extreme events rather than on changes in climate means, Mason et al. (1999) identify the significant increases in the intensity of extreme rainfall events between 1931-1960 and 1961-1990 in South Africa. However, increasing total precipitation amounts in dry regions may be compensated or overcompensated by increased evaporation in a warmer climate, and hence may not lead to increased water availability (Trenberth, 2011; Donat et al., 2016).

A lot of research find the existence of dry signals in Southern Africa, including more extreme wet and dry seasons over parts of South Africa, an increasing in high daily rainfall totals and a rise in the spatial extent of drought as well as larger inter-annual rainfall variabilities over Southern Africa since the 1970s (Fauchereau et al., 2003; Williams and Kniveton, 2011; James and Washington, 2013; Donat et al., 2016; Adisa et al., 2018; Nicholson et al., 2018). Several global-scale models suggest during December-February, equatorial regions of Africa are expected to become wetter, with drying over the tropics and subtropics, while rainfall changes are smaller (with slightly wetter conditions) over equatorial regions during June-August (Williams and Kniveton, 2011). In spite of the fact that cumulative rainfall anomalies over the summer have not shown any trend to drier or moister conditions, more extreme rainfall events in recent decades in some regions and notable variations of the inter-annual variability of rainfall over the 20th century are found. Particularly since the late 1960s, droughts become more intense and widespread in Southern Africa (Fauchereau et al., 2003). For the African continent, the rainfall sums have been predominantly below or very close to the mean in all grid points in almost every year from 19th to 21st century, however, few significant trends are evident over the entire period of record (Nicholson et al., 2018).

The clear description of temporal and spatial variations in seasonal rainfall trends from 1980 to 1998 are presented in Nicholson et al. (2018). During the months from March to May, rainfall amounts in 20 °N-35 °S are below the long-term means, but in the eastern side of Africa, within the same latitude span the rainfalls are above the long-term mean. In October and November, western equatorial regions show declining trends, while in eastern equatorial and Southern Africa there are increasing trends. But according to the annual rainfall, there are no long-term trends over Southern

Africa (Nicholson et al., 2018). Ongoma and Chen (2017) state that in East Africa (1951-2010), there are increasing temperature over entire region and significant reductions of precipitation from March to May. Although annual rainfall amounts show negative anomalies, it can be separated into two seasonal components: March-May there are negative anomalies, while positive anomalies occur in October-December in East Africa. The spatial difference of rainfall anomalies is also mentioned, with the positive anomalies in northern part and the negative anomalies in southern part. The mean variability in rainfall is insignificant, since the occurrence of extreme rainfall should be taken into consideration. In the Greater Horn region, a clear warming signal (1973-2013) is shown by changes in minimum temperature of + 0.20-0.25 °C / decade and maximum temperature of + 0.17-0.22 °C / decade depending on seasons (Camberlin, 2016). The seasonal rainfall trends have also been investigated. There are negative trends in February-July (April-May largest negative trends), and during October-December, positive trends of rainfall occurrence and amounts are found. Another study focuses on the hydrological projections using a large-scale model in Southern Africa, which includes the mean precipitation change concerning the reference period for May-October, November-April and annual mean (Li et al., 2015). The projected temperature shows an increasing tendency, while the precipitation changes vary between months and sub-regions in the near future. During the main rain periods (November-April) in Southern Africa, the central and the northwestern costal regions present 5-40 % decreases in mean precipitation change, whilst the northeastern part and the eastern coasts exhibit 5-60 % increases (Li et al., 2015). However, there are still no much real-time research concentrating on seasonal- and monthly-scale rainfall or temperature trends in Southern Africa, hence, it would be great to look deeper into this kind of direction like our study.

Despite most of the models at global and / or local scale showing different projections of rainfall under the expected scenario of future climate change, they all agree with high uncertainty over future rainfall changes as well as water availabilities over Africa (Williams and Kniveton, 2011). However, these projections have also been made at smaller spatial scales, such as the country or local level. In general, models project decrease in subtropics (dryer) and increase in tropics (wetter), for the reason that when the moisture in convection regions (e.g. tropics) increases, the tropospheric temperature rises, which enhances the convection processes and thus precipitations (Trenberth, 2011; Westra et al., 2014; Aloysius et al., 2015). Moreover, Nicholson et al. (2018) state that the

west-to-east rainfall gradient across the region over the African continent has weakened apparently in recent decades due to East Africa drying caused by the SST anomalies.

Table 1-1. The five indicators for monitoring temperature extremes world-wide proposed by Frich et al. (2002).

Indicator	Definition	Units
Fd	Total number of frost days: days with absolute minimum temperature <0°C	days
ETR	Intra-annual extreme temperature range: difference between the highest temperature observation of any given calendar year (T_h) and the lowest temperature reading of the same calendar year (T_l)	0.1 K
GSL	Growing season length: period between when T_{day} >5°C for >5 d and T_{day} < 5°C for >5 d	days
HWDI	Heat wave duration index: maximum period > 5 consecutive days with T_{max} >5°C above the 1961-1990 daily T_{max} normal	days
Tn90	Percent of time T_{min} > 90th percentile of daily minimum temperature	%

1.3. Research gaps and objectives

Different types of climate data and observational products are applied for the research in Africa (Jack et al., 2016). The direct Earth-based observed products include weather stations, radiosonde, etc. (e.g. CRU dataset), but they may suffer from spatial deficiencies due to missing station values. For example, temperature extremes require high-quality daily data for their calculation, but most of such observations do not openly exist for many areas of the globe (Perkins, 2015). On the other hand, the sources of pure space-based and blended space and Earth data products come from satellites, and the later ones are processed with the adjustments by station observations (e.g. TRMM rainfall dataset, Climate Hazards Group InfraRed Precipitation (CHIRP) rainfall dataset). Lastly, the re-analysis products or blended model / direct observations products are established by climate-model simulations with corrections by historical observations of temperature, pressures and moisture (Jack et al., 2016). In Africa, it is noticed that when the rain-gauge data are used, there is misleading information due to the sparse and uneven distribution of stations in several countries. Satellite-derived rainfall estimates can provide a solution to this problem (Williams et al., 2011). Many models applied with the gridded monthly time series (e.g. CRU dataset) (1901-2008) of precipitation and temperature as well as SSTs data set (1870-2012) show limited skill in the

simulating the seasonality, spatial patterns and magnitude of precipitation in Central Africa (Aloysisu et al., 2015). In short, it is challenging to find the most suitable climate data / products which can accurately fit different regional research.

It is necessary to understand changes in both frequencies and / or amplitudes of heavy precipitation and of periods of below / above normal rainfall, therefore the direction of research should be accessed on the daily and the monthly-to-seasonal time scales (Fauchereau et al., 2003). In Southern Africa, the study emphasise mostly monthly-to-seasonal time scales, with some of them doing climactical simulation of extreme events, but for the application of real (in-time) data on daily time scale as well as large spatial resolution, they are relatively scarce. Although climate models are the best tools available for us to understand how the climate will change under global warming as well as enhanced anthropogenic activity, they do still suffer from the heterogeneities of each variable. The quality of downscaled projections depending on the driving global climate models (GCMs) at regional scale, as well as the inconsistency of a unified definition for climate extremes (Perkins, 2015). For example, many studies employ their own heat wave definitions or use less appropriate definitions developed by ETCCDI, the projected results are diverse and it is hard to compare them (Perkins, 2015). The model stimulations are reported for yielding significantly large overestimations of rainfall totals over the escarpment areas of Southern Africa, and the pattern of the rainfall biases is also especially consistent amongst models and reanalyses (Dedekind et al., 2016; Munday and Washington, 2017). Moreover, as many aspects of climate are well represented by monthly means, it is more appropriate to use indices derived from daily data for examinations of extremes (Zhang et al., 2011). The preexisting studies generally focus on mean temperatures and precipitation or only on few indices for climate extremes in Central, West and coastal East Africa individually. The research focus more there because the subtropical rainforests are located in these regions and seen as one important carbon sink for mediating the impact of greenhouse gas emissions (Aloysius et al., 2015). The relationships between monthly temperature and precipitation are examined over the African continent. In some oceanic regions in the tropics, the positive correlations are dominant, whilst the negative correlations exist in tropical lands as well as in mid-latitudes in summer, though these patterns with significance appear less robust across datasets (James and Washington, 2013; Berg et al., 2014; Camberlin, 2016; Hao et al., 2019). However, temporal or spatial averaging of the data such as the concepts of seasons and state borders used in predetermined spans before the

analysis might lose valuable detailed data (e.g. averaging within vast geographic areas) (Kulikov and Schickhoff, 2017). Therefore, in order to understand the behaviours between precipitation and temperature extremes in Southern Africa, this study detected HWEs and applied regression model analysis between temperature and precipitation time series on a pixel basis, which can identify the complex interactions with higher spatial variations.

The specific aims in this study are to solve three research questions:

1.) Are there any trends in precipitation and maximum temperature in Southern Africa from 1981 to 2019?

2.) Are there more frequent HWEs occurring in Southern Africa. Are they with spatial variations?

3.) How do precipitation patterns change under HWEs with lag effects in rainfall periods?

The hypotheses are:

1.) There are positive trends in annual and monthly maximum temperature in the whole Southern Africa. The annual precipitations increase in tropical regions (15-23.5° S) and decrease in subtropical areas (23.5-35° S). In general, the positive trends of precipitation from October to April and the negative trends from May to September would be observed.

2.) There are more frequent HWEs in recent years, and their intensities as well as the durations increase significantly. Regarding the southern coastal regions, there are no significant phenomena mentioned above.

3.) Heat wave duration and intensity affect the amount of weekly total precipitation with lag effects of zero to two lags of weekly mean maximum temperature. Relationships between weekly precipitations and maximum temperatures with their lag effects are spatially heterogeneous over the whole study region, with the east- and north- part of Southern Africa exhibiting enhancement of rainfall amounts during HWEs, and the west part of Southern Africa having no significant connections.

This study is thus organised as follow: the first part gave an overview of the climatology of Southern Africa, and describes the extreme events such as heat waves and droughts with the background of mechanisms that drive these phenomena. The second part introduces the study region and the applied data. The detailed analysis including the methods and their procedures related to regionalisation of precipitation patterns, trend analysis, detection of HWEs and lag

regression models are presented in the third part. The discussion concerning possible aspects of climatic and orographical factors associated with the results are in the fourth and fifth parts. A conclusion of this study and the attribution issues follow as the six part.

2. Data

2.1. Study area

The study area Southern Africa is located approximately between 15° S and 35° S in latitude and between 10° E and 40° E in longitude (Figure 2-1), which includes 10 countries: Angola, Zambia, Malawi, Mozambique, Namibia, Botswana, Zimbabwe, South Africa, Lesotho and Eswatini (Swaziland). The climates are largely influenced by trade winds and subtropical highs (Buckle, 1996; Endlicher, 2000; Tyson and Preston-Whyte, 2000). Based on the Köppen-Geiger climate classification (Figure 2-2), the research area is categorised as tropical - savannah (Aw), temperate - dry winter / hot summer (Cwa), temperate - dry winter / warm summer (Cwb), arid - steppe / hot (BSh), arid - desert / hot (BWh), arid - desert / cold (BWk), arid - steppe / cold (BSk), temperate - no dry season / hot summer (Cfa), temperate - no dry season / warm summer (Cfb), temperate - dry summer / hot summer (Csa), and temperate - dry summer / warm summer (Csb) (Beck et al., 2018). The mean annual precipitation is around 20-1000 mm, with < 100 mm in the western coastal regions and up to 300 to < 500 mm in the northern boundaries. Rainfall periods occur between September to April, with the rainfall peaks in October to February.

An elevation model map representing the elevation of the study area was downloaded from SRTM 90-meter resolution data between -60 and 60 latitude by R function 'getData' in package "raster" (Hijmans et al., 2021b). The elevation map of the study area was clipped by the geographic extent of Southern Africa in R and shows a range of elevation between -251 and 3473 m a.s.l (Figure 2-1).
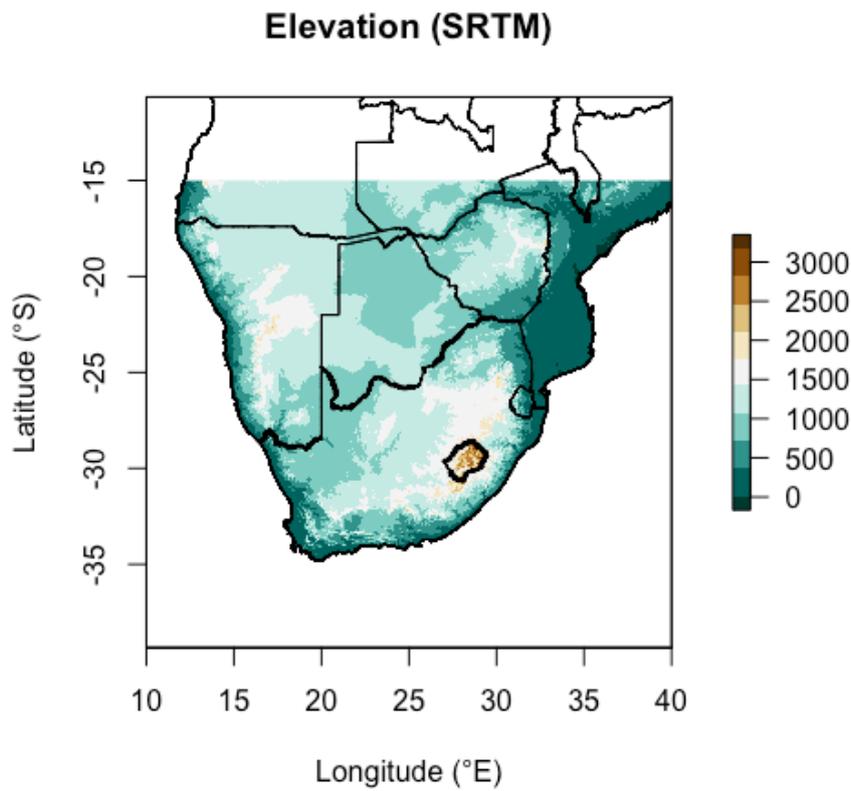
Elevation (SRTM)

Figure 2-1. Elevation map, also including the extent of the study area in Southern Africa.
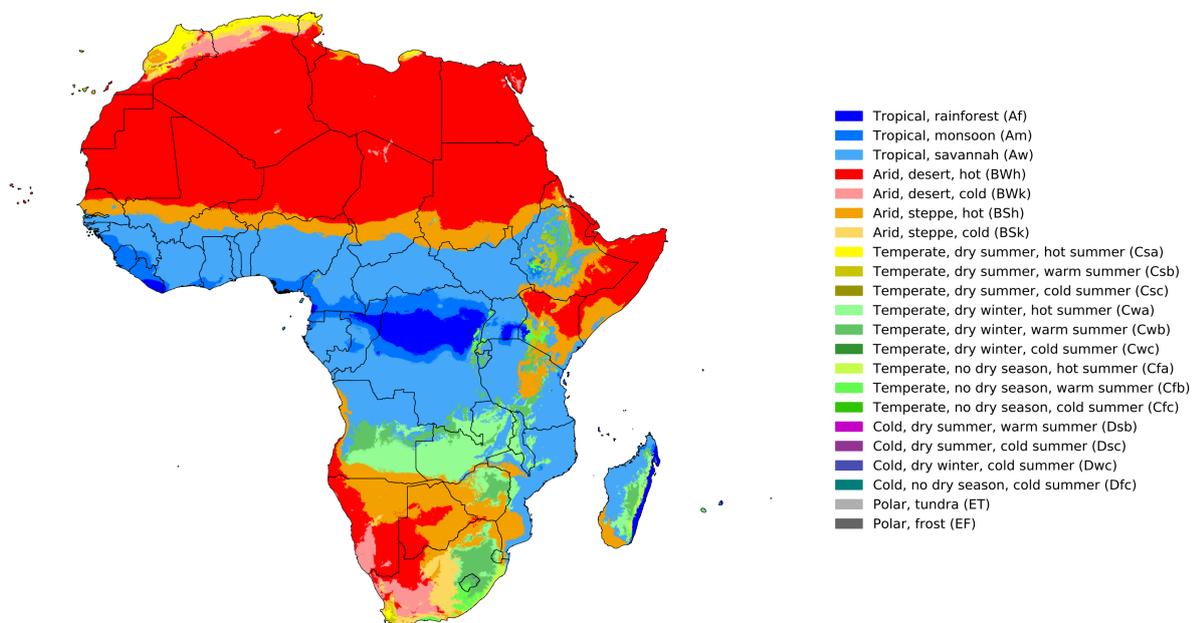
Figure 2-2. Köppen-Geiger climate classification in Africa (Beck et al., 2018).

2.2. Dataset

After comparing different available datasets (e.g. GPCC Full Data Daily V.2018, CRU TS, TRMM Multi-satellite Merged Product (3B42), PERSIANN-CDR), ERA5-Land was chosen due to both suitable spatial and temporal resolutions as well as better performances in previous studies (Climate Research Unit (CRU); European Centre for Medium-Range Weather Forecasts (ECMWF); Global Precipitation Climatology Centre (GPCC); Tropical Rainfall Measuring Mission (TRMM); Zhang et al., 2011; Zandler et al., 2019).

ERA5-Land is a global land-surface dataset providing hourly high resolution information of surface variables at 9 km resolution, and is consistent with atmospheric data from the ERA5 reanalysis (station-based gridded products) from 1950 onward. This reanalysis products ERA5-Land hourly data from 1981 to present (gridded to a regular latitude-longitude grid of 0.1×0.1 degrees; spatial resolution: $0.1°$) obtained by ECMWF, which is the officially released version available online since July 2019 (https://climate.copernicus.eu/climate-reanalysis, last access: 30 September 2020), are employed and the two variables: 2m temperature (K) and total precipitation (m) are used for analysis. The data was obtained as a NetCDF file and written as GeoTIFF format afterwards.

Both 2m temperature and total precipitation located in 5-35° S in latitude and 10-60° E in longitude were downloaded and cropped into 15.05-34.95° S and 10.05-41.05° E afterwards. There are some grid points showing error values as -2.775558e-14 in total precipitation in small number of days in the raw ERA5-Land hourly data. They were set as NA values first in order to continue the aggregation of data into daily and monthly resolutions. After the transformation of the units in 2m temperature (K to °C) and in total precipitation (m to mm), the hourly datasets were aggregated into daily resolution that span from 1981 to 2019. Total precipitation was again aggregated into monthly data for the aim of regionalisation of precipitation and trend analysis, and into weekly data for the lag regression analysis. Weekly maximum 2m temperature was computed by taking mean value of daily maximum temperature in each week for the later steps of confirming heat wave events and the lag regression analysis.

Finally, there are 14244, 2035 and 39 raster layers for daily, weekly and monthly data in each RasterBrick in R. All the approaches were processed by using R (Version 3.6.3). In these procedures, R packages "gdata", "gstat", "lubridate", "ncdf4", "raster", "rgdal", "swfscMisc", "terra" and "zoo" were used (Warnes et al., 2017; Pierce, 2019; Archer, 2021; Bivand et al., 2021; Hijmans et al., 2021a, b; Pebesma and Graeler, 2021; Spinu et al., 2021; Zeileis et al., 2021). All maps are displayed with the longitude-latitude coordinate system (WGS84).

3. Methods

3.1. Regionalisation of precipitation patterns

3.1.1. Cluster analysis

Since the whole research area is large and it includes varieties of climatic characteristic, especially in the precipitation patterns, cluster analysis has been applied in order to recognise different sub-regions based upon monthly total rainfall amounts.

There are partitioning (nonhierarchical) and hierarchical methods. In this case, due to the enormous extent and high spatial resolution of the precipitation data, partitioning clustering algorithms are more flexible and appropriate since they allow a grid cell to be reassigned to reach an optimum result (Zhang et al., 2016). Partitioning methods are applied in order to classify objects into k clusters, where k is fixed and decided by the specific evaluation processes. There are several algorithms in partitioning methods, the two well-known are k-means and k-medoids algorithms, respectively. The goal of k-means algorithm is to minimise the average squared distance and to find the centroids (the mean of all observations in the cluster), whilst k-medoids algorithm attempts to find "spherical" clusters, and theses centers are actual observations in the data. Since k-medoids algorithm concerns interval-scaled measurements and also general dissimilarity coefficients, it is more robust with respect to outliers and noise and ideal with non-normal data. The most popular heuristic for k-medoids is the Partitioning Around Medoids (PAM) algorithm (Kaufman and Rousseeuw, 1990; Roelofsen, 2018).

CLARA (Clustering LARge Applications) is one variation of k-medoids that uses sampling methods to deal with large data sets (Kaufman and Rousseeuw, 1990; Roelofsen, 2018). The clustering object is the same as PAM. The only difference is that CLARA doesn't store all dissimilarities in central memory, but the actual measurements. That is, only the distances between the observations are needed for the algorithm (because the medoids are also observations), which may cause the loss of some other features (Kaufman and Rousseeuw, 1990; Roelofsen, 2018). In CLARA, a sample of objects is selected from the data by means of a random number generator, and clustered in the way that the average distance of the representative object (medoid) to all the other objects of the same cluster is being minimised. Then each object of the entire data set is assigned to the nearest medoid of the sample. The whole procedure is repeated several times and the solution with the most ideal

overall object function is preserved. Most of its important functions are kept and the computation time remains practicable (Kaufman and Rousseeuw, 1990).

The CLARA algorithm creates multi-subsets with fixed size randomly from the original data set, and computes PAM algorithm on each subset. The corresponding k representative objects are selected as medoids and each observation of the entire data set is assigned to the closet medoid. By minimising the sum or the mean of the dissimilarities of the observations to their closest medoid during the whole calculation processes, which is a measurement of the goodness of the clustering, each sample gets its respective cluster membership finally (Kaufman and Rousseeuw, 1990). It has to be noticed that there is a trade-off between efficiency and clustering quality, which depends on the values that are chosen for random samples (S), observation of size (z) and k in total number of observations (N). In the guidelines created by Kaufman and Rousseeuw (1990) and Maechler et al. (2021), $S = 5$ and $z = 40 + 2k$ return satisfactory results, while it generally hold that $k, S, z << N$ is able to make CLARA more efficient for large values of N (Roelofsen, 2018). R packages "cluster" and "RStoolbox" are used for evaluating the results of different algorithms for k-means and k-medoids methods (Leutner et al, 2019; Maechler et al., 2021).

3.1.2. Evaluation of the optimal number of clusters

As explained in the former paragraph, partitioning clustering methods usually require the number of clusters k as an input parameter beforehand. The number of clusters k is specified based on users' prior knowledge and experiences (external cluster criterion) or based on an estimation (internal cluster criterion) (Roelofsen, 2018). There are many global and local methods to determine the optimal number of clusters k for a clustering assignment. Generally, global methods compare the criteria values for a range of k-values to decide the optimal number of clusters. In this study, Within cluster Sum of Squares (WSS), Silhouette index and Gap statistic were applied with R packages "factoextra" and "ggplot2" in order to find a congruous number of clusters and to visualise the results (Ketchen and Shook, 1996; Tibshirani et al., 2001; Kaufman and Rousseeuw, 2005; Charrad et al., 2015; Kassambara and Mundt, 2020; Maechler et al., 2021; Wickham et al., 2021a).

Dedekind et al. (2016) describe and plot the seasonal and monthly total precipitation amounts in Africa, which is ideal for the consideration of clustering according to different patterns. In this study, the average values of each month from 39 years were calculated and set as the main variable

for the clustering. As another possible variable mean monthly maximum temperature was considered and analysed together with mean monthly total rainfall amount, but the consequential clustering pattern is similar. Therefore, only mean monthly rainfall is used to display the final clustering results.

3.2. Trends of precipitation and maximum temperature

In order to detect the trend of annual and monthly precipitation and maximum temperature in Southern Africa over the 39 years, the non-parametric Mann-Kendall test is applied. The null hypothesis (H_0) states that the data come from a population with independent realisations and are identically distributed, whilst the alternative hypothesis (H_A) is that the data follow a monotonic trend (Pohlert, 2020).

The Mann-Kendall test is based on the statistic S:

$$S = \sum_{k=1}^{n-1} \sum_{j=k+1}^{n} sgn(X_j - X_k) \tag{1}$$

with

$$sgn(x) = \{1, \text{ if } x > 0$$
$$0, \text{ if } x = 0 \tag{2}$$
$$-1, \text{ if } x < 0\}$$

and the variance σ^2:

$$\sigma^2 = \left\{ n(n-1)(2n+5) - \sum_{j=1}^{p} t_j(t_j - 1)(2t_j + 5) \right\}/18 \tag{3}$$

where p is the number of the tied groups in the data set, and t_j is the number of data points in the jth tied group.

$$Z = \{ (S\text{-}1) / \sigma, \text{ if } S > 0$$
$$0, \text{ if } S = 0 \tag{4}$$
$$(S\text{+}1) / \sigma, \text{ if } S < 0 \}$$

Kendall's tau coefficient (τ) is calculated by the statistic S:

$$\tau = \frac{S}{D} \tag{5}$$

where

$$D = \left[\frac{1}{2} n(n-1) - \frac{1}{2} \sum_{j=1}^{p} t_j(t_j - 1) \right]^{1/2} + \left[\frac{1}{2} n(n-1) \right]^{1/2} \tag{6}$$

Kendall's tau coefficient (τ) ranges from -1 to +1 and is estimated by determining for each pair of observations whether they are concordant or discordant (Wilcox, 2010). Positive values of τ denote increasing (upward) trends while negative τ values show decreasing (downward) trends. When τ values are close to 0, it means there is no long-term trend (Daniel, 1990). The Z-value for recognising trends is performed at the specific α significance level. The magnitude of trends and related confidence are predicted by Theil-Sen method (Theil, 1950; Sen, 1968; Siegel, 1982). It is a non-parametric procedure showing high precision in the presence of skewed as well as heteroscedastic data and is calculated as the median from all slopes of all lines through pairs of points (Wilcox, 2010; Pohlert, 2020).

$$\beta = Median \left(\frac{x_j - x_i}{j - i} \right), j > i \tag{7}$$

where Sens's slope (β) reflects the data trend, and its values indicate the steepness of the trend. Similarly, zero value of Z-value and β-value implies no trend, while positive (negative) value indicates an increasing (decreasing) trend. In this study, significance levels $\alpha = 0.05$ is used. The details of statistical formulas can be checked in Theil (1950), Sen (1968), Siegel (1982), Daniel (1990) and Pohlert (2020). For the pixel-wise trend analysis, R package "spatialECO" is utilised,. The results of the application of the function 'raster.kendall' are given as a rasterBrick object containing seven raster layers with the values of slope, intercept, p-value, Z-value for trend, lower / upper confidence level at 95 percentile and Kendall's tau two-side test (Evans et al., 2021).

3.3. Detection of heat wave events (HWEs)

Heat wave studies commonly focus on three main features: intensity, duration, and frequency (Perkins, 2015), which can be computed based on the event scale or for each grid point (Barbier et al., 2018; Schlegel and Smit, 2021a, b). There are several methods with different thresholds which can define the occurrence of heat wave events. Lyon (2009) applies both criteria in Southern Africa during the summer time: a minimum of 3 or 5 consecutive days and/or the 90th or 95th percentile criteria, and finds out that the latter stricter criteria did not alter the main results, but only identified fewer cases. Since understanding the relationships between precipitation and temperature extremes is the goal in this study, the criteria with higher thresholds identifying the most extreme heat wave events are selected. Zhang et al. (2011) report that gridding indices from daily data are not always direct and proper because averaging daily information from many stations tends to weaken gridded extremes. Hence, a pixel-wise analysis for detection of HWEs is conducted in this study. The daily climatologies in this application have been calculated over the long-term average period of 1981-2010, which is the current WMO climatological standard for long-term averages (World Meteorological Organization, 2017).

The established criteria for this study are stated in the following:

1) A period of at least 5 consecutive days when the daily maximum temperature (T_{max}) exceeds the statistical 95th percentile of the climatological T_{max} series dependent on a 15-day moving window. The T_{max} percentiles are obtained by calculating daily climatology over 1981-2010. Since there might be spatial variations in temperature associated with elevations, percentiles are used rather than absolute values of T_{max}.

2) Area covered in each sub-region, expressed as a percentage relative to the whole sub-region. The detected heat waves are transformed into weekly time scale. There are two reasons. First, since the start of heat waves in each grid point occurs on different dates, if the heat waves are confirmed only with the agreement of more than 30 %, 40% and 50% grid points, it is hard to identify clear events in each sub-region. Second, the further regression analysis with total precipitation amounts is meaningful using weekly data, because as one heat wave event is identified with the accumulated high-temperature condition, rainfall amounts might be influenced by lag effects after the accumulation of heats in the atmosphere. In consequence, if

the starts of the heat waves occur in the same week, they are computed as the same heat wave period and calculated for the percentages relative to the whole-subregion.

3) Occurrence during the rainfall periods determined separately in each sub-region. Rainfall periods are defined as when the mean of monthly total precipitation is more than 5% of the annual total precipitation amounts.

The utilisation of R packages "dplyr", "doParallel" and "heatwaveR" are included in this part (Schlegel and Smit, 2018, 2021b; Wallig et al., 2020; Wickham et al., 2021b). The functions 'ts2clm' and 'detect_event' in R package "heatwaveR" and the vignettes provided by Schlegel and Smit (2021a) are used for the creation of daily climatology and the detection of pixel-wise heat wave events.

3.4. Lag regression models

Since total precipitation is considered to be influenced by HWEs at various lags, both weekly precipitation and maximum temperature are selected during each heat wave event with additional four weeks before and after for the lag regression models. In lag regression models analysed with zero- to two-week lags, weekly total precipitation amount is applied as the dependent variable, and weekly mean maximum temperature as the independent (explanatory) variable:

$$P_t = \alpha + \beta_0 T_{max,t} + \beta_1 T_{max,t-1} + \beta_2 T_{max,t-2} + \varepsilon_t$$

where the response variable P_t is the precipitation at time t, the predictor variable is the maximum temperature (T_{max}) with its lag effects $T_{max,\,t}$, $T_{max,\,t-1}$ and $T_{max,\,t-2}$, α is the intercept, β_0, β_1 and β_2 are the lag coefficients (slopes) of $T_{max,\,t}$, $T_{max,\,t-1}$ and $T_{max,\,t-2}$, and ε_t is the random error. It is noted that the model is unique for each sub-region (location-dependent). The coefficients may vary obviously between geographic locations due to different terrain characteristics and atmospheric circulations. Hence, lag regression models are created pixel-wise for each heat wave event and presented by adjusted R-squared values as well as the maps masked by the significance results ($p < 0.05$), and the slopes of each lag effect.

R packages "broom", "raster", "RColorBrewer", "xts" and "zoo" are applied for the analysis and the output of figures (Neuwirth, 2014; Ryan et al., 2020; Hijmans et al., 2021b; Robinson et al., 2021; Zeileis et al., 2021).

4. Results

4.1. Cluster analysis

According to the result of Within cluster sum of squares (WSS), Silhouette index and Gap statistic, the appropriate number of clusters are three, two and six, respectively (Figure 4-1). After the CLARA program was applied and the different results visualised, in compliance with the references describing seasonal and monthly total precipitation amounts in Africa (Dedekind et al., 2016), it is hard to recommend using two or three clusters for the regionalisation of precipitation patterns in the extensive research area. Furthermore, the winter precipitations in the southwestern region can be only identified with at least eight clusters. The 10-cluster result is decided in order to represent the rainfall patterns in the northern part of the research area (Angola, Zambia and Malawi) explicitly (Figure 4-2).

The code number of ten sub-regions are C1 to C10 in this study (Figure 4-2). C1 (3667 grids) includes southern coastal area of Angola, coastal Namibia and South Africa. C2 (4116 grids) extends from southern coastal Angola, Namibia, South Africa and Botswana. C3 (3349 grids) has the extension of Angola, Namibia, Botswana, small areas of South Arica and Zimbabwe. C4 (2771 grids) contains mostly eastern coastal South Arica, Lesotho, Eswatini, small areas of Zimbabwe and Mozambique. C5 (2276 grids) and C6 (5063 grids) are covered by Angola, Zambia, Zimbabwe, Mozambique and Malawi, and C6 has additionally a small area of Namibia. Southern Angola, northern Namibia and Botswana, Zimbabwe and Mozambique and very less grids of Zambia and Malawi comprise C7 (4330 grids). C8 (4613 grids) involves South Africa, Eswatini, Botswana, Zimbabwe and southern Mozambique. C9 (4876 grids) is located in the middle of the study region, and its spatial ranges are a tiny area of Angola, Namibia, Botswana, South Africa, northern Zimbabwe and Mozambique. The position of C10 (1206 grids) is in the southern coastal area of South Africa.

The rainfall periods in 10 sub-regions are shown as below:

C1: October to August. The peak rainfall period is from January to April with more than 10 % annual rainfall amount in each month.

C3 and C5: November to April. The peaks occur from December to March (higher than 14 %), and the total rainfall are higher than 20 % of annual rainfall in January and February.

C2, C4, C8 and C9: October to April. The peaks delineated by higher than ca. 15 % exist from December to February.

C6 and C7: November to March. The peaks extend from December to February (higher than 20 %).

C10: January to December (the whole year), ca. 7.1-9.2 % of the annual rainfalls in each month.

The elaborated mean percentages of monthly precipitation amount in each sub-region from 1981 to 2019 can be found in Appendix A. (Table A-1). In Figure 4-3 (a.-j.) the monthly precipitations over 1981-2019 are visualised as box plots for C1 to C10 sub-regions and the associated spatial maps can be seen in Appendix A. (Figure A-1).
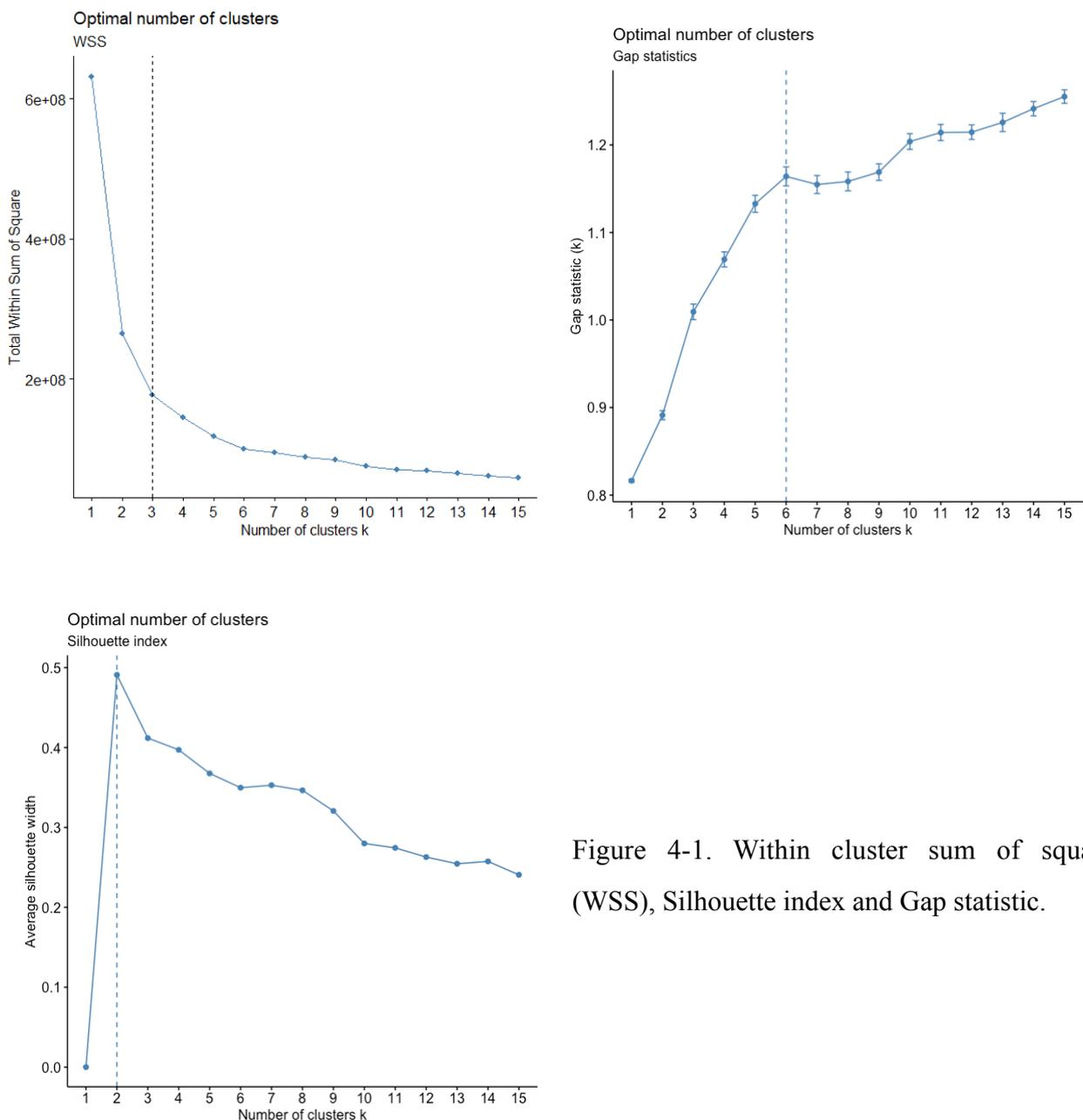
Figure 4-1. Within cluster sum of squares (WSS), Silhouette index and Gap statistic.
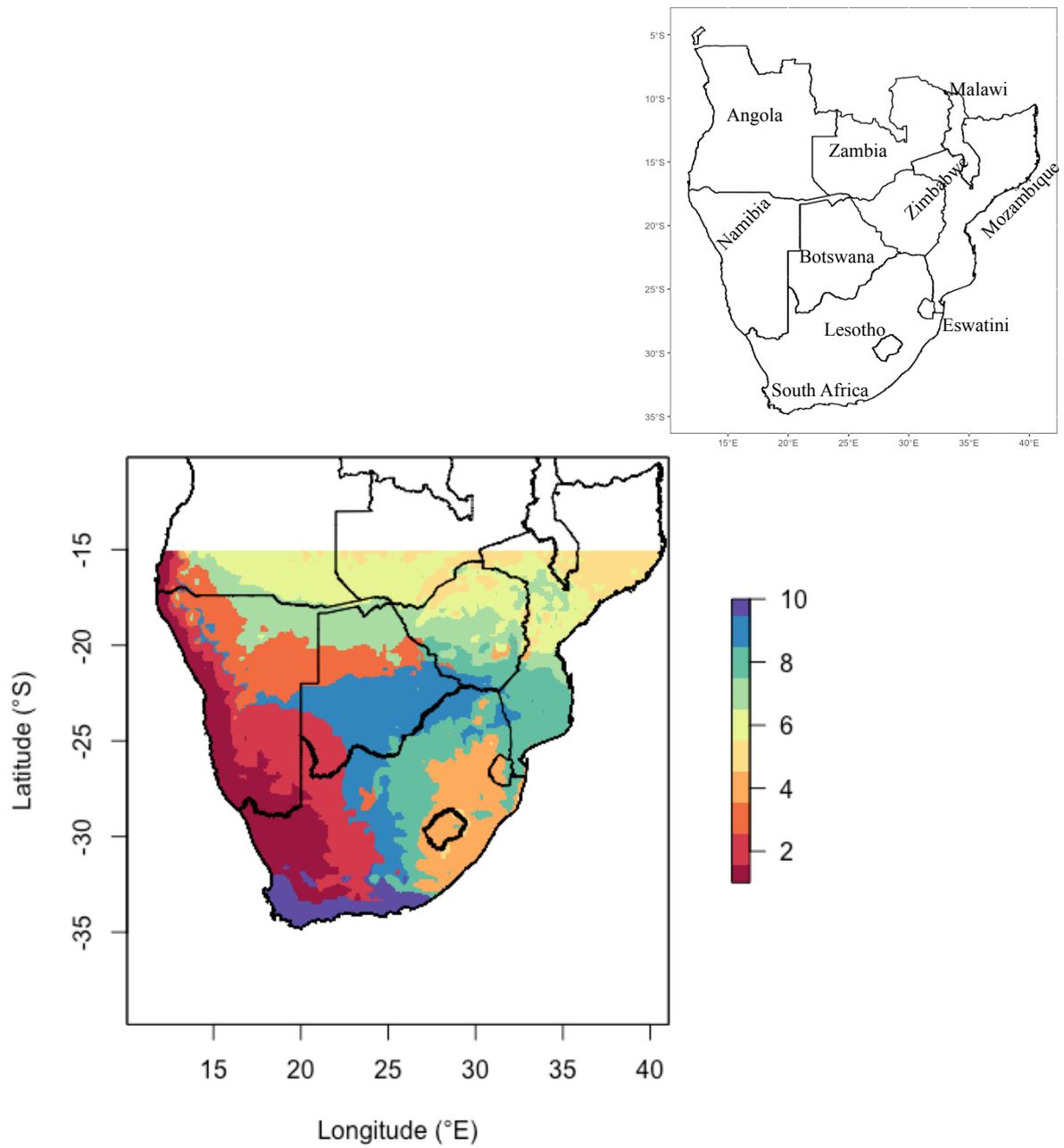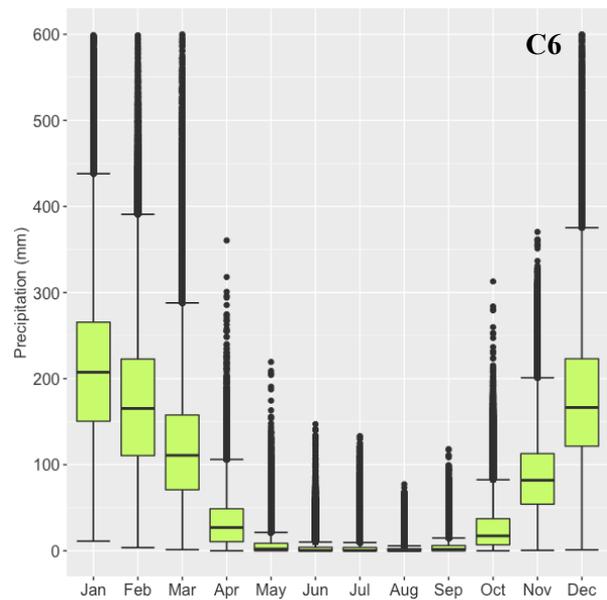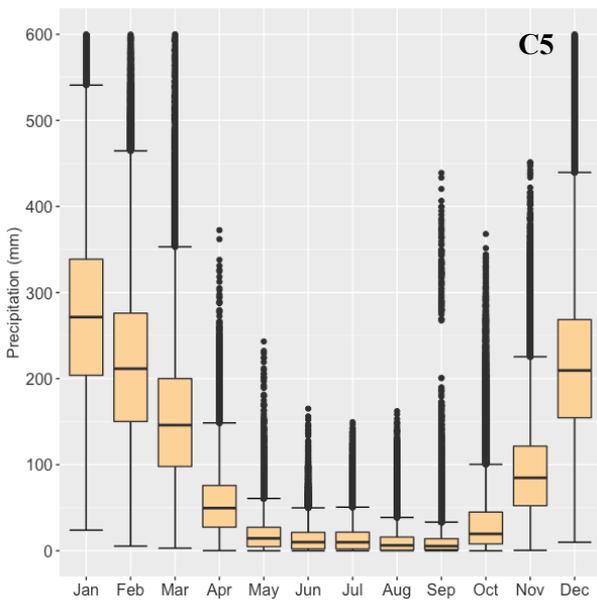
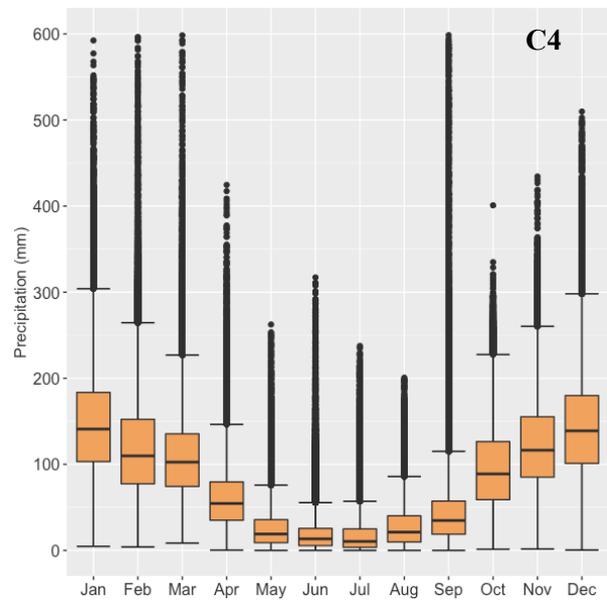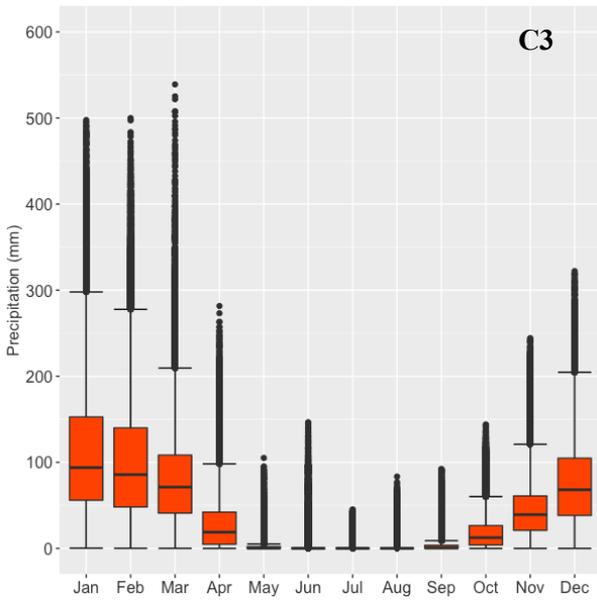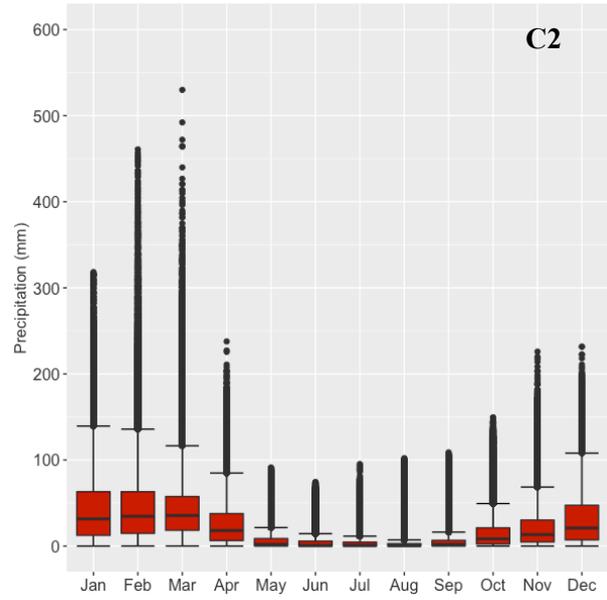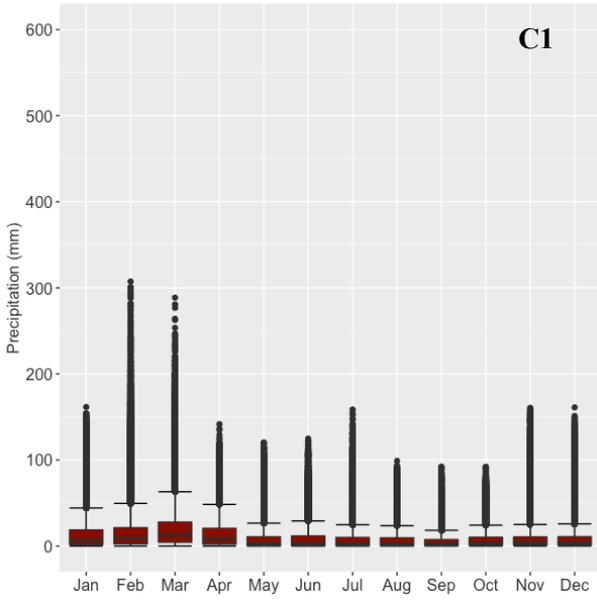**Regionalisation of monthly precipitation**

Figure 4-2. Regionalisation of precipitation patterns in Southern Africa. Colours show regions belonging to the same cluster.
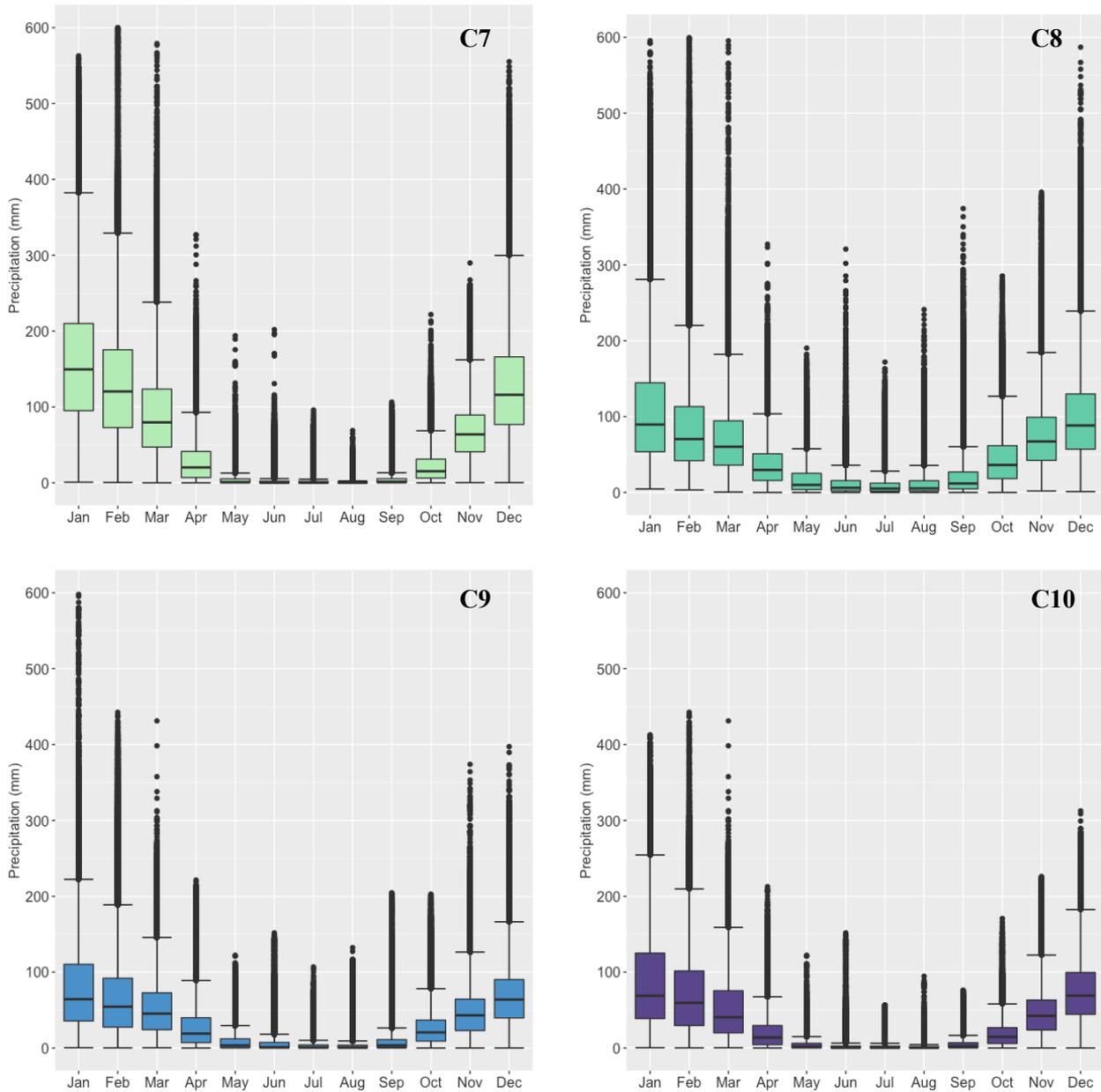
Results

Figure 4-3. Monthly precipitation in sub-regions C1 to C10 illustrated as box plots. Boxes range from 25 % to 75 % quantile. Thick black lines represent median (50 % quantile), lower / higher whiskers extend to 1.5 * IQR (interquartile range), and outliers are truncated at 600 mm.

4.2. Trends of precipitation and maximum temperature

Based on Kendall's tau coefficient (τ) and Sen's slope (β), the annual total precipitations show increasing trends in most of the northern part of the whole study region, and decreasing trends in the southern part (Figure 4-4 a, c). Excepting the west-central part (Namibia, western Botswana, and some sections of South Africa), there are increasing trends in the annual maximum temperatures (Figure 4-4 b, d). Sen's slopes exhibit large magnitudes of decreasing rainfall around Lesotho (C4 sub-region). Though Z-values present a little different spatial trend pattern (larger peripheral area) (Figure 4-4 e, f), when they are masked with the significant level ($p < 0.05$), only the negative trends remain in both annual total precipitation and maximum temperature (Figure 4-4 g, h).

On a monthly scale, from December to April there are positive trends of precipitation in most of the northern part of the study area, excluding Mozambique and eastern Zimbabwe in February (Appendix B, Figure B-1). In May, only the central part of South Africa shows increasing rainfall trends, while from August to October, Southern Africa presents mainly decreasing trends (Appendix B, Figure B-1, B-2, B3). The slopes indicate greater magnitudes of positive trends in southern Angola in December and relatively large magnitudes of negative trends in Mozambique in February and over Lesotho from October to November (Appendix B, Figure B-2). Z-values imply significant decreasing precipitations particularly from May to September, whilst the other regions showing positive trends are not significant signals during the same months ($p > 0.05$) (Appendix B, Figure B-3). Except for April, positive trends of monthly maximum temperatures are detected in South Africa (Appendix B, Figure B-4, B-6). From August to September Southern Africa exhibits increasing maximum temperatures with the exclusion of west-coastal regions. During May-June-July, there are decreasing trends of maximum temperatures in the central part of Southern Africa, and these trends extend broadly gradually from January to April (the main rainfall periods) (Appendix B, Figure B-4, B-5, B-6). The comparatively great magnitudes of positive trend indicated by the slopes occur during October and November in South Africa as well as the coastal regions in Namibia (Appendix B, Figure B-5). Similarly, the significant trends exist only in negative Z-values, and very small areas are with significance during September-October-November (Appendix B, Figure B-6).
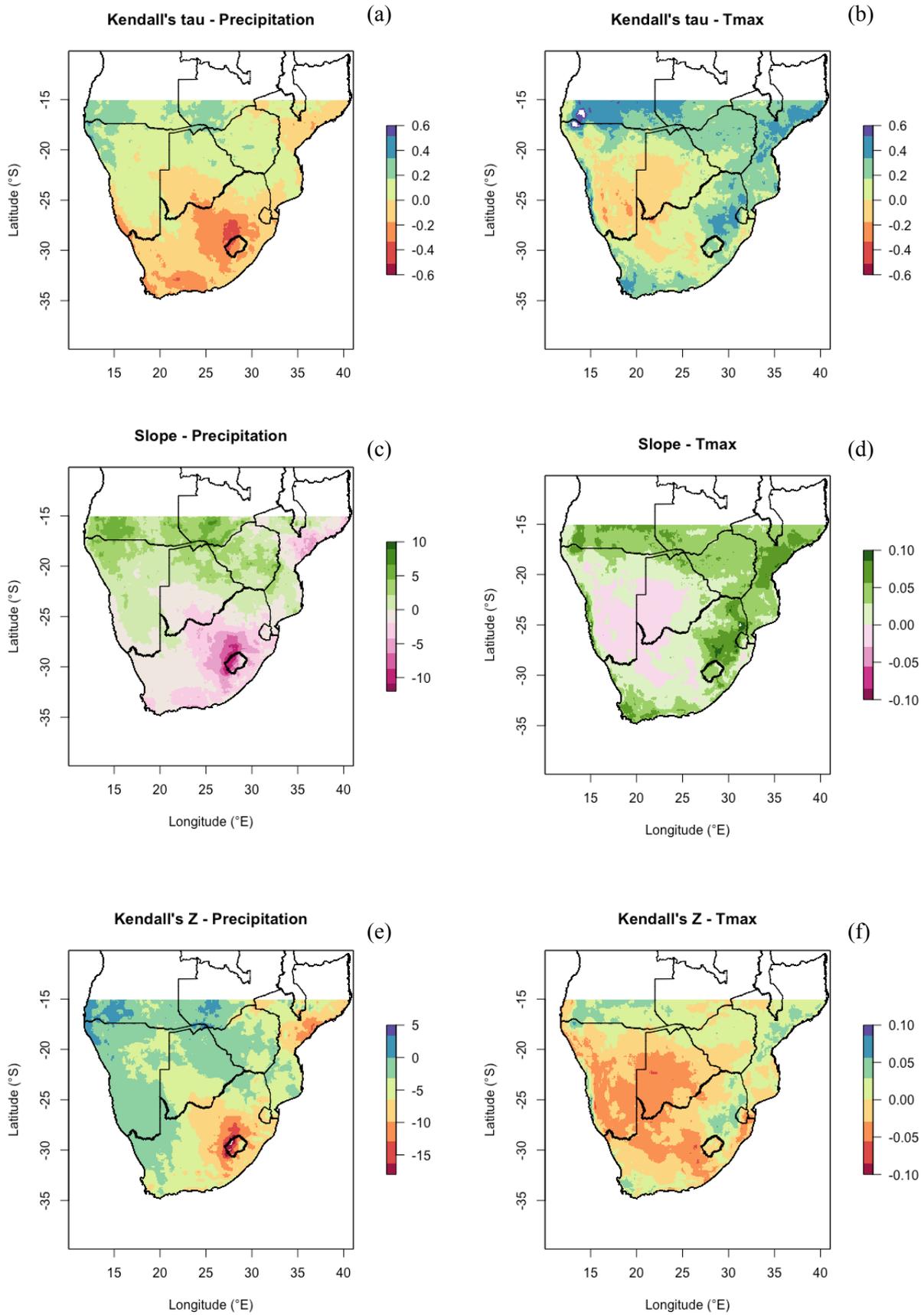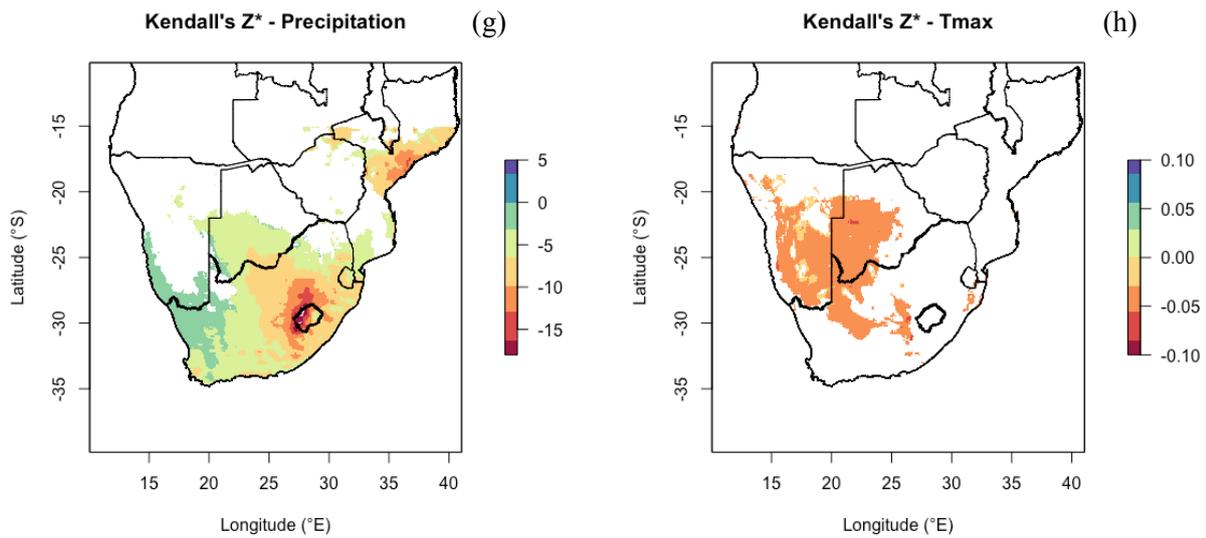
Figure 4-4. Trends of annual precipitation and maximum temperatures in Southern Africa from 1981 to 2019. Annual values of tau (a, b), Sen's slope (c, d), *Z*-value (e, f) and *Z*-value masked with significance (g, h) of Mann-Kendall Test.

4.3. HWEs

There are zero to six heat wave events detected per year in each sub-region which can be found in more than 30 % area during the rainfall periods. One to 24 events in each sub-region are detected from 1981 to 2019. The mean durations, the mean intensity and the cumulative intensity of HWEs over 39 years in 10 sub-regions are 5.0 ± 0.09 - 23.7 ± 7.97 days, 3.6 ± 0.30 - 11.7 ± 1.18 °C and 20.4 ± 6 - 143.4 ± 47.7 °C × day, respectively. The detailed results can be viewed in Table 4-1. However, there are no increasing tendencies in the number as well as in the cumulative intensity of HWEs in all sub-regions. But if all grids are involved and counted for each individual heat wave event, there are more HWEs since 2014 and with a peak in 2019 except for in the C10 sub-region (Appendix C, Figure C-1). Different extensions of impacted area elucidated by the percentage of area are displayed in Table 4-1.

28

Table 4-1. The indices of HWEs based on the criteria (5 consecutive days when the daily T_{max} exceeds the statistical 95th percentile of the climatological T_{max} series) including mean and max durations (day) and cumulative intensity (°C × day), and percentages of impacted area in 10 sub-regions from 1981 to 2019.

HWEs (Year/Week)	Start date	Mean duration (day)	Max. duration (day)	Mean intensity (°C)	Max. intensity (°C)	Cumulative intensity (°C × day)	Impacted area (%)
C1							
1985/W46	11 Nov.	7.8 ± 1.41	10	8.8 ± 1.54	10.0	68.6 ± 14.84	49.7
1992/W53	28 Dec.	6.1 ± 0.36	7	7.6 ± 1.13	8.6	45.9 ± 6.51	50.7
2016/W34	22 Aug.	5.8 ± 0.56	8	9.9 ± 1.66	11.1	57.2 ± 10.16	46.4
C2							
1981/W44	26 Oct.	6.3 ± 0.74	8	6.2 ± 1.07	7.4	38.4 ± 3.94	50.9
1983/W12	21 Mar.	6.8 ± 13.31	12	5.1 ± 0.61	6.0	35.0 ± 8.73	30.3
1985/W46	11 Nov.	5.9 ± 1.06	9	7.2 ± 1.36	7.9	42.9 ± 12.54	38.6
1987/W53	28 Dec.	5.4 ± 0.75	8	5.4 ± 0.61	6.4	29.3 ± 4.93	51.1
1992/W10	2 Mar.	5.7 ± 0.83	9	5.8 ± 0.48	6.7	32.9 ± 6.74	53.6
1997/W50	8 Dec.	5.5 ± 0.78	8	5.7 ± 0.76	6.5	31.5 ± 5.33	48.8
1998/W06	2 Feb.	6.9 ± 1.36	10	6.0 ± 0.53	7.1	41.0 ± 6.73	68.0
1998/W18	27 Arp.	5.1 ± 0.54	9	5.7 ± 0.72	6.2	29.2 ± 4.42	32.7
2003/W10	3 Mar.	5.6 ± 0.76	9	5.2 ± 0.31	5.8	28.9 ± 3.15	35.0
2012/W01	2 Jan.	5.9 ± 0.93	9	5.3 ± 0.57	6.3	31.2 ± 5.97	37.4
2015/W53	28 Dec.	8.3 ± 2.53	12	6.0 ± 0.82	7.1	48.2 ± 10.92	31.5

HWEs (Year/Week)	Start date	Mean duration (day)	Max. duration (day)	Mean intensity (°C)	Max. intensity (°C)	Cumulative intensity (°C × day)	Impacted area (%)
2016/W43	24 Oct.	6.6 ± 1.69	11	6.1 ± 0.64	6.9	40.1 ± 11.44	33.1
2016/W48	28 Nov.	6.9 ± 1.14	9	5.9 ± 0.73	7.1	40.7 ± 9.85	31.6
2018/W45	5 Nov.	7.5 ± 2.01	12	6.3 ± 1.26	7.7	46.5 ± 12.04	33.6
2019/W18	29 Apr.	7.3 ± 2.4	23	5.1 ± 0.89	5.7	36.3 ± 9.27	30.3
C3							
1983/W07	14 Feb.	7.8 ± 1.05	11	7.3 ± 0.54	8.6	56.9 ± 10.21	61.2
1984/W07	13 Feb.	5.5 ± 0.77	9	7.1 ± 0.71	7.8	39.4 ± 6.30	46.8
1987/W10	2 Mar.	6.9 ± 1.15	9	7.0 ± 0.67	7.8	48.5 ± 9.11	35.0
1987/W14	30 Mar.	11.6 ± 1.44	13	5.9 ± 0.78	7.0	68.4 ± 13.71	54.8
1992/W08	17 Feb.	8.6 ± 4.56	18	6.9 ± 0.75	8.2	58.7 ± 28.86	36.2
1992/W09	24 Feb.	8.7 ± 4.51	17	7.3 ± 0.54	8.3	61.7 ± 29.24	40.6
1992/W10	2 Mar.	6.2 ± 0.93	10	6.9 ± 0.54	7.8	42.2 ± 6.38	61.7
1994/W50	12 Dec.	7.0 ± 1.72	11	5.6 ± 0.6	6.6	39.7 ± 12.46	56.7
1995/W04	23 Jan.	6.1 ± 1.04	9	7.2 ± 0.67	8.0	43.9 ± 9.81	44.0
1995/W16	17 Apr.	9.0 ± 1.49	12	5.1 ± 0.73	6.2	45.7 ± 7.74	40.3
1995/W45	6 Nov.	5.4 ± 0.67	7	5.1 ± 0.43	5.8	27.4 ± 3.73	46.7
1998/W05	26 Jan.	9.4 ± 2.01	14	7.0 ± 0.50	8.6	65.3 ± 13.46	34.2
2003/W03	13 Jan.	5.2 ± 0.38	7	7.1 ± 0.92	8.2	36.4 ± 5.02	49.2
2013/W11	11 Mar.	7.9 ± 2.02	13	5.6 ± 0.37	6.5	44.5 ± 11.25	33.1

HWEs (Year/Week)	Start date	Mean duration (day)	Max. duration (day)	Mean intensity (°C)	Max. intensity (°C)	Cumulative intensity (°C × day)	Impacted area (%)
2015/W46	9 Nov.	7.7 ± 2.40	12	5.7 ± 0.82	6.5	43.5 ± 13.01	61.2
2016/W01	4 Jan.	5.6 ± 0.49	7	7.1 ± 0.89	8.9	40.1 ± 7.05	38.0
2016/W16	18 Apr.	5.7 ± 1.78	17	3.6 ± 0.30	4.2	20.4 ± 6.00	32.2
2018/W46	12 Nov.	7.4 ± 1.42	11	5.0 ± 0.31	6.0	37.1 ± 6.70	58.3
2019/W04	21 Jan.	5.6 ± 1.03	11	6.5 ± 0.41	7.5	36.3 ± 6.23	39.6
2019/W09	25 Feb.	7.4 ± 5.36	84	6.7 ± 0.47	7.7	49.1 ± 26.97	48.3
2019/W11	11 Mar.	11.5 ± 3.75	26	6.4 ± 0.37	8.1	73.4 ± 21.34	42.8
2019/W14	1 Apr.	9.3 ± 10.66	55	4.8 ± 0.49	5.7	43.8 ± 45.86	36.1
2019/W16	15 Apr.	17.4 ± 12.99	40	4.0 ± 0.35	5.0	67.6 ± 49.93	31.1
2019/W17	22 Apr.	13.7 ± 6.96	33	3.8 ± 0.36	4.8	50.8 ± 24.53	30.1
C4							
1981/W45	2 Nov.	6.1 ± 0.50	7	7.5 ± 0.50	8.5	46.3 ± 5.78	32.0
1992/W11	9 Mar.	6.9 ± 1.14	12	6.0 ± 0.75	7.2	41.8 ± 9.28	34.2
2003/W40	29 Sep.	5.2 ± 0.41	7	7.2 ± 0.63	7.9	37.6 ± 3.85	30.6
2015/W40	28 Sep.	9.5 ± 2.04	12	8.1 ± 0.72	9.2	76.0 ± 16.42	43.9
2015/W45	2 Nov.	7.0 ± 1.15	9	8.5 ± 0.60	10.7	59.0 ± 9.68	42.3
2016/W43	24 Oct.	6.9 ± 1.91	11	7.9 ± 0.63	9.5	54.4 ± 15.38	41.7
2017/W44	30 Oct.	6.0 ± 0.74	8	7.1 ± 0.58	8.6	42.3 ± 6.75	31.0
2018/W50	10 Dec.	10.5 ± 4.84	17	6.2 ± 0.71	8.3	65.3 ± 31.84	32.6

HWEs (Year/Week)	Start date	Mean duration (day)	Max. duration (day)	Mean intensity (°C)	Max. intensity (°C)	Cumulative intensity (°C × day)	Impacted area (%)
2019/W42	14 Oct.	7.9 ± 3.51	14	8.5 ± 1.12	10.0	64.9 ± 24.44	43.5
C5							
1982/W12	22 Mar.	5.9 ± 0.98	9	4.3 ± 0.78	4.9	25.3 ± 7.73	31.7
1994/W46	14 Nov.	6.0 ± 0.64	9	6.9 ± 1.07	8.1	41.3 ± 7.23	68.2
1994/W50	12 Dec.	7.4 ± 1.14	10	5.8 ± 0.98	7.2	43.6 ± 10.38	34.7
1994/W51	19 Dec.	7.1 ± 1.54	18	5.5 ± 0.77	6.5	38.6 ± 8.65	31.3
1995/W16	17 Apr.	9.0 ± 1.81	14	5.6 ± 0.92	6.9	49.9 ± 9.93	45.7
2005/W10	7 Mar.	5.0 ± 0.09	6	5.2 ± 1.15	5.8	25.9 ± 5.72	67.2
2016/W07	15 Feb.	7.2 ± 1.98	12	4.8 ± 1.06	6.7	34.6 ± 12.67	32.8
C6							
1983/W07	14 Feb.	9.6 ± 3.50	20	4.8 ± 0.46	6.0	46.1 ± 17.61	33.3
1987/W14	30 Mar.	10.1 ± 2.98	23	4.8 ± 0.65	5.7	49.4 ± 16.70	34.3
1987/W47	16 Nov.	6.0 ± 0.61	11	6.4 ± 0.43	7.9	38.5 ± 3.89	39.4
1992/W08	17 Feb.	8.4 ± 3.65	25	6.5 ± 1.48	9.0	55.2 ± 25.26	32.2
1992/W10	2 Mar.	6.3 ± 1.12	14	4.8 ± 0.75	6.0	30.5 ± 7.79	38.5
1994/W12	21 Mar.	7.2 ± 1.64	12	4.4 ± 0.37	5.5	31.8 ± 6.97	38.6
1994/W46	14 Nov.	6.0 ± 0.89	11	7.1 ± 1.20	8.4	42.3 ± 7.08	42.9
1994/W50	12 Dec.	7.9 ± 2.54	49	5.8 ± 0.75	7.0	46.0 ± 18.55	47.3
1995/W11	13 Mar.	5.7 ± 0.69	13	5.0 ± 0.72	5.9	28.4 ± 5.86	42.3

HWEs (Year/Week)	Start date	Mean duration (day)	Max. duration (day)	Mean intensity (°C)	Max. intensity (°C)	Cumulative intensity (°C × day)	Impacted area (%)
2005/W10	7 Mar.	5.0 ± 0.10	6	6.7 ± 1.54	7.8	33.8 ± 7.67	36.9
2015/W46	9 Nov.	9.3 ± 5.31	21	6.2 ± 0.46	7.2	58.0 ± 34.74	44.8
2019/W09	25 Feb.	9.6 ± 5.25	42	5.0 ± 0.58	6.0	48.2 ± 28.09	36.7
2019/W11	11 Mar.	23.7 ± 7.97	74	5.8 ± 0.58	7.5	136.2 ± 42.01	37.9
C7							
1987/W14	30 Mar.	10.1 ± 1.93	17	5.6 ± 0.72	6.6	57.1 ± 15.77	69.8
1992/W08	17 Feb.	8.2 ± 2.53	20	7.0 ± 1.18	8.9	57.9 ± 19.51	46.8
1992/W49	30 Nov.	5.3 ± 0.45	6	6.2 ± 0.75	7.0	32.7 ± 3.84	31.5
1994/W50	12 Dec.	7.9 ± 1.72	15	6.2 ± 0.37	7.1	49.0 ± 11.49	55.2
1995/W04	23 Jan.	7.7 ± 1.45	10	7.2 ± 0.67	8.4	56.1 ± 13.33	47.0
1995/W11	13 Mar.	5.6 ± 0.53	7	6.1 ± 0.46	7.0	34.1 ± 3.60	49.3
1995/W45	6 Nov.	5.4 ± 0.62	8	5.3 ± 0.27	5.9	28.7 ± 3.37	42.5
1997/W50	8 Dec.	5.5 ± 0.50	6	6.2 ± 0.46	7.0	34.4 ± 4.23	33.2
2015/W11	9 Mar.	10.1 ± 2.58	15	6.4 ± 0.43	7.4	64.9 ± 17.46	30.3
2015/W46	9 Nov.	7.8 ± 3.77	21	6.3 ± 0.85	7.2	48.6 ± 20.77	68.4
2019/W11	11 Mar.	22.6 ± 8.99	71	6.4 ± 0.50	8.4	143.3 ± 47.40	30.3
C8							
1987/W14	30 Mar.	8.1 ± 1.85	13	5.9 ± 0.53	6.9	48.3 ± 14.21	36.4
1992/W49	30 Nov.	5.2 ± 0.59	7	7.6 ± 1.18	8.6	39.5 ± 5.87	42.9

33

HWEs (Year/Week)	Start date	Mean duration (day)	Max. duration (day)	Mean intensity (°C)	Max. intensity (°C)	Cumulative intensity (°C × day)	Impacted area (%)
2015/W40	28 Sep.	9.2 ± 1.92	11	7.3 ± 0.47	8.4	66.7 ± 12.08	34.2
2019/W48	25 Nov.	6.5 ± 1.02	9	7.3 ± 0.74	8.6	46.9 ± 9.02	50.1
C9							
1981/W45	2 Nov.	5.6 ± 0.6	7	6.4 ± 0.65	7.5	35.9 ± 5.70	32.6
1983/W01	3 Jan.	5.0 ± 0.19	8	7.0 ± 0.50	8.3	35.1 ± 2.66	30.0
1984/W07	13 Feb.	6.7 ± 1.03	9	6.8 ± 0.49	7.8	45.4 ± 5.26	37.0
1987/W14	30 Mar.	10.3 ± 1.72	13	6.5 ± 0.39	7.6	66.5 ± 11.62	60.0
1992/W10	2 Mar.	5.6 ± 0.73	9	6.0 ± 0.37	6.7	33.9 ± 5.21	39.2
1992/W49	30 Nov.	5.3 ± 0.52	7	6.7 ± 0.92	7.8	35.8 ± 4.90	41.5
1994/W50	12 Dec.	7.8 ± 1.53	10	5.7 ± 0.37	6.4	45.1 ± 9.84	49.4
1995/W04	23 Jan.	5.5 ± 0.50	7	7.1 ± 0.58	8.1	38.8 ± 3.99	50.9
1995/W40	2 Oct.	6.2 ± 0.75	8	6.9 ± 0.98	8.3	42.9 ± 7.13	30.6
1995/W45	6 Nov.	5.8 ± 1.05	9	5.9 ± 0.61	6.7	34.2 ± 6.42	44.2
2003/W03	13 Jan.	5.5 ± 0.51	7	7.0 ± 0.68	8.3	38.9 ± 4.71	41.9
2003/W40	29 Sep.	6.2 ± 2.25	12	5.8 ± 0.76	6.5	35.7 ± 10.80	50.6
2015/W40	28 Sep.	9.9 ± 2.06	12	6.6 ± 0.88	7.6	64.1 ± 10.64	38.6
2015/W46	9 Nov.	5.8 ± 0.59	7	7.7 ± 1.13	8.7	44.5 ± 8.05	38.7
2015/W51	14 Dec.	6.3 ± 1.47	11	6.0 ± 0.42	7.1	37.8 ± 9.94	36.9
2016/W01	4 Jan.	5.9 ± 0.53	7	7.2 ± 0.45	9.5	42.5 ± 4.54	41.8

HWEs (Year/Week)	Start date	Mean duration (day)	Max. duration (day)	Mean intensity (°C)	Max. intensity (°C)	Cumulative intensity (°C × day)	Impacted area (%)
2016/W43	24 Oct.	7.8 ± 1.67	11	7.1 ± 0.78	8.4	55.2 ± 13.52	51.7
2016/W48	28 Nov.	6.8 ± 0.89	9	6.7 ± 0.73	8.2	46.0 ± 9.33	47.0
2018/W46	12 Nov.	7.0 ± 0.98	10	6.0 ± 0.82	6.7	41.8 ± 8.27	33.3
2019/W09	25 Feb.	6.4 ± 1.27	28	6.8 ± 0.50	7.8	43.5 ± 9.10	40.1
2019/W48	25 Nov.	6.3 ± 0.99	9	6.7 ± 0.72	7.7	42.1 ± 8.23	47.6
C10							
2016/W34	22 Aug.	5.2 ± 0.40	7	11.7 ± 1.18	13.1	60.5 ± 5.24	64.1

4.4. Lag regression models

For better graphic representation and elaboration, lag regression models are displayed and clarified with the cases of more than 40% area-covered HWEs. In C1 and C2 sub-regions, the subtropical dry climate with the coastal deserts dominate. These two regions are largely influenced by the South-Atlantic subtropical high, which is stable and dry in front of the coast with upwelling cold deep water from the Benguela Current. The sea breeze, mountain wind and South-Hemispheric Westerlies (in austral winter) work morphogenetic, which creates wind blown depression in the southern Namib Sand Sea with sand dunes in the central (Buckle, 1996; Endlicher, 2000). The steep fringe of the Great Escarpment extents to 100 km far from the coasts and exhibits large gaps. With the sea breeze the moist-cold Atlantic (Southeast trade wind) air masses are transported eastward. In austral summer, when the two subtropical highs move polewards, the possible moist tropical air masses from the East arrive in the coastal steppe fore-Namib and bring weak rainfalls (Endlicher, 2000). The C1 sub-region shows the coastal areas from 15 to 33° S and around 100-500 km landwards from the North to the South is the C2 sub-region (Figure 4-5, 4-6). Both sub-regions present the same spatial variation of relationships of the weekly rainfall amounts and the weekly maximum temperature. The slopes for lag = 0-week are positive from 15.5 to 23.5° S in C1 sub-region and from 15.5 to 17° S in C2 sub-region, and the slope values are negative from 23.5 (17) to 35(31)° S in C1 (C2) sub-regions, which shows the increase / decrease of rainfalls during the heat waves. There are converse values of the slope in lag = 1-week and 2-week, which indicates 1 to 2 weeks after the heat waves, there are more rainfalls in the southern part of these two sub-regions (C1 with significant relationships) (Appendix D, Figure D-1, D-2; Appendix E). The regression models of lag = 0~1-weeks describe similar spatial patterns, whilst the regression models of lag = 0~2 weeks show slight differences in the marginal areas, for instance, the southern side of C1 (27.5-34° S, 18-22 ° E) and the western side of C2 (21-26° S, 15-16.5° E) sub-regions (Figure 4-5, 4-6).

The C3 sub-region is located mostly in subtropical dry climate and marginally in the wet-dry torrid zone. There is slightly more rainfall as compared with C1 and C2 sub-region. In Botswana with the Kalahari Basin and the highlands of middle Namibia (more than 1000 m a.s.l.), the trade winds and the mid-tropospheric Botswana High describe the summer weather (Endlicher, 2000; Driver and

Reason, 2017). In the 2015 heat wave event (61.2 % area), most parts exhibit negative slopes in the single regression models of lag = 0-week, 1-week, and 2-week (Figure 4-7; Appendix D, Figure D-3). With the increasing lags the marginal spaces shift to positive slopes, which is the extended part of C2 sub-region. Only in the 2-week and 0~2 weeks lag regression models the middle of the C3 sub-region (19-22.5° S, 17-22° E, 1500-1800 m a.s.l.) is supposed to have more rainfall amounts (insignificant relationships). In the 2003 and 1994 heat waves (49.2 and 56.7 % area), the slopes of lag = 1-week and 2-week in the lag regression models 0~1 weeks and 0~2 weeks exhibits different spatial patterns (Appendix D, Figure D-3; Appendix E). Most of the western part showing positive slopes but smaller as well as scattered areas with significance.

Most of the C4 sub-region belongs to the always moist subtropical climate of southern and southeastern coasts with maximum summer rains (Endlicher, 2000). Tropical and subtropical disturbances combined with more or less unstable layered air masses from the Northeast to the Southeast are responsible for the precipitation. In summer, the subtropical inversion is weakly formed and convectively softened by powerful irradiation (insolation). In winter, there is disturbance-free high pressure weather on the coasts and high-humidity weather triggered by tropical moist Indian air masses in the highlands (Buckle, 1996; Endlicher, 2000). The lag regression models in different years show slight spatial patterns in this southeastern region in South Africa (Figure 4-8; Appendix D, Figure D-4; Appendix E). Nevertheless, all agree with the result that there are few areas with significant relationships. For example, the slopes of lag = 0-week of the regression models referring to the heat waves in 2015 and 2016 are negative and the slopes of lag =1-week and 2-week are positive, which may imply after the occurrences of heat wave event, there are more intense weekly rainfalls. In 2019, most areas present negative slopes with lag = 0~1 weeks and lag = 0~2 weeks as well, which shows dissimilar patterns of rainfalls affected by high temperatures (Appendix E).

The wet-dry torrid zone dominates C5, C6 and C7 sub-regions, which is the transition zone of the continent (Endlicher, 2000). Angola highlands, Zambia, Zimbabwe in the East and Namibia in the West in the wet-dry outer tropic is influenced by the diverted Atlantic monsoon with moist Congo air masses in the North in summer-half year (Buckle, 1996; Endlicher, 2000). The position of southern Zimbabwe with the Lowveld and the Highveld is in the summer moist subtropic. In spring and summer, the northeast part of these sub-regions are also affected by the Intertropical

Convergence Zone (ITCZ). Together with the convergence of the Congo Air Boundary in the tropics, in-situ convection leads to precipitation-generating phenomenon overall (Endlicher, 2000; Howard and Washington, 2019). The C5 sub-region is the most northern part of the whole research area. The most severe heat waves detected in the C5 sub-region are in 2005 (week 10, 7-13 Mar., 67.2 % impacted area), 1994 (week 46, 14-20 Nov., 68.2 % impacted area) and 1995 (week 16, 17-23 Apr., 45.7 % impacted area). Most of the areas show negative slopes with 0- and 1-week lags of the HWEs, then turn into positive slopes with 2-week lag, which suggests that the rainfalls increase two weeks later under the extreme high temperatures (Figure 4-9; Appendix D, Figure D-5; Appendix E). Notwithstanding the high relationships, the impacted areas are with low significance. During the HWEs in 2015 (week 46, 9-15 Nov.), the high adjusted R-squared values with significance show negative effects on rainfalls in C6 and C7 sub-regions, and shift to positive effects in eastern part of the two sub-regions one week later, whilst there are positive effects in most of the two whole sub-regions in 1-week-lag period in 1994 (week 50, 12-18 Dec.) and 1995 (week 11, 13-19 Mar.) (Figure 4-10, 4-11; Appendix D, Figure D-6, D-7; Appendix E). The effect of high temperatures on rainfalls shows spatial variation with 2-week-lag, but most of the cases reach an agreement of negative effects on the area between 1000 and 1800 m a.s.l. near the Kalahari Basin (18-20° S, 20-25° E).

The C8 and C9 sub-regions in east of the Great Escarpment cross over the summer rain subtropical climate of the central highlands and the wet-dry torrid zone inside the continent (Endlicher, 2000). The convective structure of tropical summer rain brings about strong regional differences in precipitations (e.g. drought- and flooding regions can be very close to each other). The maritime moist-saturated southeastern trade winds make central and southern Mozambique hot and sultry (C8 sub-region) (Endlicher, 2000). With the exclusion of the heat wave event in 1987 (week 14, 30 Mar.-5 Apr.), all the regression models in 1992 (week 49, 2-8 Dec.) and 2019 (week 48, 25 Nov.-1 Dec.) with 0- to 2-week lags in C8 sub-region present negative slopes (reduced rainfalls) during the occurrence of heat waves (with significance) and 1 or 2 weeks later with positive slopes (enhanced rainfalls) (but less significant) (Figure 4-12; Appendix D, Figure D-8; Appendix E). Botswana with the Kalahari and the Okavango Basins in C9 sub-region are influenced by trade winds but at the same time influenced by the subtropical high, thus there are precipitation decreases in the southern central area (Endlicher, 2000). Most of the northern C9 sub-region shows negative slopes in 0-

week-lag period and positive slopes in the southern part (29-33° S, 23.5-26.5° E, 1500-1800 m a.s.l.) (Figure 4-13). Even though the spatial patterns are considerably diverse in 1- and 2-week-lag periods, the areas with significant relationships exhibit positive slopes, which confirms the fact that larger amounts of the precipitation come up after the HWEs (Appendix D, Figure D-9; Appendix E).

C10 sub-region is located at the Southwest tip of the African continent, which lies in front of the Great Escarpment and behind another chain of mountains of the Western Cape land. The climate classification is winter rain subtropic. Because the strong chambered landscapes protect this region from the influence of the Atlantic anticyclone during the summer-half year. During this dry period, the southern and the southeastern trade winds are dominant and bring the foehn wall effect (Endlicher, 2000). Conversely, the northwestern wind in winter is linked with the passage of wandering cyclones, and its cold front windward of the Cape chains causes the relative productive precipitation. The Lows occur in the west wind drift and hit with their fronts on the continent, when the barrier effect of subtropical high reduces (Buckle, 1996; Endlicher, 2000). The only heat wave event detected in 2016 covered by 64.1 % area exhibits less significant relationships of weekly rainfalls and maximum temperature explained by lag regression models (Figure 4-14). Only in the western coastal area the regression models of 0-week and 2-week describe significant decrease and increase rainfalls, respectively (Appendix D, Figure D-10). In all 10 sub-regions, we can see that when the number of lag regression models increases, the areas with significant relationships of weekly precipitation and maximum temperature are smaller and more fragmented.

C1 1985/W46   **Impacted area: 49.7 %**
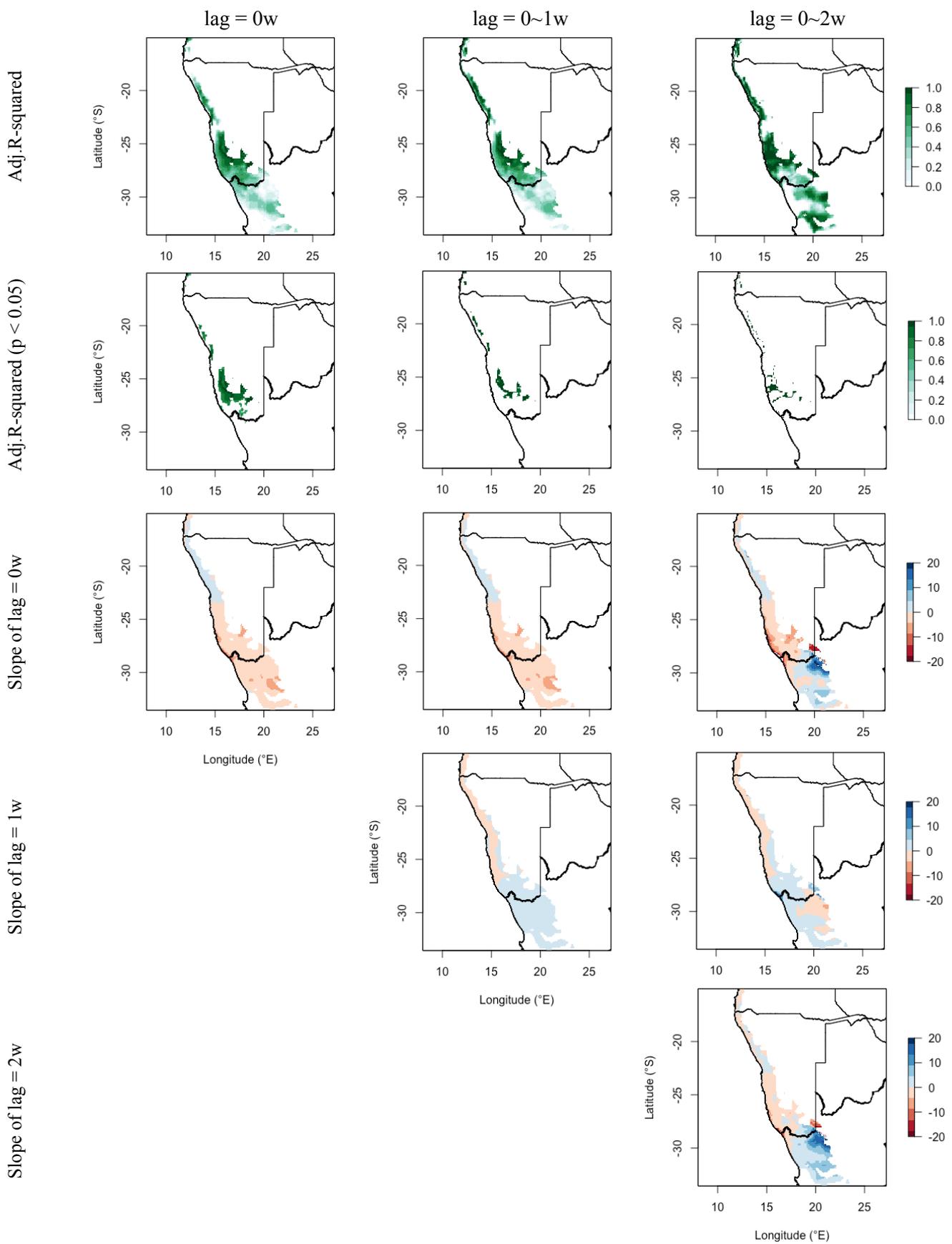
Figure 4-5. The overview results of lag regression models of 0, 0~1 and 0~2weeks in C1 sub-region.

C2 1987/W53   **Impacted area: 51.1 %**
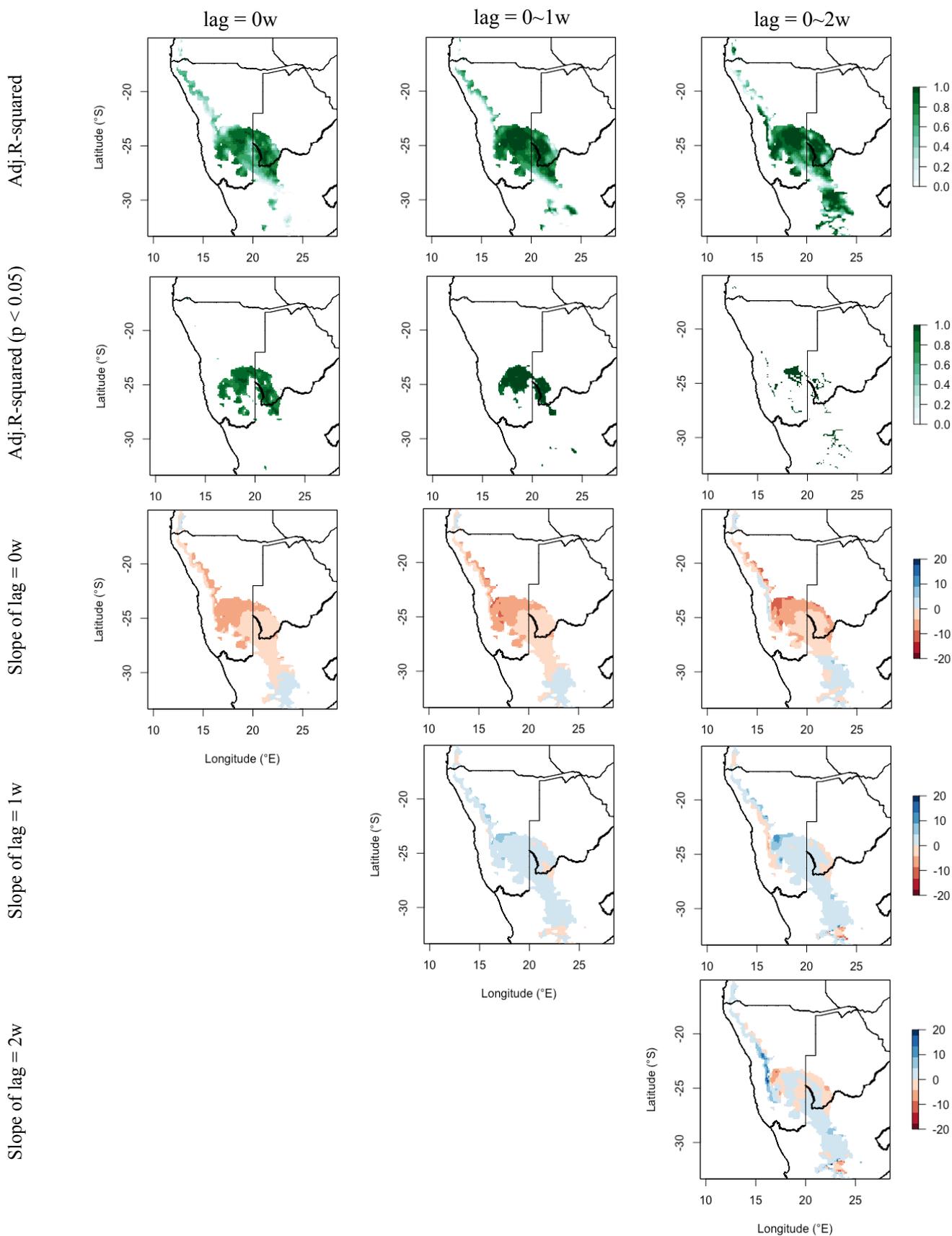
Figure 4-6. The overview results of lag regression models of 0, 0~1 and 0~2weeks in C2 sub-region.

C3 2015/W46   **Impacted area: 61.2 %**
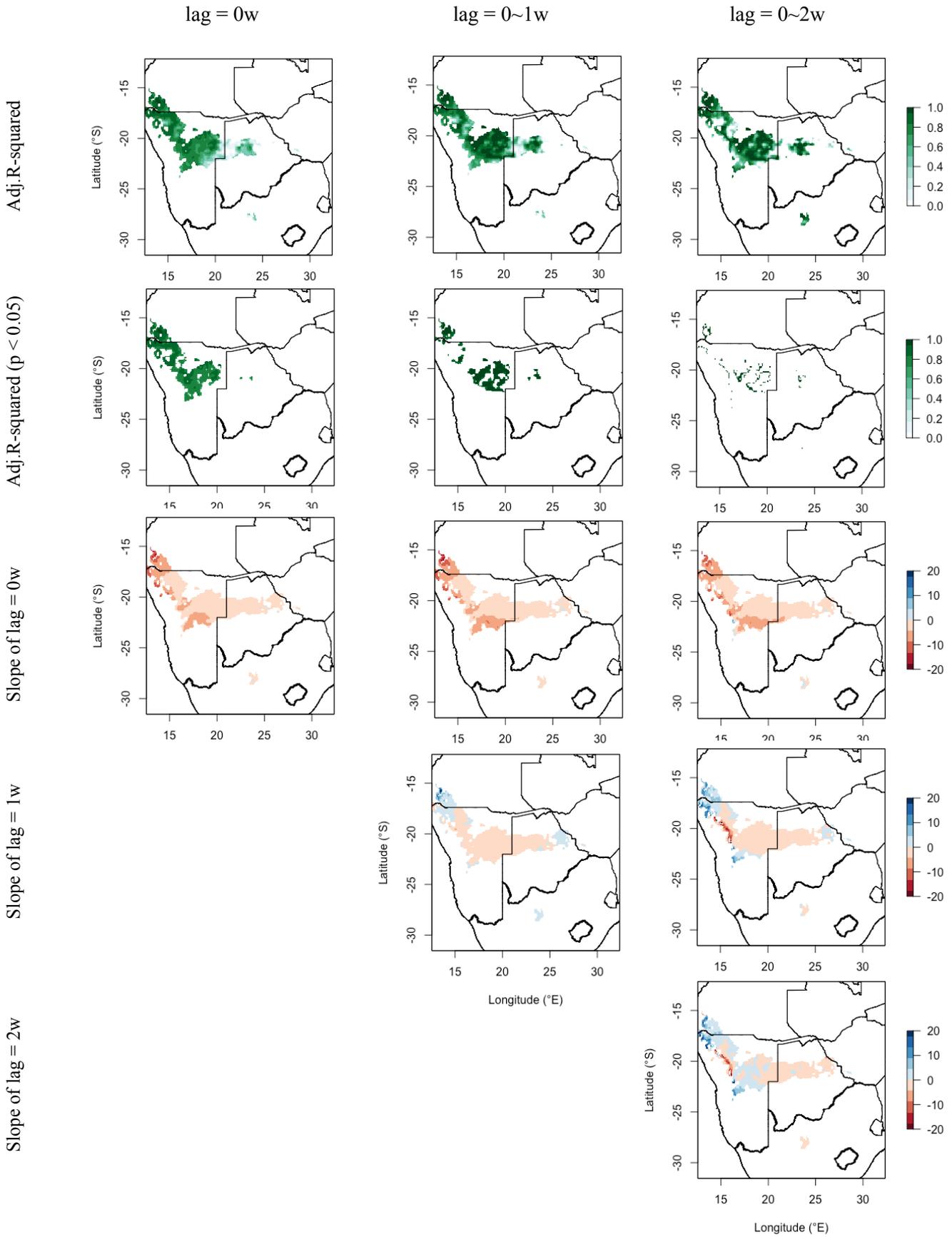
Figure 4-7. The overview results of lag regression models of 0, 0~1 and 0~2weeks in C3 sub-region.

C4 2016/W43   **Impacted area: 41.7 %**
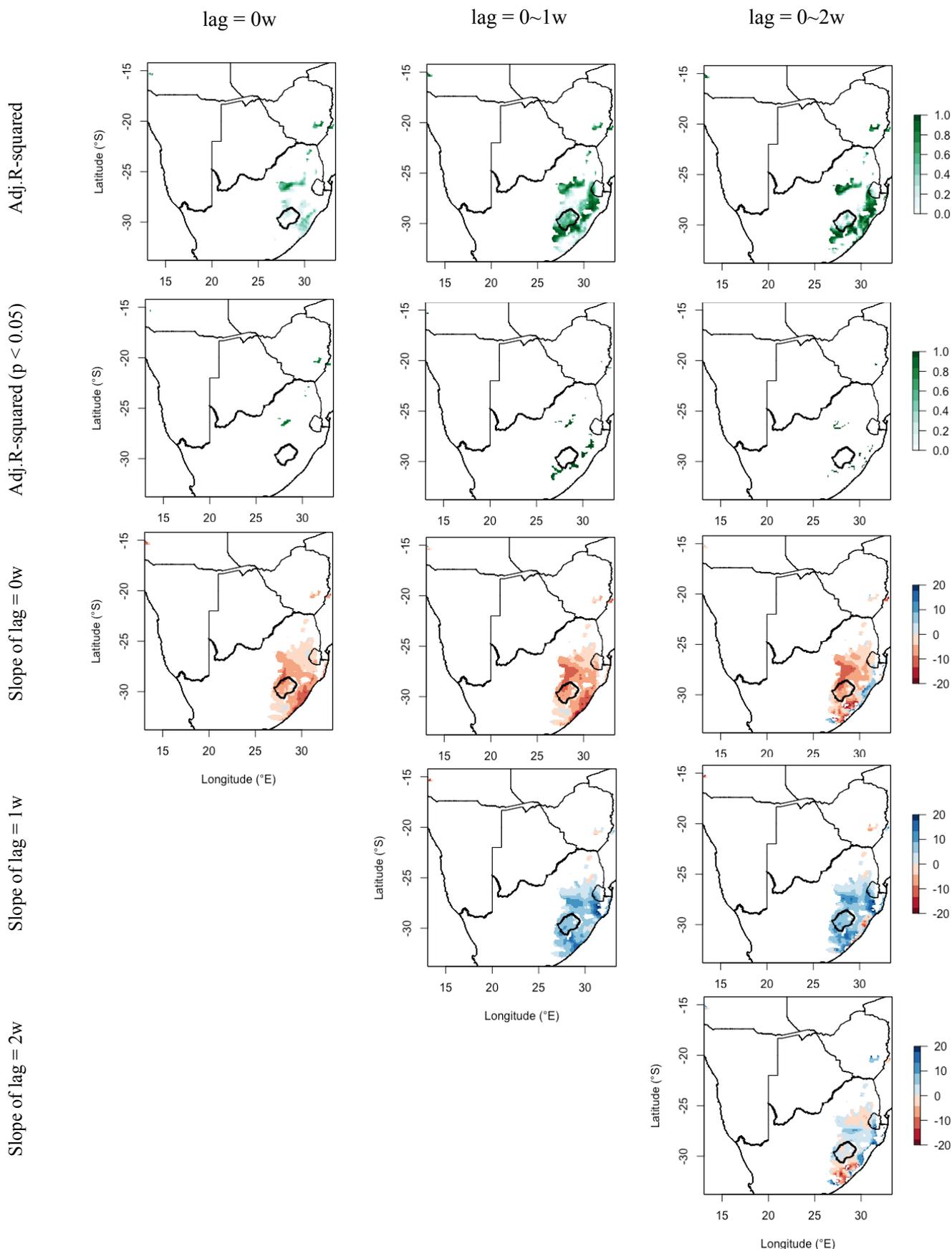
Figure 4-8. The overview results of lag regression models of 0, 0~1 and 0~2weeks in C4 sub-region.

43

C5 1994/W46   **Impacted area: 68.2 %**
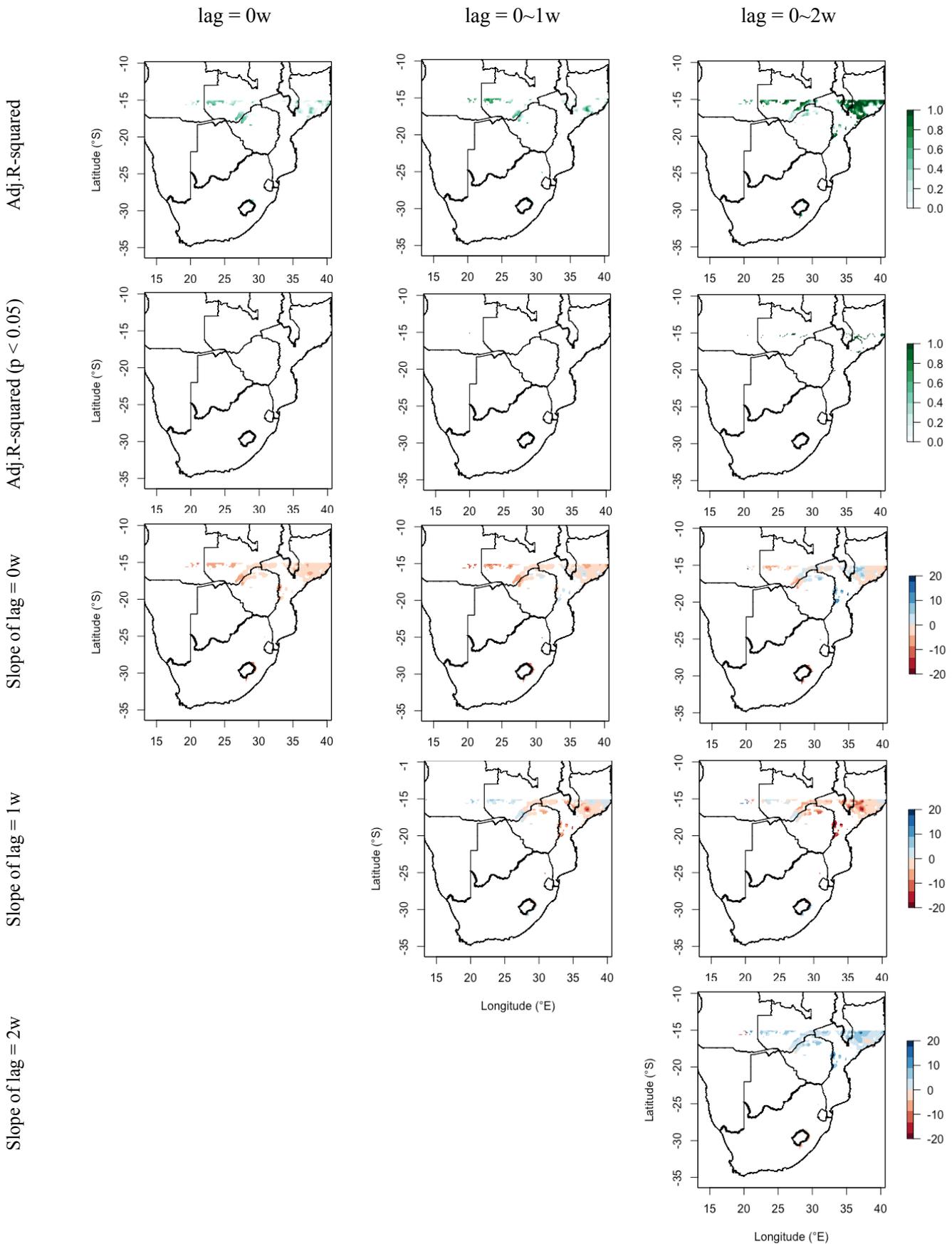
Figure 4-9. The overview results of lag regression models of 0, 0~1 and 0~2weeks in C5 sub-region.

C6 2015/W46   **Impacted area: 44.8 %**
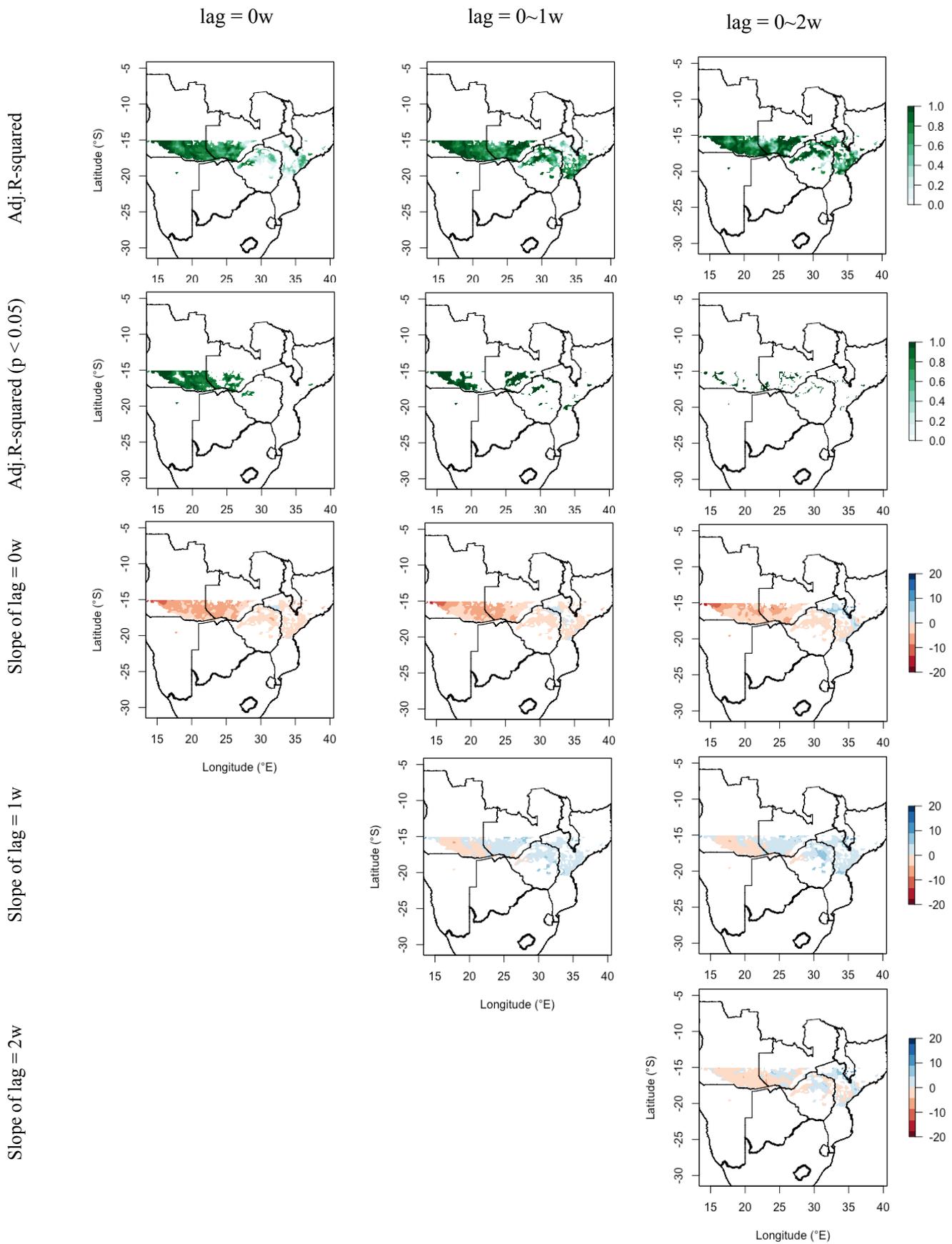
Figure 4-10. The overview results of lag regression models of 0, 0~1 and 0~2weeks in C6 sub-region.

C7 2015/W46   **Impacted area: 68.4 %**
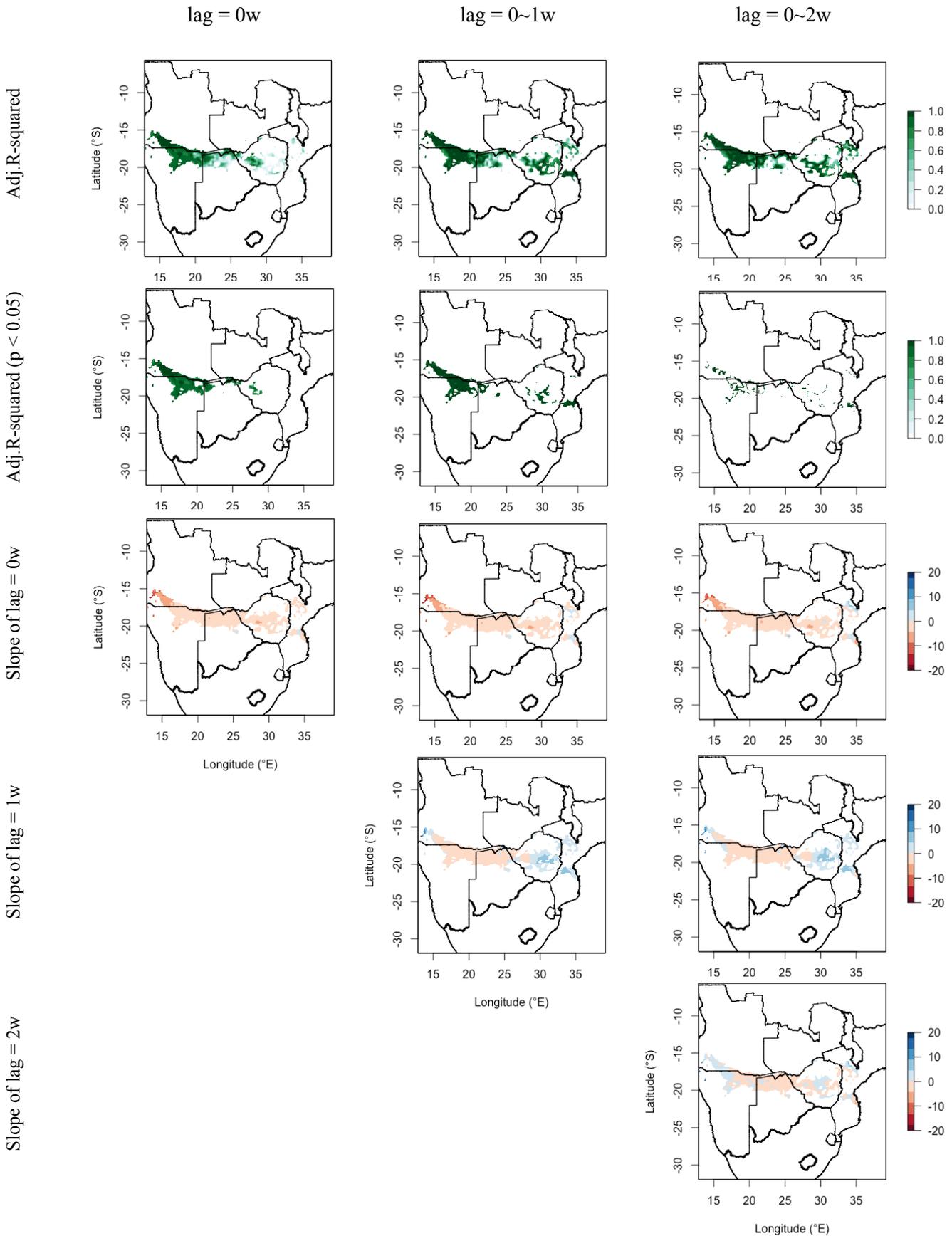
Figure 4-11. The overview results of lag regression models of 0, 0~1 and 0~2weeks in C7 sub-region.

C8 2019/W48   **Impacted area: 50.1 %**
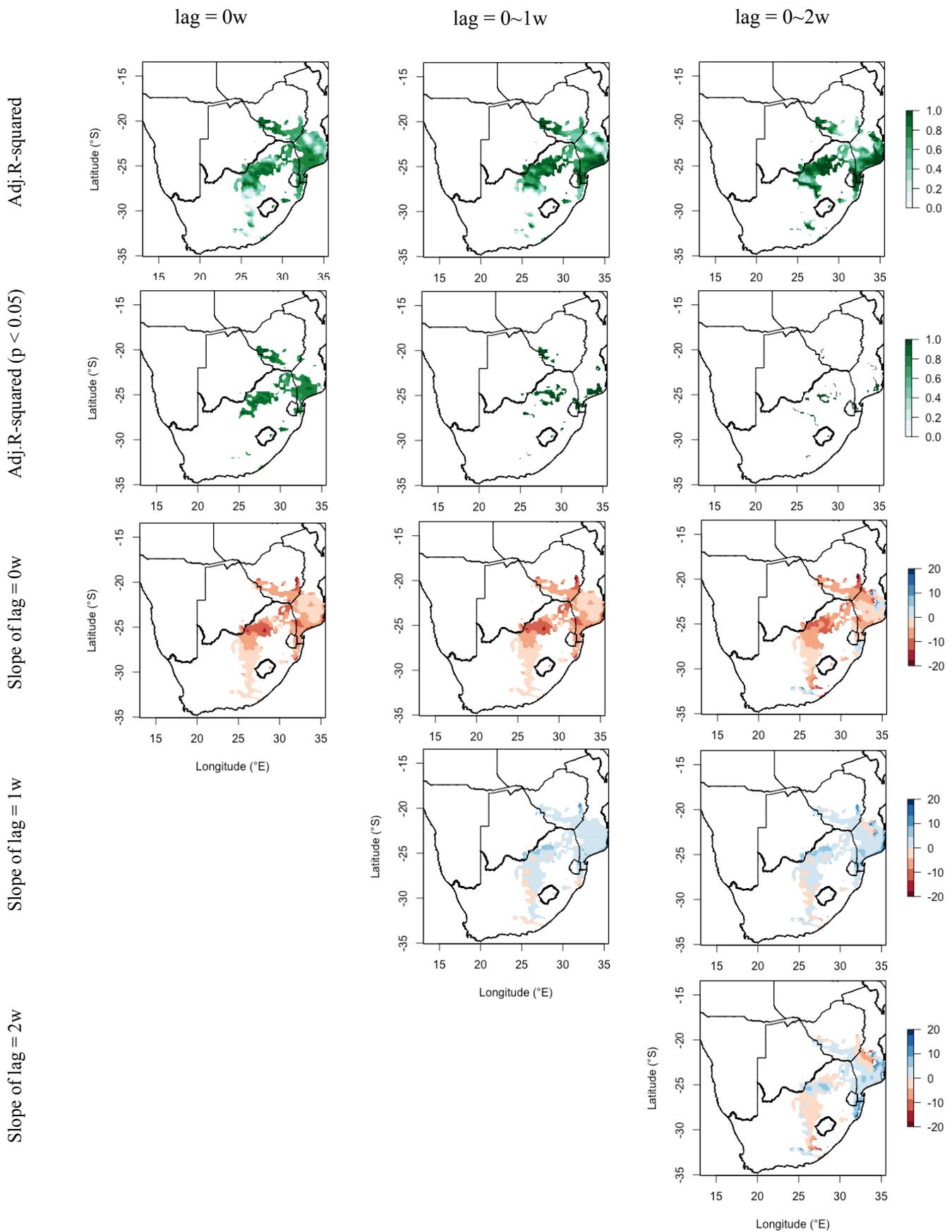
Figure 4-12. The overview results of lag regression models of 0, 0~1 and 0~2weeks in C8 sub-region.

C9 2016/W43   **Impacted area: 51.7 %**
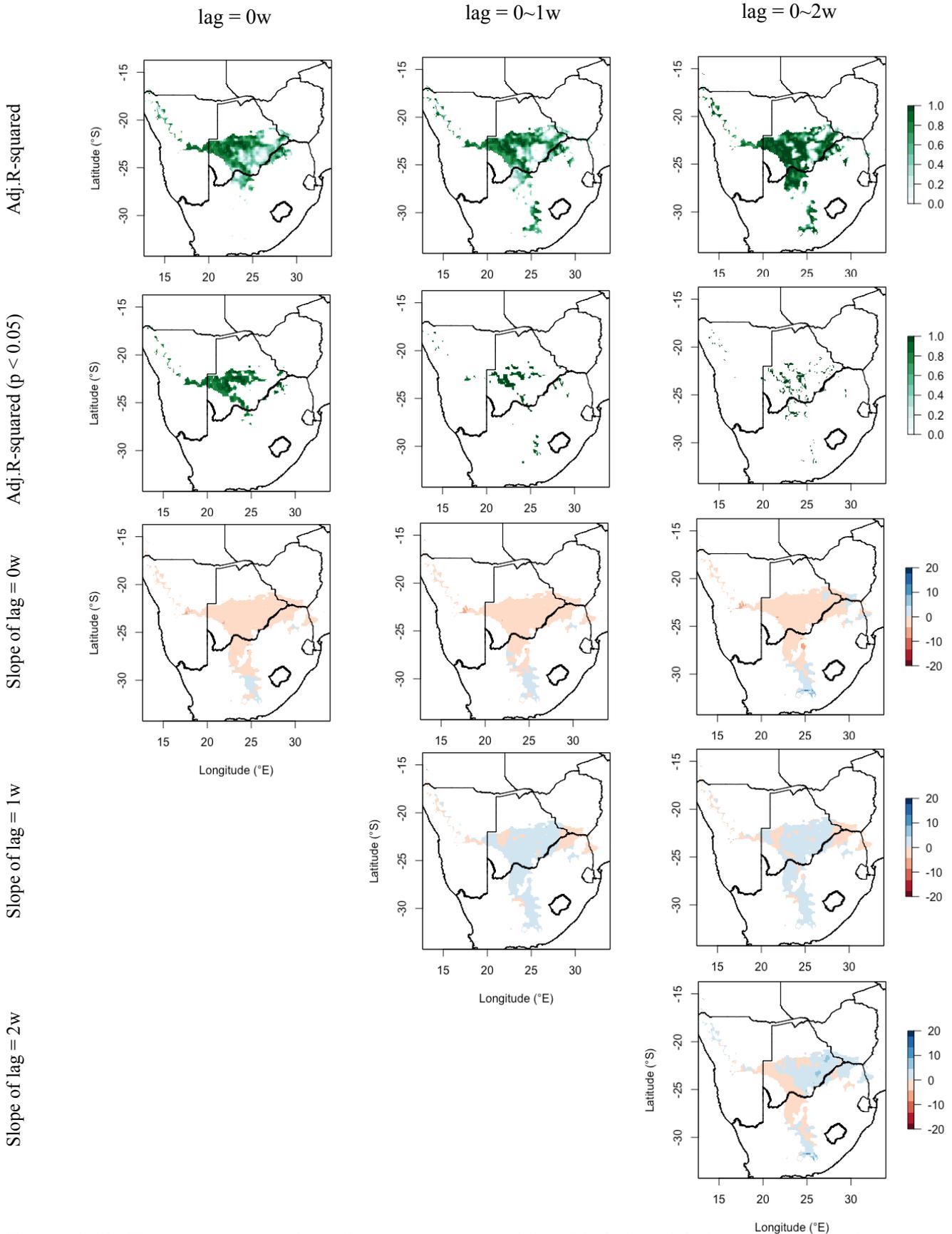
Figure 4-13. The overview results of lag regression models of 0, 0~1 and 0~2weeks in C9 sub-region.

C10 2016/W34   **Impacted area: 64.1 %**
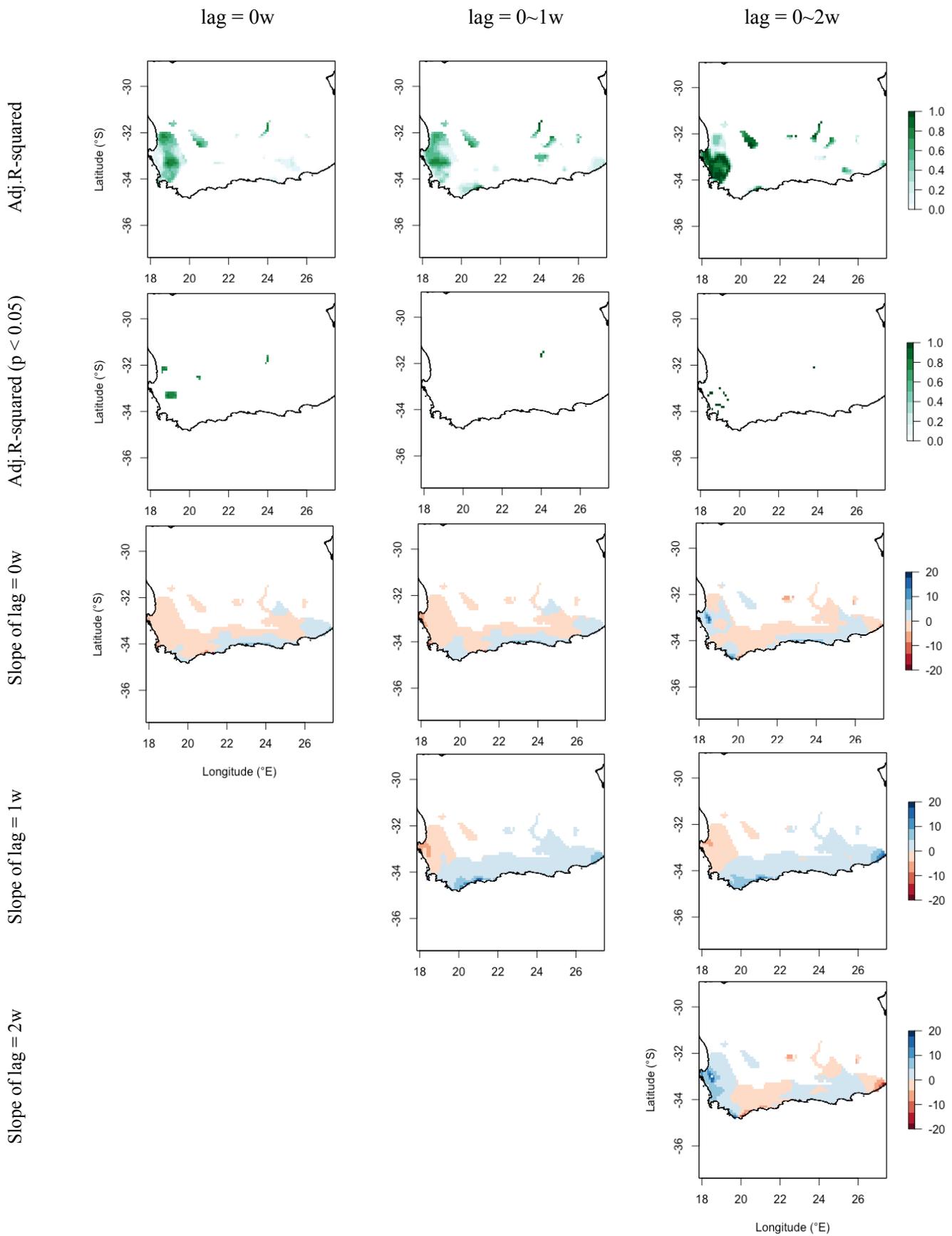
Figure 4-14. The overview results of lag regression models of 0, 0~1 and 0~2weeks in C10 sub-region.

5. Discussion

5.1. Regionalisation of precipitation patterns

It is essential to define homogeneous precipitation regions for hydrological and climate modelling under the high temporal and spatial variations of precipitation (Zhang et al., 2016). The 10 sub-regions determined by CLARA exhibit the clear outline map of regionalisation by the mean temporal rainfall patterns, which differs from the most presented annual precipitation or cumulative rainfall maps in Southern Africa, and thus is sensible for the further analysis related to inter-annual variability in precipitation. The k-means method for the cluster analysis is more common in most of the hydrological research and is recommended, because it can produce more stable cluster boundaries (Zhang et al., 2016). In this study, the general patterns analysed by k-means and k-medoids methods are similar, but the results of k-means method shows more obscure boundaries than that of k-medoids method regardless of the number of clusters. Moreover, it is more efficient to apply CLARA without losing important information when dealing with large data like our case (Kaufman and Rousseeuw, 1990; Roelofsen, 2018). The selection of k is more subjective in this study, since there are no consistent results from the three objective evaluations, also, the suggested numbers are too small to describe the precise inter-annual rainfall patterns in the whole Southern Africa with respect to the Köppen-Geiger climate classification and the spatial distribution of monthly rainfall totals displayed by using CRU and TRMM observed datasets (Dedekind et al., 2016).

5.2. Trends of precipitation and maximum temperature

Our results ascertaining the trends of annual and monthly precipitations are partly in agreement with most of the studies at both global and local scales, which shows the tropical regions close to the equator are wetter as well as the drying trends in subtropics with spatial heterogeneity (Kruger and Shongwe, 2004; Williams and Kniveton, 2011; James and Washington, 2013; Nicholson et al., 2018; Ilori and Ajayi, 2020; Onyutha, 2021). The coastal regions in Mozambique present reduced annual rainfall amounts in all months except for January (Appendix B, Figure B-1). However, from May to November there are large extents of negative trends in rainfall totals (ca. 0.1-4.5 mm reductions), especially in October with the most severe levels (Appendix B, Figure B-2), which supports the observed dry signals over Southern Africa (Faucherau et al., 2003; Williams and

50

Kniveton, 2011; James and Washington, 2013; Donat et al., 2016; Adisa et al., 2018; Nicholson et al., 2018). Excluding the adjacent regions of the Kalahari Basin and the Lunda Plateau, the annual maximum temperatures are higher in Southern Africa. From August to November, there are increases from 0.01 up to 0.15 °C over the whole study region. When compared to the warming signals in the Greater Horn, the change in degrees is smaller in Southern Africa (Camberlin, 2016). Generally, the increasing trends of monthly maximum temperatures and large spatial deviations of trends in precipitation are contradicting to the findings in East Africa and only consistent with the results of November-April in the future projections in Southern Africa (Li et al., 2015; Ongoma and Chen, 2017). Nevertheless, most of the trend analysis are conducted with longer time scale (e.g. at least 50 years), and the magnitudes of different periods might be able to be compared together in order to realise the real meaningful trends of different indices related to climatic extremes. For instance, a study using long-term monthly values of maximum and minimum temperatures finds out that the 1979-2015 warming is stronger than that of 1901 to 1940 over the African continent (Onyutha, 2021).

5.3. The characteristics of HWEs

Several studies reveal that Africa has experienced hotter, longer and more spatially extensive heat waves in this century and the projections in the future suggest unusual heat waves under present climate conditions will occur on a regular basis along with rising global mean temperatures (Perkins et al., 2012; Russo et al., 2014, 2016; Perkins, 2015; Barbier et al., 2018). Many monthly global products of temperature are supplied with the time back to the late 1800s or early 1900s, but the quality of daily data for many regions cannot be accessed to a comparable standard before 1950 (Perkins, 2015). In this study, the increasing tendencies of the magnitude, the duration and the extension are not found, which is possibly due to the relatively shorter period that does not involve the temperature data from 1950 to 1980. The entire ERA5-Land dataset from 1950 to present is expected to be available for public release later in 2021, which can be helpful for robust long-term heat wave research in the future (ECMWF). However, our results of the most severe heat waves since 1981 are in agreement with the findings from Russo et al. (2016) despite the different index used (e.g. Heat-wave magnitude index daily (HWMId)). For instance, the events in 1983 (March-May), 1987 (April-June), 1997-1998 (December-February), 2015 (March-May, July-September) and 2015-2016 (November-January) have all been found in both studies (Figure 5-1). Warm ENSO

events can also impact the heat waves through the longer persistence of drought conditions (Russo et al., 2016). Three strong ENSO events (1982-1983, 1997-1998, 2014-2016) and five smaller ones (2002-2003, 2004-2005, 2006-2007, 2009-2010, 2018-2019) occur from 1981 to 2019 (Australian Bureau of Meteorology; United States Climate Prediction Center). There are more than four sub-regions with detected heat waves (cover more than 30% area) during the 1982-1983, 1997-1998 and 2014-2016 ENSO episodes, with all 10 sub-region having HWEs in the last severe ENSO period (2014-2016). Their magnitude and duration depend neither on the regional maximum temperatures nor from the strength of El Niño, which corresponds to the statement that HWEs might occur more often in the future without ENSO events as well (Lyon, 2009; Russo et al., 2016). In South Africa, El Niño and La Niña events do not play a relevant role in the increasing temperatures observed (Kruger and Shongwe, 2004).

Moreover, Perkins et al. (2012) find out that trends of the thresholds regarding the calendar day 90th percentile based on a 15-day window for T_{max} and T_{min} are larger and exhibit more significance for warm spells over Northern America, Eurasia and Australia, which implies non-summer events are driving annual trends over these regions. There are sparse data as well as limited comprehensive records in Africa, therefore it is unknown if this kind of changing climate exists in Southern Africa, knowing this could help us to understand a better concept of the long-term development of HWEs. Though an increase in seasonal average temperature is thought to be the main driver for increased heat wave occurrence and duration (Perkins, 2015), the geographic variability of the observed and modelled heat wave intensities in 21st century are analysed and reported as large with significant uncertainties. At regional scale there are different changing patterns, especially the increases in heat wave intensity did not certainly follow the warming patterns (Ganguly et al., 2009). Thus, despite slightly increasing trends of T_{max} in most of the regions in Southern Africa (Figure 4-4), the intensity of HWEs dose not escalate in our study, which is consistent with the statement from Ganguly et al. (2009).

The study of summer temperature extremes in Europe indicated that the use of different variants of the percentile-based definition (e.g. 90th or 95th percentile of T_{max} or T_{min}) may affect the intensity and spatial extent of an extreme temperature event (Sulikowska and Wypych, 2020). Though according to the unpublished results but clear statements from Lyon (2009), the application of different thresholds didn't change the main results, it would be interesting to know based upon

different thresholds how far the intensity or the spatial extent of HWEs differ from each other. The number of days applied for a moving window is debated as well (Zhang et al., 2011; Perkins, 2015; Barbier et al., 2018; Sulikowska and Wypych, 2020). The percentile depended on a short moving window (e.g. 5-day moving window) might lead to a steady seasonal distribution over the occurrence, and consequently obtain a wide range of heat wave intensities from extreme heat waves to less extreme warm spells (Barbier et al., 2018). The magnitude of day-to-day variability is larger when a short moving window is applied (i.e. a 5-day v.s. a 15-day moving windows) (Sulikowska and Wypych, 2020). In our study, it is found that with shorter periods (11-day) of a moving window, slightly less HWEs are detected, though the extension of the same events (percentages of HWEs in each sub-region) didn't differ greatly (mean ± 0.4 %, max. ± 1.9 %).

The different indices for determining heat waves are discussed in order to clarify the possibility unrobustness (Lyon, 2009; Russo et al., 2014; Barbier et al., 2018). When most of the research define the heat waves at annual scale (e.g. maximum magnitude of the heatwaves in a year), our results focus on the individual events at weekly scale for the purpose of executing lag regression models connected with rainfall extremes, which might be the reason for the difficulty to examine the severity of HWEs and to compare comprehensively across regions and time. In the Sahel from 1950 to 2012, the synoptic intra-seasonal heat waves didn't tend to be more frequent and there was no strong climatological trend of heat wave occurrences (Barbier et al., 2018). The authors elucidate that climate and heat wave temperature trends do not necessarily increase at the same rate, because their T_{max} and T_{min} significantly increased by 1.6 and 2.6 °C, respectively. In South Africa, the annual absolute maximum temperatures do not reflect the general trends in the other indices (e.g. annual percentage of days when T_{max} > 90th percentile, annual percentage of days when T_{min} > 90th percentile), which indicates that individual extreme events can not always be associated with observed long-term climatic trends (Kruger and Sekele, 2013). In addition, our analysis excludes the HWEs that didn't occur during the rainfall periods, whereas Russo et al. (2016) mention heat waves could occur with a frequency of every season in Africa by the end of the century. More suitable indices and time scales for studying the frequency, magnitude and degree of severity of HWEs should be improved in Southern Africa in the future.
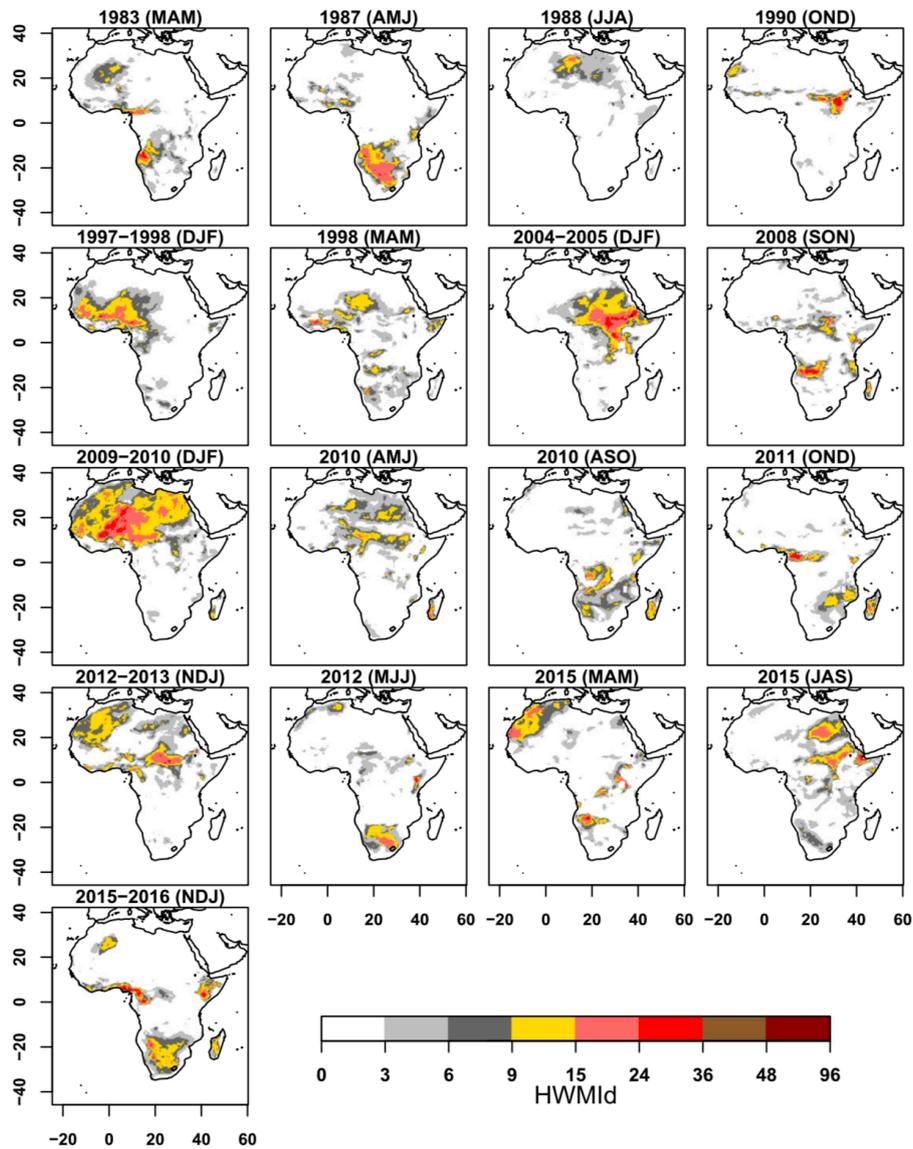
Figure 5-1. Spatial distribution of the Heat Wave Magnitude Index daily (HWMId) with ERA-I reanalysis, interpolated to the Africa cordex domain, of the most severe heat waves since 1979. The HWMId values represent the seasonal maximum magnitude at each grid point (Russo et al., 2016).

Fischer et al. (2012) examine the difference responses of heat stress in urban and rural regions in Europe and Africa. Since urbanisation can alter the partition of the surface energy budget by shifting the balance from latent to sensible heat fluxes, that is, urban areas reradiate the heat

absorbed and stored during the day at nighttime (Hulley et al., 2020). It is found that Southern Europe and tropical Africa experience the greatest increase in number of high-heat-stress nights. Moreover, urban areas are projected so see larger increases in heat stress (heat waves coupled with humidity) at nighttime (Fischer et al., 2012). Another research on heat waves in America (Southern California) from 1950 to 2020 also showed increasing trends in frequency, duration and intensity of HWEs in inland urban communities, which is assumed to be connected with nighttime warming and nighttime humidity (Hulley et al., 2020). Furthermore, they investigate the atmospheric circulation (i.e. the persistence and the location of high- and low-pressure systems) as well as the moisture source and found out that ocean warming trends and changes in the California current system lead to an anomalous moisture source off the coast. It is in agreement with the fact that the drivers of heat waves include synoptic systems (e.g. blocking high-pressure systems), soil moisture, land surface interactions and climate variability phenomena (e.g. ENSO) (Perkins, 2015). Because climate in Southern Africa is deeply influenced by the subtropical highs and the equatorial trough as well as the ocean currents, it would be a good direction to do further research for verifying interactions of these roles and their impacts on HWEs in terms of T_{max} or T_{min} in urban or rural regions.

5.4. Relationships between precipitations and HWEs

In the whole research region, during the weeks within the occurrence of HWEs, most of the areas are showing reduction of rainfalls. After one to two weeks, they are shifting to rainfall enhancement. Only the western coastal regions in Namibia, some parts of Mozambique and the coastal as well as central regions of Southern Africa display another pattern. Though the majority of the area does not present significant relationships between the rainfall and the temperature extremes, the high adjusted R-squared coefficients (> 0.8) can somehow illustrate the connection between them. As the heat wave impacted areas are wider (higher percentages), the area with significant relationships are also larger, except for C5 sub-region (the North-West boundary of the research are).

However, there are still spatial variations from HWEs happened in different years in all sub-regions, which might be explained by the moving impacted areas. Since the detection of extreme heat waves are agreed with more than 40-60 % area, different grid points are representative for each individual

event, and therefore when the lag regression models are applied in the whole sub-regions, there are less obvious consistent relationships between the precipitation and maximum temperature variables in the grid points where they themselves do not show the existences of heat waves.

5.4.1. The North and the East

Over Mozambique, Zimbabwe and Zambia, a stable stratification (layering) and a minor precipitation preparedness are created because the southeast trade wind is subject to the surface and flow convergence. The upper winds and lee effect from the surrounding ridges are important to the mountain winds in the coastal plains (Endlicher, 2000). In these region, heat waves have a positive effect on rainfalls with 2-week lag on northeastern coasts and the windward sides, while inland on the leeward sides, the rainfalls increase already 1 week after the HWEs. The ITCZ moves southwards and reaches about 20° S during the austral summer and the rain belt covers the North of our study region, which is the main factor for the rainfall seasonality here (Dedekind et al., 2016). Since the south ITCZ stays shorter over Zambia with drier air, the rain is limited to short spells alternating with drier weather (Buckle, 1996). The heat waves detected here occur mostly in March-April and November-December, which is not the time of the maximum cover by the rain belt of the ITCZ. The air is relatively stable and dry, under these circumstances, time for accumulating enough water vapour in the atmosphere and creating the opportunities for intense precipitation is supposed to be longer, which matches the results of the northeastern coastal regions in this study.

The highest percentage of heat wave impacted area in C4 sub-region is 44%, which is lower than other sub-regions. The maritime-moist southeast trade wind (the source of latent energy) formed over the warm Indian Ocean flows landward on the east coast until the Great Escarpment with its highest peak in the Drakensberg (3482 m). The coastal plain in southern Mozambique is particularly wide and the friction convergence developed here can lead to a dissolution of the Easterlies inversion, and contribute to the precipitation in the eastern half of the subcontinent, whilst in lee direction the rainfall amount drops (Endlicher, 2000). The significant relationships are also observed only on the windward side. These petite regions with significance may be explained by the lower percentage of heat wave impacted areas.

5.4.2. The Central and the South

The precipitations in the central part of Southern Africa increase 1 or 2 weeks after the heat waves exist. The relief conditions has thermal and dynamical effects on the climate in Southern Africa. The highlands are high-altitude heating surface for the atmosphere. As a result, with sufficiently intense irradiations a thermal low is formed and the air masses can flow in. The dynamic effect refers to air flows, which are forced to rise up and to trigger the convection and foehn effects (Buckle, 1996; Endlicher, 2000). The subcontinent is an extensive internal highland with altitudes of 1000 to 2000 m, which is enclosed from the approximately 5000 km long Great Escarpment. Hence, albeit the Indian air masses and landward southeastern trade winds are dried through the continent, the foehn effect of the eastern fringe steps can contribute to the rainfall events under the low-pressure system, which partially explains that the southern-central part of the research area shows increased rainfalls for the duration of the HWEs (0-week lag, without significance). In general, inland basins consist of the Kalahari Basin with the Sandveld and Hardveld from 600 up to 1200 m, the Bushveld in the East (a small part of northwestern South Africa, northeastern Botswana and southwestern Zimbabwe) and the Okavango Basin in the North (northern Botswana) show reduced rainfalls with 0- and 2-week-lags of high temperature effects. Though some of the parts in 1-week-lag period exhibit slightly increased rainfalls, the results imply the drier conditions under the HWEs in these inland basins. The different spatial patterns of the slopes in 1987 heat wave event are reasonably explained by the time (the end of March), which is not the rainfall peak in this region. The effectiveness of such dynamic effects depend on the angle of air flow, the speed and the stability of contributed air masses might change and create different atmospheric conditions from the lee side of the mountain (Endlicher, 2000). The Highveld plateaus arises between 1200 and 1800 m in South Africa, where the rainfall and temperature extremes exhibit mostly significant relationships due to the topographic impact. Though the experiments on the effect of increasing temperature on annual mean rainfall suggest a reduction in rainfall here (Walker and Schultz, 2008).

The southward coastal steps in South Africa are relatively narrow. At the southern tip of the continent, the Great Escarpment curves circa 200 km inland and yields cape fold mountains (the Swartberg mountains up to 2325 m) and semi-desert zones (Great Karoo) of South Africa. The cyclonical west wind drifts only swipe the southern tip of the continent during the winter half-year. Concurrently, the 2000 m high peripheries of the Great Escarpment prevent the wide incursion of

Southeast trade winds going throw the entire tropospheric high as well as the low trade wind inversion into the interior of Southern Africa (Endlicher, 2000). A significant influence on climatic conditions is due to the coastal ocean currents as well. Cold water of Benguela Current shapes the air temperature near the coast, and thus only one extreme heat wave event is detected over 39 years, and the significant positive effects with 1- and 2-week-lags of the maximum temperature on the precipitation are found near Cape Town (0-500 m a.s.l.) and until the Great Escarpment (32° S, 24° E, 500-1000 m a.s.l.).

5.4.3. The West

Besides being extremely arid and semi-arid regions, the western coastal region belongs to the fog deserts, with a whole-year radiation decrease in the tropic and might be the reason for the relatively low number of HWEs detected here. The large temperature contrast between cold Benguela Current and vegetation-free overheating desert surface builds the fierce refresh circulation. With these winds the fogs shift landward and serve as the sources of moisture for the near-surface grown vegetation, which is insufficient moisture for actual rain (Buckle, 1996; Endlicher, 2000). The main precipitation form is not induced by convection processes related to higher temperature, therefore the relationships of rainfall and temperature extremes in this area are indistinguishable. Only the highland near Windhoek in Namibia at altitudes of 2484 m and the marginal region of Kalahari Basin present significant relationships, since the topography can act as an additional trigger for convective precipitation (Endlicher, 2000). The importance of steep local topography and adiabatic descent (foehn, winds) for the development of heat waves in coastal locations is emphasised (Lyon, 2009). Higher probabilities of heat waves conditioned on drought are largely seen in interior sections of South Africa. Particularly during ENSO events, there are enhanced heat wave probabilities accompanied by drought and above-average tropospheric temperatures during austral summer (Lyon, 2009). These results are able to explain why heatwave-induced rainfall extremes have not existed in our study.

5.5. Other climatic factors

5.5.1. The relationships between heat waves and droughts

Under warmer climates, increased risks of both droughts and floods are being noticed and connected with each other. As theories showing increase of water vapour leads to more intense

precipitation events, it takes longer to recharge the atmosphere with water vapour, and the frequency and duration of precipitation extremes would not be absolutely higher. Contemporaneously, surface drying caused by higher evaporation may be intense and more frequent (Trenberth, 2011). In view of the occurrence of HWEs, a strong relationship between the number of hot days in the regions, hottest month and preceding precipitation deficits at the global scale is observed (Mueller and Seneviratne, 2012). Since the occurrence probability of an above-average number of hot days is over 70% after precipitation deficits and below 30-40% after wet conditions, the authors concluded that moisture deficits derive predictive information on occurrence of hot extremes a few weeks later (Mueller and Seneviratne, 2012). The interactions between soil moisture and temperature are shown to increase summer temperature variability over Australia, which results in extreme temperatures with low soil moisture conditions (Perkins, 2015). On the opposite, extremely high temperatures contribute to droughts (Trenberth, 2011). If the frequency, duration and extension of land drying enlarge and become normal, the local atmospheric circulation will be changed and thereby build up a positive feedback between temperature extremes and droughts. Drought conditions may have remote effects on areas around or outside the actual drought region due to changes in atmospheric circulation and advection of air masses (Fisher et al., 2007). The duration and the cumulative intensity of HWEs in our study are checked with both mean and maximum values, but still there are no increasing tendencies found. The mechanisms of the formation of HWEs described above might provide another explanation, namely that long-term persistence of droughts could bring more frequent hot days and higher maximum temperature, and thus HWEs would be only detected by the most severe conditions based on the percentile of 1981-2010 climatology values.

5.5.2. Atmospheric conditions, clouds and topographic features

On the subject of the heat wave-induced rainfall extremes, there are few significant performances of lag regression model, partly because changes in rainfall are a more indirect consequence of local land-atmosphere interactions than a single direct climate variable (i.e. short-term temperature extremes in this study). The ITCZ shifts north and south following the path of the sun as well as the seasonal expansion and contraction of the subtropical highs (Buckle, 1996). Therefore, different atmospheric conditions that influence the properties of the two subtropical highs annually might indirectly affect the significance of relationships between two variable extremes. By analysing

changes in baroclinicity in the Southern Hemisphere, a poleward shift and upward expansion of subtropical high-pressure systems in an ensemble of 21st century climate simulations are projected, where many extratropical storm tracks move poleward and therefore can cause a drying tendency in the subtropics (Yin, 2005). Because cloudy skies, less solar radiation, more rain and soil moisture are dominant in cyclonic regimes over land, normally there is more energy going into evaporative processes (i.e. evaporative cooling of the surface), while less goes into sensible heating, and consequently lower temperatures exist (Trenberth, 2011). The number and strength of cyclones which contribute mainly to the rainfalls in austral summer in Southern Africa would be important to explain the intensity of rainfall events in different years when HWEs occurred. Donat et al. (2016) investigate the extreme precipitation in the world with the concept of 'wet-' and 'dry' grid cells and found a statistically significant relationship between daily extreme precipitation increases in dry regions and the mean temperature response in the individual model simulations. However, they also declare the rate of increase of precipitation extremes is affected by multiple factors such as the vertical velocity profile and its changes. Camberlin (2016) points out that daily maximum and minimum temperatures play different role on daily precipitation in different topographic conditions in the Greater Horn. In cool highland areas, rainfall occurs above the normal minimum temperature, and below this variable in lowland or hot environments. It is conceivable to add minimum temperature for establishing time-lag multiple regression models in the future in order to understand their mechanisms with precipitation extremes. Daily maximum temperature is affected by variations in cloud cover, proximity to large water bodies, prevailing wind direction and thermal advection (Buckle, 1996; Lyon, 2009; Camberlin, 2016). Since cloud cover reduces incoming shortwave radiation and the outflow of indirect heat through terrestrial radiation, which can contribute to reduce maximum temperature and enhance minimum temperature (Buckle, 1996; Camberlin, 2016). The other factors such as the combination of cloud cover with warm or cold air advection, types and height of clouds might make the relationship between temperature and cloudiness strongly space- and time-dependent (Camberlin, 2016).

The role of the strengths of the Angola Low and the Botswana High is associated with the variability of precipitation over Southern Africa (Driver and Reason, 2017; Munday and Washington, 2017). The Angola Low is a cyclonic feature formed during the austral summer. In the model simulation, it enhances southward moisture by northeasterly and northwesterly moisture

transport, which contributes the increase of moisture convergence in the central areas and the decrease of moisture divergence across Mozambique's coast. The consequences can lead to up to 70 % variability in rainfall amount during the rain seasons (December to February) particularly (Munday and Washington, 2017). On the other hand, the Botswana High not only influences the seasonal and inter-annual variably of rainfall but those of temperature (Driver and Reason, 2017). The formation of the Botswana High begins in August in Angola, and it is built up stronger and moves southward over Southern Africa during the spring and summer. The development and its position are linked with the movement of the regions with heavy rainfalls in tropical Southern Africa, while the ITCZ lies northeast to it (Driver and Reason, 2017). Hence, the strengths of the Low and the High differ intra-annually, which might cause variations of regional circulation and amounts of summer rainfall in this manner.

5.5.3. Precipitation and temperature dependence

Furthermore, the (co-)variations of the dependence between precipitation and temperature (P-T dependence) under global warming plays a crucial role in characterising the joint behaviour of these two variables (Hao et al., 2009; Berg et al., 2014). The different degrees of correlation, changes and the slopes in different months between global precipitation and temperature are discovered. For example, the negative dependence in the monthly variations of P-T dependence is found from December to February in Southern Africa from both observations (e.g. CRU) and CMIP5 climate models (Hao et al., 2009). Temperature-precipitation correlations are contributed through the soil moisture on surface heat flux partitioning (soil moisture-atmosphere interactions), which has been shown to play an amplifying role in warm extremes (Berg et al., 2014). The soil moisture is affected by temperature and circulation patterns (Fisher et al., 2007; Lyon, 2009). If the precipitation is below-average, the reduced soil moisture and latent heat flux as well as increased insolation (surface sensible heating) cause higher (near-)surface air temperatures and therefore enhanced surface radiation and evaporative fraction (Lyon, 2009; Trenberth, 2011; Berg et al., 2014). On the other hand, cloud cover and dry air advection contribute these consequences as well (Buckle, 1996; Mueller and Seneviratne, 2012; James and Washington, 2013; Camberlin, 2016). Since local and regional changes in the character of precipitation are largely dependent on variability patterns of atmospheric circulation (Trenberth, 2011), these factor should be taken into consideration in the

future especially for the analysis of the relationships between precipitation and temperature extremes.

5.5.4. Sea surface temperatures (SSTs)

According to the Clausius-Clapeyron (C-C) equation describing the water-holding capacity of the atmosphere as a function of temperature, the expectation of increases in water vapour amount as the climate warms is investigated, and a strong relationship between total column water vapour and SSTs over the oceans is found, whilst over the land there is a lower increase of water vapour possibly due to limits of water availability (Trenberth, 2011). Therefore, the availability of moisture seems to be vital, and the relationships are spatially different. In Northern Eurasia, warming air temperatures have been accompanied by higher precipitation intensity but lower frequency as well as a slight change in annual precipitation total (Ye et al., 2016). However, if temperatures are above the specific threshold, precipitation intensity reverses to decreasing with rising air temperature, which can be explained by the fact that decreasing water vapour is associated with extreme high temperatures (Ye et al., 2016). The extension and fluctuation of these relationships are also impacted by the ENSO events, which might diminish the strength of them. Besides, increased amounts of water vapour affect the hydrological cycle, because there are increases in moist static energy and gross moist instability that facilitate stronger convection and the formation of all storms. However, along the movements of winds, increases in evaporation and moisture lead to the consequence that more moisture is transported from divergence regions (30° S) to convergence zones (lower latitude near the equator and 60° S) (Trenberth, 2011). This may be the reason that there is less moisture in Southern Africa for the supply of regional water sources to form the precipitations induced by hot weathers. Anomalous deep convections triggered by the change of SSTs can release more latent heat and drive the atmospheric teleconnections that cause the remote impacts of ENSO (e.g. rainfall variabilities and anomalies) (Fauchereau et al., 2003; Perry et al., 2017). For example, in 1896-2002 the number of warm days in Southern Africa during ENSO events in austral summer increased (Kenyon and Hegerl, 2008). However, it is reported that since the late-1970s, SSTs variability in the tropical Western Indian Ocean has become significantly less dependent upon ENSO. Warm (cold) SSTs in the tropical Western Indian Ocean have become associated with wet (dry) conditions over the north-eastern half of South Africa and northern Namibia (Landman and Mason, 1999; Washington and Preston, 2005).

Moreover, the Northern Hemisphere SSTs are found with a later peak in temperature (original in August), which leads to a large scale shift in the annual cycle of precipitation globally by changing the West Africa Monsoon (WSM), and is responsible for the explanation of drying in Southern Africa during September-November (James and Washington, 2013). During some ENSO events, the Angola Low is proved to be suppressed and thus moisture circulation is changed by reducing poleward moisture transport (Reason and Jagadheesha, 2005; Munday and Washington, 2017). Besides, the Botswana High is stronger during ENSO events, and this atmospheric condition intensifies the occurrence of dry spells, maximum temperatures and the number of days with extreme temperature in summer in Southern Africa (Driver and Reason, 2017). In short, the character of SSTs and El Niño or La Niña events play an important role in changing regional atmospheric circulation directly and / or indirectly, which might break the theory that describes high temperature extreme induces intense precipitation.

Many detected HWEs in this study occur during the ENSO conditions, although they do not have absolutely stronger intensities, some of the lag regression models display both steeper negative and positive slopes with the lag effects of maximum temperature on precipitations (e.g. week 07, 1983 in C3 sub-region and week 07, 2016 in C5 sub-region) (Appendix E). As the whole research area extends widely across 20 degrees of latitude and 25 degrees of longitude, and with high temporal as well as spatial resolutions, the inter- and intra-annual variations of atmospheric condition, SSTs, displacements of the ITCZ, movements of the oceanic as well as the continental highs and lows, and diverse topographic features altogether construct the complexity of relationships between precipitation and temperature extremes in Southern Africa.

6. Conclusion

Based on the high temporal and spatial resolutions ERA5-Land reanalysis data, the presented study aims to regionalise the precipitation patterns, to evaluate the trends of precipitation and maximum temperature, and to establish the lag regression models of precipitation and maximum temperature extremes in Southern Africa from 1981 to 2019.

The CLARA program is efficient for the application with big datasets. The generated map with clear boundaries in each clusters confirms the robustness of cluster analysis in this study. The clustering result illustrate great precipitation period patterns over the 39 years, which combines the outcomes of recent regional climatic research and the categories of Köppen-Geiger climate classification.

The positive trends in annual precipitation in the northern part (15-23.5° S) and the significant negative trends in the southern part (23.5-35° S) of Southern Africa are observed, and are mainly contributed by the monthly precipitations from December to April. Generally, there are upward trends in maximum temperature (particularly in August-November) excluding the west-central part of Southern Africa. The upwelling cold water of the Benguela Current flowing through the west-costal regions can influence the air temperature, together with the topographic features (< 1000 m a.s.l.), which might be the reasons of decreasing trends of maximum temperature here.

Notwithstanding that there are several indices used for defining heat waves all over the world, the more strict one that describes when the daily T_{max} exceeds the statistical 95th percentile of the 30-year climatological T_{max} series for at least 5 consecutive days is applied. In order to detect heat waves pixel-wisely in the whole study region with spatial variation of elevations, the criteria are set up by the further conditions including the percentage of impacted area and the rainfall periods. Finally, there are one to 24 HWEs detected in each sub-region during the recent 39 years. However, the frequency, the duration and the intensity do not indicate increasing trends, which might be explained by the relatively short time scale comparing to other research with time series data since 1950.

In this study, the applied lag regression models display the reduction of rainfalls during HWEs and the enhancement of rainfalls after one to two weeks of the events. The spatial patterns of relationships between weekly precipitations and maximum temperatures with their lag effects are heterogeneous, different sub-regions (grid points) may show opposing results in different years. High adjusted R-squared values (> 0.8) imply the connections of increased weekly rainfall totals and temperature extremes with their lag effects until 2 weeks after HWEs, albeit there are no significant performances for supporting our theoretical hypothesis.

Previous studies mainly focused on changes in annual or seasonal precipitation amounts under global warming but ignored other features, such as intensity, duration as well as type of precipitation and variable regional behaviours (Westra et al., 2014; Donat et al., 2016). Moreover, the most reliable changes in precipitation with climate change are those with the thermodynamic aspects both in regional and remote atmospheric circulations (Seneviratne et al., 2012; Munday and Washington, 2017; Shepherd, 2019). We do not consider effects of minimum temperature, cloud cover, atmospheric moisture and topographic features in this study, which should be taken into consideration in future research. Overall, a deeper understanding of these processes and mechanisms in precipitation and temperature extremes could not only help improve climatic hazard predictions, but provide risk assessments in vulnerable regions like Southern Africa (Hulley et al., 2020).

Bibliography

Adisa, O.M., Botai, C.M., Botai, J.O., Hassen, A., Darkey, D., Tesfamariam, E., Adisa, A.F., Adeola, A.M. & Ncongwane, K.P. (2018). Analysis of agro-climatic parameters and their influence on maize production in South Africa. *Theoretical and Applied Climatology,* 134, 991-1004. DOI: 10.1007/s00704-017-2327-y.

Aloysius, N.R., Sheffield, J., Saiers, J.E., Li, H. & Wood, E.F. (2015). Evaluation of historical and future simulations of precipitation and temperature in Central Africa from CMIP5 climate models. *Journal of Geophysical Research Atmospheres,* 121(1), 130-152. DOI: 10.1002/2015JD023656.

Archer, E. (2021). *swfscMisc: Miscellaneous Functions for Southwest Fisheries Science Center.* R package version 1.5. URL: https://cran.r-project.org/web/packages/swfscMisc/index.html.

Australian Bureau of Meteorology. *El Niño - Detailed Australian Analysis.* http://www.bom.gov.au/climate/enso/enlist/index.shtml. Last visit on July 21, 2021.

Barbier, J., Guichard, F., Bouniol, D., Couvreux, F. & Roehrig, R. (2018). Detection of intraseasonal large-scale heat waves: characteristics and historical trends during the Sahelian spring. *Journal of Climate,* 31(1), 61-80. DOI: 10.1175/JCLI-D-17-0244.1.

Beck, H.E., Zimmermann, N. E., McVicar, T. R., Vergopolan, N., Berg, A. & Wood, E. F. (2018). Present and future Köppen-Geiger climate classification maps at 1-km resolution. *Nature Scientific Data,* 5, 180214. DOI:10.1038/sdata.2018.214.

Berg, A., Lintner, B.R., Findell, K., Seneviratne, S.I., Van den Hurk, B., Ducharne, A., Chéruy, F., Hagemann, S., Lawrence, D.M., Malyshev, S., Meier, A. & Gentine, P. (2014). Interannual coupling between summertime surface temperature and precipitation over land: processes and implications for climate change. *American Meteorological Society,* 28, 1308-1328. DOI: 10.1175/JCLI-D-14-00324.1.

Bivand, R., Keitt, T., Rowlingson, B., Pebesma, E., Sumner, M., Hijmans, R., Baston, D., Rouault, E., Warmerdam, F., Ooms, J. & Rundel, C. (2021). *rgdal: Bindings for the 'Geospatial' Data Abstraction Library.* R package version 1.5-23. URL: https://cran.r-project.org/web/packages/rgdal/index.html.

Buckle, C. (1996). *Weather and climate in Africa.* Addison Wesley Longman Limited, Malaysia. 312 pp.

Bibliography

Camberlin, P. (2016). Temperature trends and variability in the Greater Horn of Africa: interactions with precipitation. *Climate Dynamics,* 48, 477-498. DOI: 10.1007/s00382-016-3088-5.

Charrad, M., Ghazzali, N., Boiteau, V. & Niknafs, A. (2015). *NbClust: Determining the Best Number of Clusters in a Data Set.* R package version 3.0. URL: https://cran.r-project.org/web/packages/NbClust/index.html.

Climate Research Unit (CRU). University of East Anglia. https://crudata.uea.ac.uk/cru/data/hrg/. Last visit on July 28, 2020.

Cowpertwait, P.S.P. & Metcalfe, A.V. (2009). *Introductory Time Series with R.* Springer Dordrecht, Heidelberg.

Daniel, W.W. (1990). "Kendall's tau". *Applied Nonparametric Statistics (2nd ed.).* Boston, PWS-Kent. pp. 365-377.

Dedekind, Z., Engelbrecht, F.A. & van der Merwe, J. (2016). Model simulations of rainfall over Southern Africa and its eastern escarpment. *Water SA,* 42(1), 129-143. DOI: 10.4314/wsa.v42i1.13.

Donat, M.G., Lowry, A.L., Alexander, L.V., O'Gorman, P.A. & Maher, N. (2016). More extreme precipitation in the world's dry and wet regions. *Nature Climate Change,* 6, 508-514. DOI: 10.1038/NCLIMATE2941.

Driver, P. & Reason, C.J.C. (2017). Variability in the Botswana High and its relationships with rainfall and temperature characteristics over Southern Africa. *International Journal of Climatology,* 37 (Suppl.1), 570-581. DOI: 10.1002/joc.5022.

ECMWF. https://www.ecmwf.int/en/era5-land. Last visit on July 12, 2021.

Endlicher, W. (2000). "III Afrika südlich des Maghreb." in Weischet, W., Endlicher, W.: *Regionale Klimatologie, Teil 2 Die Alte Welt, Europa, Afrika, Asien.* B.G. Teubner, Stuttgart, Leipzig. p. 245-336.

Evans, J.S., Murphy, M.A. & Ram, K. (2021). *spatialEco: Spatial Analysis and Modelling Utilities.* R package version 1.3-7. URL: https://cran.r-project.org/web/packages/spatialEco/index.html.

Expert Team on Climate Change Detection, Monitoring and Indices (ETCCDI). *Climate Change Indices.* http://etccdi.pacificclimate.org/list_27_indices.shtml. Last visit on July 4, 2021.

Fauchereau, N., Trzaska, S., Rouault, M. & Richard, Y. (2003). Rainfall variability and changes in Southern Africa during the 20th century in the global warming context. *Natural Hazards,* 29, 139-154.

Fischer, E.M., Seneviratne, S.I., Lüthi, D. & Schär, C. (2007). Contribution of land-atmosphere coupling to recent European summer heat waves. *Geophysical Research Letters,* 34, L06707, DOI:10.1029/2006GL029068.

Fischer, E.M., Oleson, K.W. & Lawrence, D.M. (2012). Contrasting urban and rural heat stress responses to climate change. *Geophysical Research Letters,* 39(3), L03705. DOI: 10.1029/2011GL05057.

Frich, P., Alexander, L.V., Della-Marta, P., Gleason, B., Haylock, M., Klein Tank, A.M. & Peterson, T. (2002). Observed coherent changes in climatic extremes during the second half of the twentieth century. *Climate Research,* 19(3), 193-212.

Ganguly, A.R., Steinhaeuser, K., Erickson, D.J., Branstetter, M., Parish, E.S., Singh, N., Drake, J.B. & Buja, L. (2009). Higher trends but larger uncertainty and geographic variability in 21st century temperature and heat waves. *PNAS,* 106(37), 15555-15559. DOI: 10.1073/pnas.0904495106.

Global Precipitation Climatology Centre (GPCC), Deutscher Wetterdienst. https://www.dwd.de/EN/ourservices/gpcc/gpcc.html. Last visit on July 28, 2020.

Hart, N., Blamey, R. & James, R. (2016). "Southern Africa - Studying variability and future change." in Future Climate for Africa: *Africa's climate: Helping decision-makers make sense of climate information.* p. 17-22. URL: https://futureclimateafrica.org.

Hao, Z., Phillips, T.J., Hao, F. & Wu, X. (2019). Changes in the dependence between global precipitation and temperature from observations and model simulations. *International Journal of Climatology,* 39, 4895-4906. DOI: 10.1002/joc.6111.

Hijmans, R.J., Bivand, R., Forner, K., Ooms, J. & Pebesma, E. (2021a). *terra: Spatial Data Analysis.* R package version 1.3-4. URL: https://cran.r-project.org/web/packages/terra/index.html.

Hijmans, R.J., van Etten, J., Sumner, M., Cheng, J., Baston, D., Bevan, A., … & Wueest, R. (2021b). *raster: Geographic Data Analysis and Modeling.* R package version 3.4-13. URL: https://cran.r-project.org/web/packages/raster/index.html.

Howard, E & Washington, R. (2019). Drylines in Southern Africa: rediscovering the Congo Air Boundary. *Journal of Climate,* 32(23), 8223-8242. DOI: 10.1175/JCLI-D-19-0437.1.

Hulley, G.C., Dousset, B. & Kahn, B.H. (2020). Rising trends in heatwave metrics across Southern California. *Earth's Future,* 8(7), e2020EF001480. DOI: 10.1029/2020EF001480.

Ilori, O.W. & Ajayi, W. (2020). Change detection and trend Analysis of future temperature and rainfall over West Africa. *Earth Systems and Environment,* 4, 493-512. DOI: 10.1007/s41748-020-00174-6.

Jack, C., Wolski, P., Pinto, I. & Indasi, V. (2016). "Southern Africa - Tools for observing and modelling climate." in Future Climate for Africa: *Africa's climate: Helping decision-makers make sense of climate information.* p. 23-30. URL: https://futureclimateafrica.org.

James, R. & Washington, R. (2013) Changes in African temperature and precipitation associated with degrees of global warming. *Climate Change,* 117, 859-872. DOI 10.1007/s10584-012-0581-7.

Kassambara, A. & Mundt, F. (2020). *factoextra: Extract and Visualize the Results of Multivariate Data Analyses.* R package version 1.0.7. URL: https://cran.r-project.org/web/packages/factoextra/index.html.

Kaufman, L. & Rousseeuw, P.J. (1990). *Finding groups in data: an introduction to cluster analysis.* Wiley, New York, United States of America. 342 pp.

Kenyon, J. & Hegerl, G. C. (2008). Influence of modes of climate variability on global temperature extremes. *Journal of Climate,* 21, 3872-3889. DOI: 10.1175/2008JCLI2125.1.

Ketchen, D.J. & Shook, C.L. (1996). The application of cluster analysis in strategic management research: An analysis and critique. *Strategic Management Journal,* 17(6), 441-458.

Kruger, A.C. & Sekele, S.S. (2013). Trends in extreme temperature indices in South Africa: 1962-2009. *International Journal of Climatology,* 33, 661-676. DOI: 10.1002/joc.3455.

Kruger, A.C. & Shongwe, S. (2004). Temperature trends in South Africa: 1960-2003. *International Journal of Climatology,* 24, 1929-1945. DOI: 10.1002/joc.1096.

Kulikov, M. & Schickhoff, U. (2017). Vegetation and climate interaction patterns in Kyrgyzstan spatial discretization based on time series analysis. *Erdkunde,* 71(2), 143-165.

Landman, W.A. & Mason, S.J. (1999). Change in the association between Indian Ocean sea-surface temperatures and summer rainfall over South Africa and Namibia. *International Journal of Climatology,* 19(13), 1477-1492. DOI: 10.1002/(SICI)1097-0088(19991115)19:13%3C1477::AID-JOC432%3E3.0.CO;2-W.

Leutner, B., Horning, N., Schwalb-Willmann, J. & Hijmans, R.J. (2019). *RStoolbox: Tools for Remote Sensing Data Analysis.* R package version 3.5.0. URL: https://cran.r-project.org/web/packages/RStoolbox/index.html.

Li, L., Diallo, I., Xu, C.-Y. & Stordal, F. (2015). Hydrological projections under climate change in the near future by RegCM4 in Southern Africa using a large-scale hydrological model. *Journal of Hydrology,* 528, 1-16. DOI: 10.1016/j.jhydrol.2015.05.028.

Lyon, B. (2009). Southern Africa summer drought and heat waves observations and coupled model behavior. *Journal of Climate,* 22, 6033-6046. DOI: 10.1175/2009JCLI3101.1.

Maechler, M., Rousseeuw, P., Struyf, A., Hubert, M., Hornik, K., Studer, M., Roudier, P., Gonzalez, J., Kozlowski, K., Schubert, E. & Murphy, K. (2021). *cluster: "Finding Groups in Data": Cluster Analysis Extended Rousseeuw et al.* R package version 3.4.0. URL: https://cran.r-project.org/web/packages/cluster/index.html.

Mason, S.J., Waylen, P.R., Mimmack, G.M., Rajaratnam, B. & Harrison, J.M. (1999) Changes in extreme rainfall events in South Africa. *Climate Change,* 41, 249-257.

Mueller, B. & Seneviratne, S.I. (2012). Hot days induced by precipitation deficits at the global scale. *PNAS,* 109(31), 12398-12403. DOI: 10.1073/pnas.1204330109.

Munday, C. & Washington, R. (2017). Circulation controls on Southern African precipitation in coupled models: The role of the Angola Low. *Journal of Geophysical Reserach Atmospheres,* 122(2), 861-877. DOI: 10.1002/2016JD025736.

Neuwirth, E. (2014). *RColorBrewer: ColorBrewer Palettes.* R package version 1.1-2. URL: https://cran.r-project.org/web/packages/RColorBrewer/index.html.

Nicholson, S.E., Nash, D.J., Chase, B.M., Grab, S.W., Shanahan, T.M., Verschuren, D., Asrat, A., Lézine, A.-M. & Umer, M. (2013). Temperature variability over Africa during the last 2000 years. *Holocene,* 23, 1085-94. DOI: 10.1177/0959683613483618.

Nicholson, S.E., Funk, C. & Fink, A.H. (2018). Rainfall over the African continent from the 19th through the 21st century. *Global and Planetary Change,* 165, 114-127. DOI: 10.1016/j.gloplacha.2017.12.014.

Ongoma, V. & Chen, H. (2017). Temporal and spatial variability of temperature and precipitation over East Africa from 1951 to 2010. *Meteorology Atmospheric Physics,* 129, 131-144. DOI: 10.1007/s00703-016-0462-0.

Onyutha, C. (2021). Trends and variability of temperature and evaporation over the African continent: relationships with precipitation. *Atmósfera,* 34(3), 267-287. DOI: 10.20937/ATM.52788.

Pebesma, E. & Graeler, B. (2021). *gstat: Spatial and Spatio-Temporal Geostatistical Modelling, Prediction and Simulation.* R package version 2.0-7. URL: https://cran.r-project.org/web/packages/gstat/index.html.

Perkins, S.E., Alexander, L.V. & Nairn, J.R. (2012). Increasing frequency, intensity and duration of observed global heatwaves and warm spells. *Geophysical Research Letters,* 39, L20714: 1-5. DOI:10.1029/2012GL053361.

Perkins, S.E. (2015). A review on the scientific understanding of heatwaves - Their measurement, driving mechanisms, and changes at the global scale. *Atmospheric Research,* 164-165, 242-267, DOI:10.1016/j.atmosres.2015.05.014.

Perry, S.J., McGregor, S., Gupta, A.S. & England, M.H. (2017). Future changes to El Niño-Southern Oscillation temperature and precipitation teleconnections. *Geophysical Research Letters,* 44(20), 10608-10616. DOI: 10.1002/2017GL074509.

Pierce, D. (2019). *ncdf4: Interface to Unidata netCDF (Version 4 or Earlier) Format Data Files.* R package version 1.17. URL: https://cran.r-project.org/web/packages/ncdf4/index.html.

Pohlert, T. (2020). *Non-parametric trend tests and change-point detection.* Creative Commons License (CC BY-ND 4.0). URL: http://creativecommons.org/licenses/by-nd/4.0/.

Reason, C. J. C. & Jagadheesha, D. (2005). A model investigation of recent ENSO impacts over Southern Africa. *Meteorology Atmospheric Physics,* 89(1-4), 181-205. DOI:10.1007/s00703-005-0128-9.

Robinson, D., Hayes, A., Couch, S., Patil, I., Chiu, D., Gomez, M., … & Yamamoto, J. (2021). *broom: Convert Statistical Objects into Tidy Tibbles.* R package version 0.7.8. URL: https://cran.r-project.org/web/packages/broom/index.html.

Roelofsen, P. (2018). *Time series clustering.* Master thesis, Vrije Universiteit Amsterdam. 76 pp.

Russo, S., Dosio, A., Graversen, R.G., Sillmann, J., Carrao, H., Dunbar, M.B., Singleton, A., Montagna, P., Barbola, P. & Vogt, J.V. (2014). Magnitude of extreme heat waves in present climate and their projection in a warming world. *Journal of Geophysical Research Atmospheres,* 119(22), 12500-12512. DOI: 10.1002/2014JD022098.

Russo, S., Marchese, A.F., Sillmann, J. & Immé, G. (2016). When will unusual heat waves become normal in a warming Africa? *Environmental Research Letters,* 11, 054016. DOI: 10.1088/1748-9326/11/5/054016.

Ryan, J.A., Ulrich, J.M., Bennett, R. & Joy, C. (2020). *xts: eXtensible Time Series.* R package version 0.12.1. URL: https://cran.r-project.org/web/packages/xts/index.html.

Schlegel, R.W. & Smit, A.J. (2018). heatwaveR: A central algorithm for the detection of heatwaves and cold-spells. *Journal of Open Source Software,* 3(27), 821. DOI: 10.21105/joss.00821.

Schlegel, R.W. & Smit, A.J. (2021a). *Detection events in gridded data.* URL: https://cran.r-project.org/web/packages/heatwaveR/vignettes/gridded_event_detection.html.

Schlegel, R.W. & Smit, A.J. (2021b). *heatwaveR: Detect Heatwaves and Cold-Spells.* R package version 0.4.5. URL: https://cran.r-project.org/web/packages/heatwaveR/index.html.

Sen, P.K. (1968). Estimates of Regression Coefficient Based on Kendall's tau. J*ournal of the American Statistical Association,* 63(324), 1379-1389.

Seneviratne, S.I., Nicholls, N., Easterling, D., Goodess, C.M., Kanae, S., Kossin, J., … & Zhang, X (2012). Changes in climate extremes and their impacts on the natural physical environment. In: Field, C.B., Barros, V., Stocker, T.F., Qin, D., Dokken, D.J., Ebi, K.L., … & Midgley, P.M. (eds.) *Managing the Risks of Extreme Events and Disasters to Advance Climate Change Adaptation. A Special Report of Working Groups I and II of the Intergovernmental Panel on Climate Change (IPCC).* Cambridge University Press, Cambridge, UK, and New York, NY, USA, pp. 109-230.

Shepherd, T.G. (2019). Storyline approach to the construction of regional climate change information. *Proceedings of the Royal Society A,* 475(2225), 20190013. DOI: 10.1098/rspa.2019.0013.

Siegel, A.F. (1982). Robust Regression Using Repeated Medians. *Biometrika,* 69(1), 242-244.

Spinu, V., Grolemund, G., Wickham, H., Lyttle, I., Costigan, I., Law, J., Mitarotonda, D., Larmarange, J., Boiser, J., Lee, C.H. & Google Inc. (2021). *lubridate: Make Dealing with Dates a Little Easier.* R package version 1.7.10. URL: https://cran.r-project.org/web/packages/lubridate/index.html.

Sulikowska, A. & Wypych, A. (2020). Summer temperature extremes in Europe: how does the definition affect the results? *Theoretical and Applied Climatology,* 141, 19-30. DOI: 10.1007/s00704-020-03166-8.

Theil, H. (1950). A rank invariant method of linear and polynomial regression analysis, i, ii, iii. *Proceedings of the Koninklijke Nederlandse Akademie Wetenschappen, Series A Mathematical Sciences,* 53, 386-392, 521-525, 1397-1412.

Tibshirani, R., Walther, G. & Hastie, T. (2001). Estimating the number of clusters in a dataset via the gap statistic. *Journal of the Royal Statistical Society: Series B (Statistical Methodology),* 63, 411-423.

Trenberth, K.E. (2011). Changes in precipitation with climate change. *Climate Research,* 47, 123-138. DOI: 10.3354/cr00953.

Tropical Rainfall Measuring Mission (TRMM). https://trmm.gsfc.nasa.gov/. Last visit on July 28, 2020.

Tyson, P.D. & Preston-Whyte, R. (2000). *The weather and climate of Southern Africa (2nd Edition).* Oxford University Press, South Africa. 396 pp.

United States Climate Prediction Center. *Historical El Niño/La Niña episodes (1950-present).* https://origin.cpc.ncep.noaa.gov/products/analysis_monitoring/ensostuff/ONI_v5.php. Last visit on July 21, 2021.

United States Environmental Protection Agency. *Temperature and precipitation.* Report on the Environment. https://cfpub.epa.gov/roe/indicator.cfm?i=89. Last visit on March 28, 2021.

Walker, N. & Schultz, R. (2008). Climate change impacts on agro-ecosystem sustainability across three climate regions in the maize belt of South Africa. *Agriculture Ecosystems and Environment,*124(1-2), 114-124.

Wallig, M., Microsoft Corporation, Weston, S. & Tenenbaum, D. (2020). *doParallel: Foreach Parallel Adaptor for the 'parallel' Package.* R package version 1.0.16. URL: https://cran.r-project.org/web/packages/doParallel/index.html.

Warnes, G.R., Bolker, B., Gorjanc, G., Grothendieck, G., Korosec, A., Lumley, T., MacQueen, D., Magnusson, A. & Rogers, J. (2017). *gdata: Various R Programming Tools for Data Manipulation.* R package version 2.18.0. URL: https://cran.r-project.org/web/packages/gdata/index.html.

Westra, S., Fowler, H.J., Evans, J.P., Alexander, L.V., Berg, P., Johnson, F., Kendon, E.J., Lenderink, G. & Roberts, N.M. (2014). Future changes to the intensity and frequency of short-duration extreme rainfall. *Reviews of Geophysics,* 52(3), 522-555. DOI: 10.1002/2014RG000464.

Wickham, H., Chang, W., Henry, L., Pedersen, T.L., Takahashi, K., Wilke, C., Woo, K., Yutani, H., Dunnington, D. & RStudio (2021a). *ggplot2: Create Elegant Data Visualisations Using the*

Grammar of Graphics. R package version 3.3.5. URL: https://cran.r-project.org/web/packages/ggplot2/index.html.

Wickham, H., François, R., Henry, L., Müller, K. & RStudio (2021b). *dplyr: A Grammar of Data Manipulation.* R package version 1.0.7. URL: https://cran.r-project.org/web/packages/dplyr/index.html.

Wilcox, R.R. (2010). *Fundamentals of modern statistical methods: substantially improving power and accuracy, 2nd ed.* Springer, New York. DOI: 10.1007/978-1-4419-5525-8.

Williams, C.J.R. & Kniveton, D.R. (2011). "Introduction" in Williams, C.J.R. & Kniveton, D.R. (eds.): *African climate and climate change. Advances in Global Change Research 43,* 1-12. DOI: 10.1007/978-90-481-3842-5_1.

Williams, C.J.R., Kniveton, D.R. & Layberry, R. (2011). "Extreme rainfall events over Southern Africa" in Williams, C.J.R. & Kniveton, D.R. (eds.): *African climate and climate change. Advances in Global Change Research 43,* 71-100. DOI: 10.1007/978-90-481-3842-5_4.

World Meteorological Organization (2017) *Guidelines on the calculation of climate normals (WMO-No. 1203).* 2017 edition, Geneva.

Ye, H. (2016). Increasing daily Precipitation intensity associated with warmer air temperatures over Northern Eurasia. *Journal of Climate,* 29(2), 623-636. DOI: 10.1175/JCLI-D-14-00771.1.

Yin, J.H. (2005). A consistent poleward shift of the storm tracks in simulations of 21st century climate. *Geophysical Research Letter,* 32, L18701. DOI:10.1029/2005GL023684.

Zandler, H., Haag, I. & Samimi, C. (2019). Evaluation needs and temporal performance differences of gridded precipitation products in peripheral mountain regions. *Scientific Reports,* 9, 15118. DOI: 10.1038/s41598-019-51666-z.

Zeileis, A., Grothendieck, G., Ryan, J.A., Ulrich, J.M. & Andrews, F. (2021). *zoo: S3 Infrastructure for Regular and Irregular Time Series (Z's Ordered Observations).* R package version 1.8-9. URL: https://cran.r-project.org/web/packages/zoo/index.html.

Zhang, X., Alexander, L., Hegerl, G.C., Jones, P., Tank, A.K., Peterson, T.C. & Zwiers, F.W. (2011). Indices for monitoring changes in extremes based on daily temperature and precipitation data. *Wiley Interdisciplinary Reviews Climate Change,* 2(6), 851-870.

Zhang, Y., Moges, S. & Block, P. (2016). Optimal cluster analysis for objective regionalization of seasonal precipitation in regions of high spatial-temporal variability application to western Ethiopia. *Journal of Climate,* 29, 3697-3717. DOI: 10.1175/JCLI-D-15-0582.1.

Appendix A.

Table A-1. The percentages (%) of monthly precipitation in 10 sub-regions (1981-2019).

	January	February	March	April	May	June	July	August	September	October	November	December
C1	10.6	13.1	15.3	11.5	6.4	6.5	5.8	5.5	4.4	6.1	6.8	8.0
C2	17.4	18.5	16.7	10.3	3.0	2.0	1.6	1.5	2.5	5.9	8.2	12.3
C3	23.6	21.9	16.9	6.1	0.5	0.3	0.1	0.1	0.7	3.9	9.5	16.3
C4	15.7	12.9	11.7	6.4	2.7	2.1	2.0	3.1	4.8	10.2	13.1	15.4
C5	24.7	19.6	13.8	5.0	1.7	1.2	1.2	0.9	1.1	3.0	8.3	19.4
C6	25.0	20.3	14.0	3.9	0.8	0.5	0.5	0.3	0.6	3.0	10.2	20.7
C7	24.8	20.5	14.0	4.3	0.7	0.4	0.4	0.2	0.7	3.4	10.7	19.8
C8	17.8	14.9	11.8	6.3	2.9	1.9	1.6	2.1	3.4	7.6	12.6	17.0
C9	19.4	17.2	12.9	6.9	2.2	1.7	0.9	1.2	2.4	6.6	11.7	16.9
C10	7.1	7.3	8.7	9.1	7.4	9.1	8.7	9.1	7.5	9.1	9.2	7.7
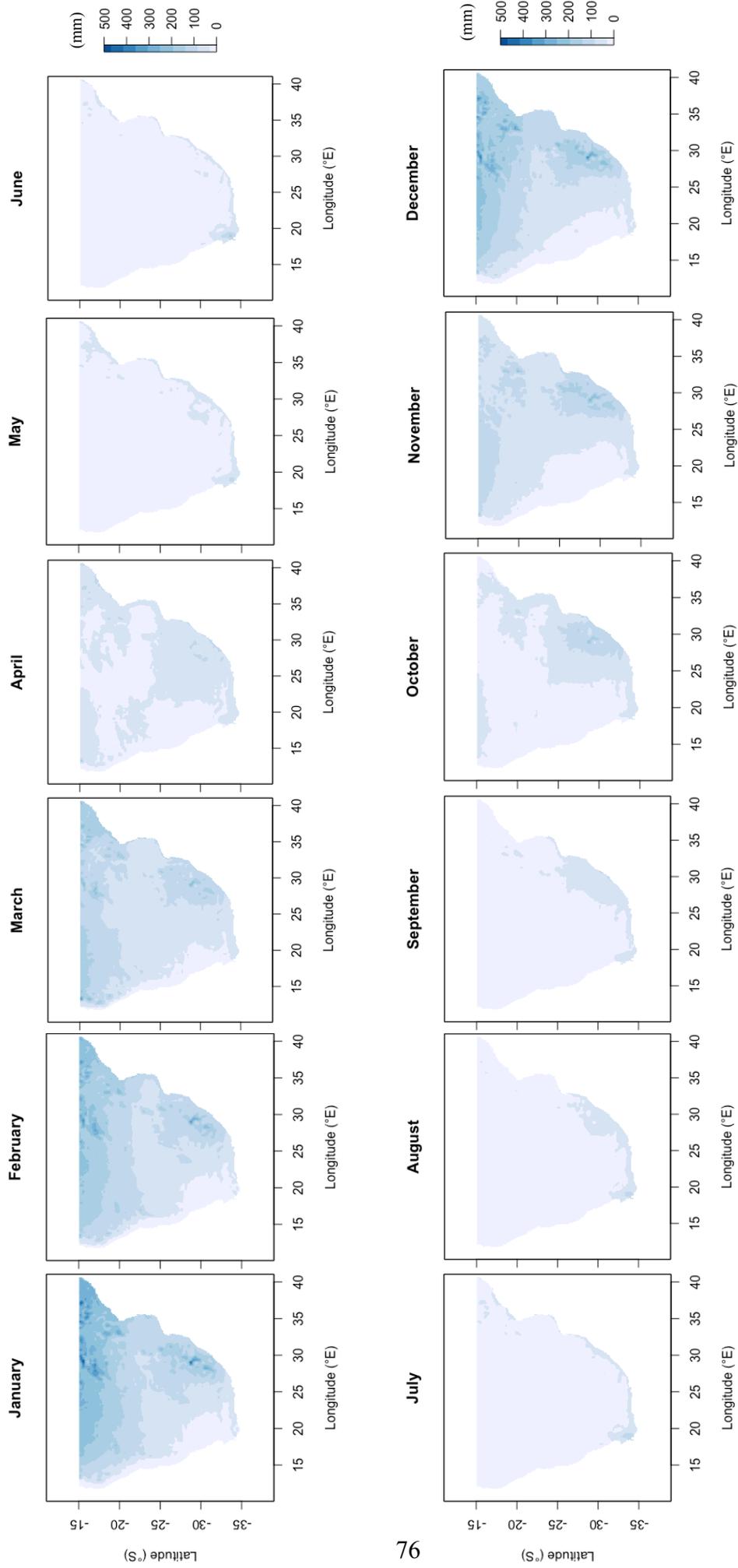
Figure A-1. Mean monthly total precipitation from 1981 to 2019.

Appendix B.
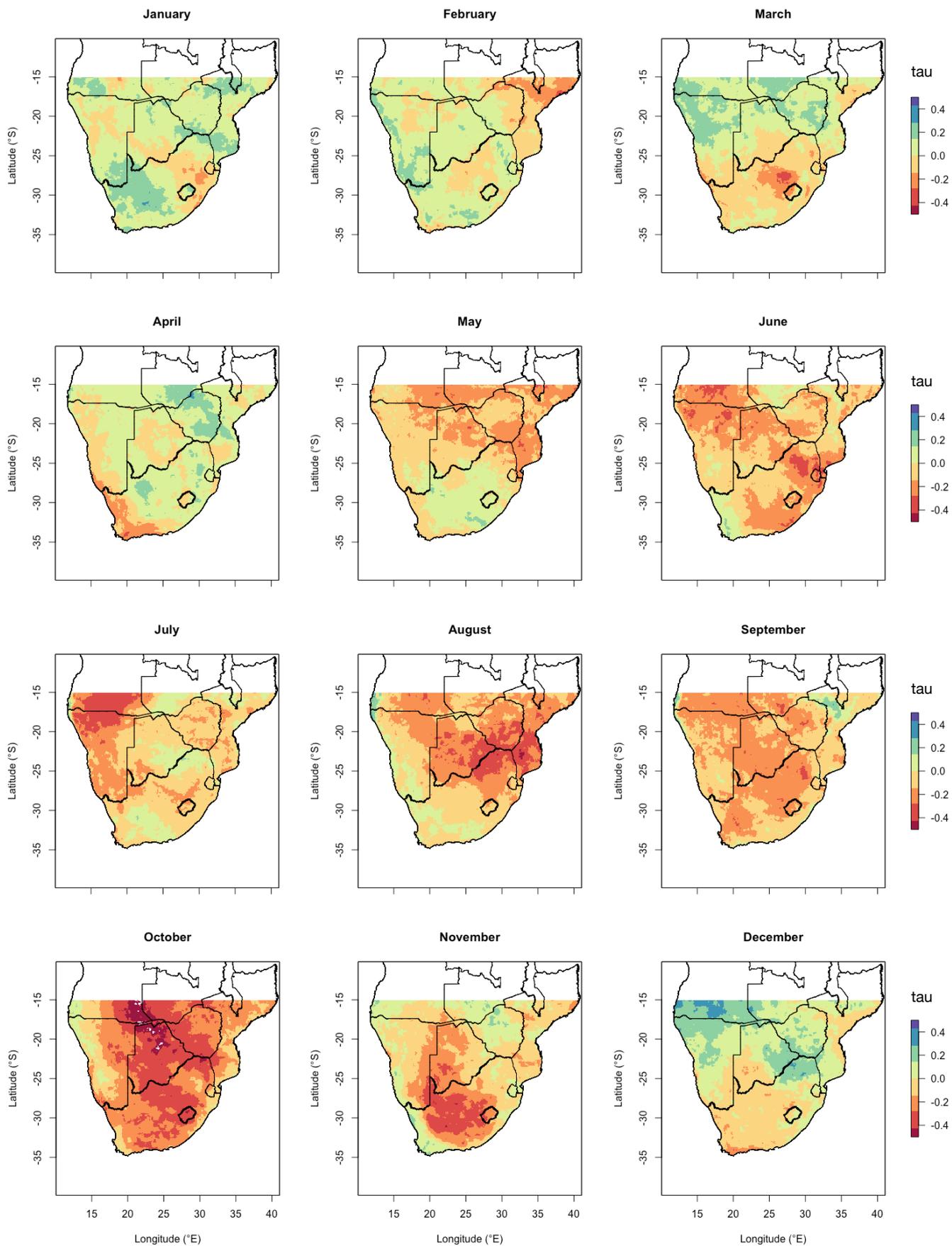
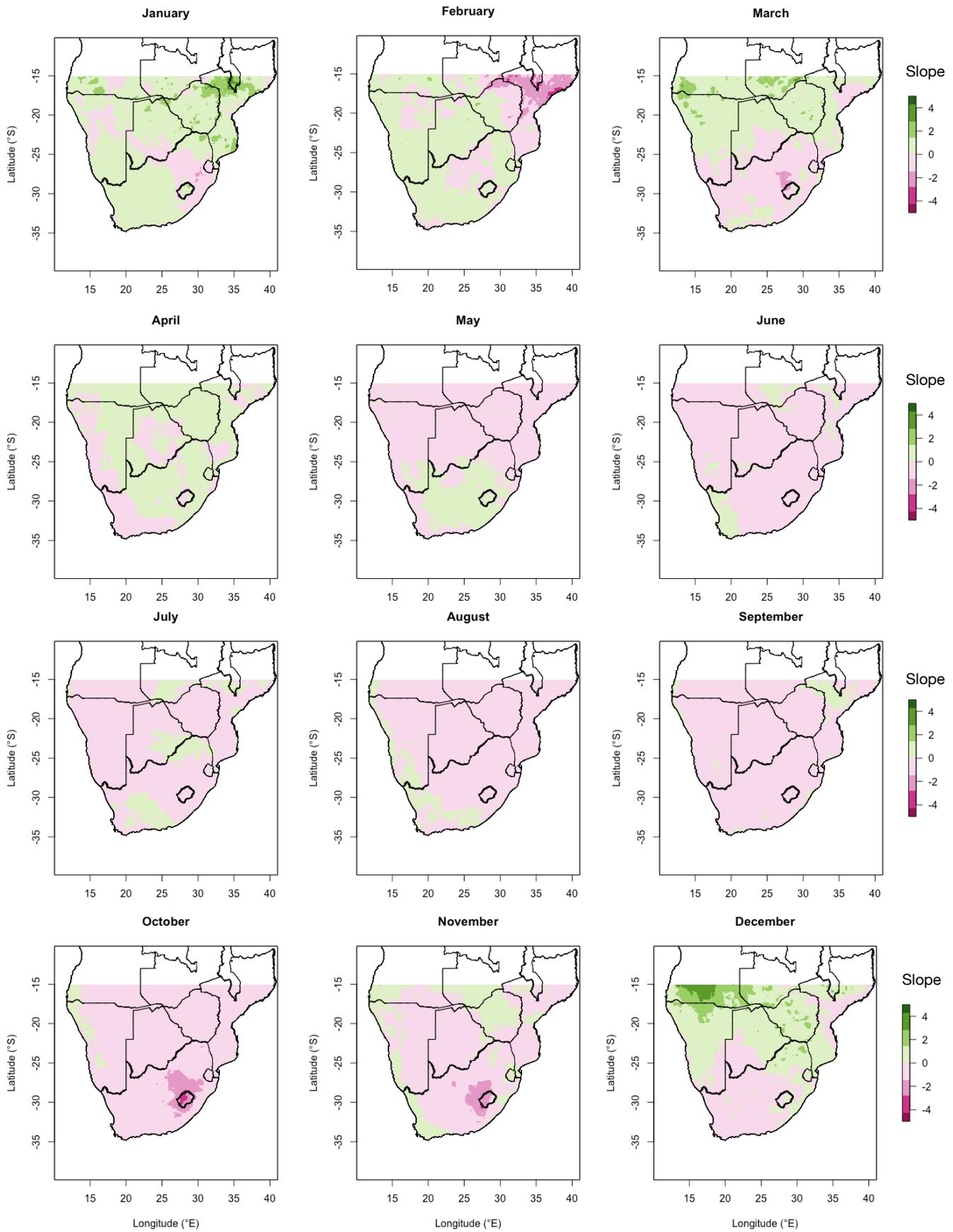Figure B-1. Monthly values of tau for precipitation in Mann-Kendall Test.

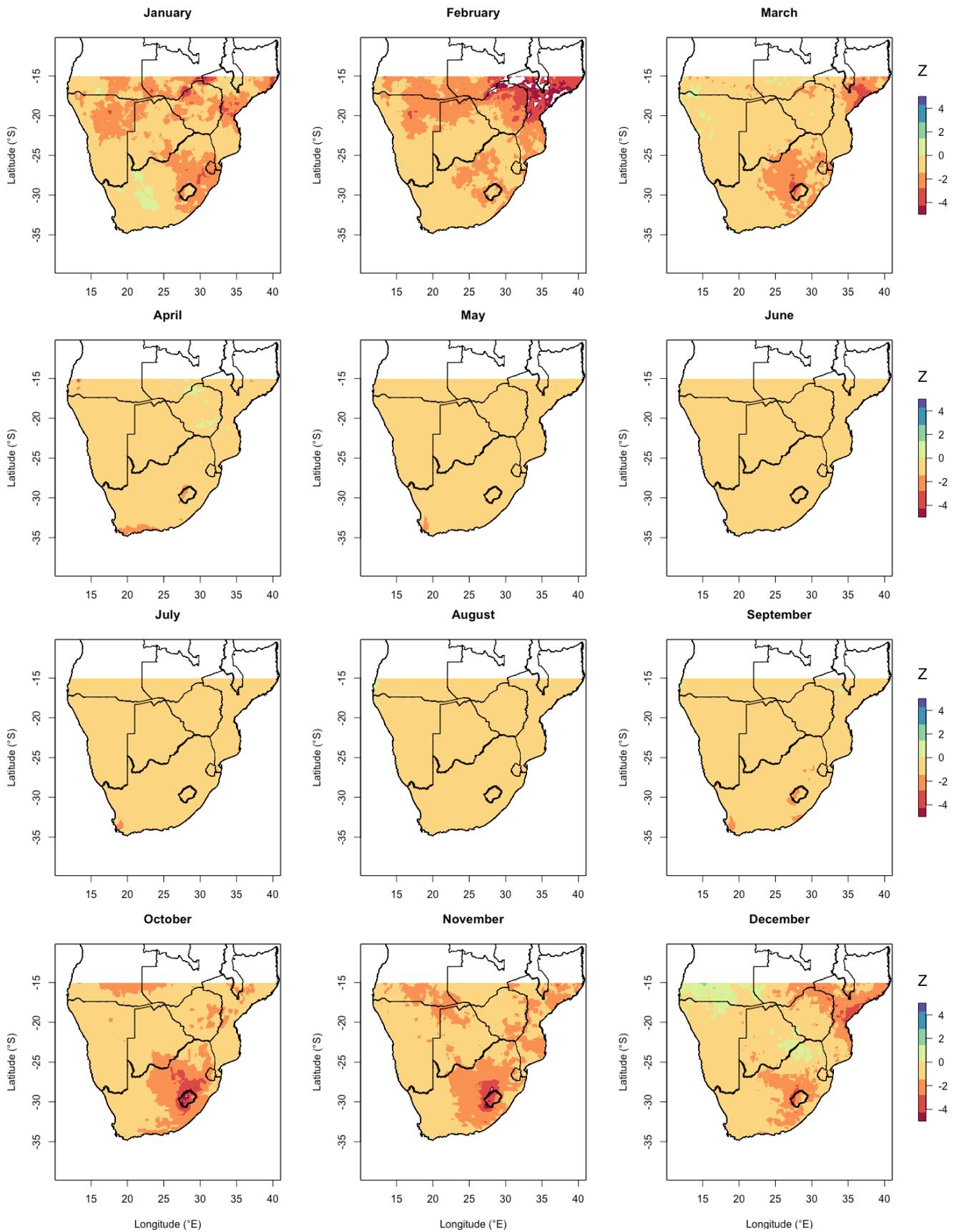Figure B-2. Monthly values of Sen's slope for precipitation in Mann-Kendall Test.

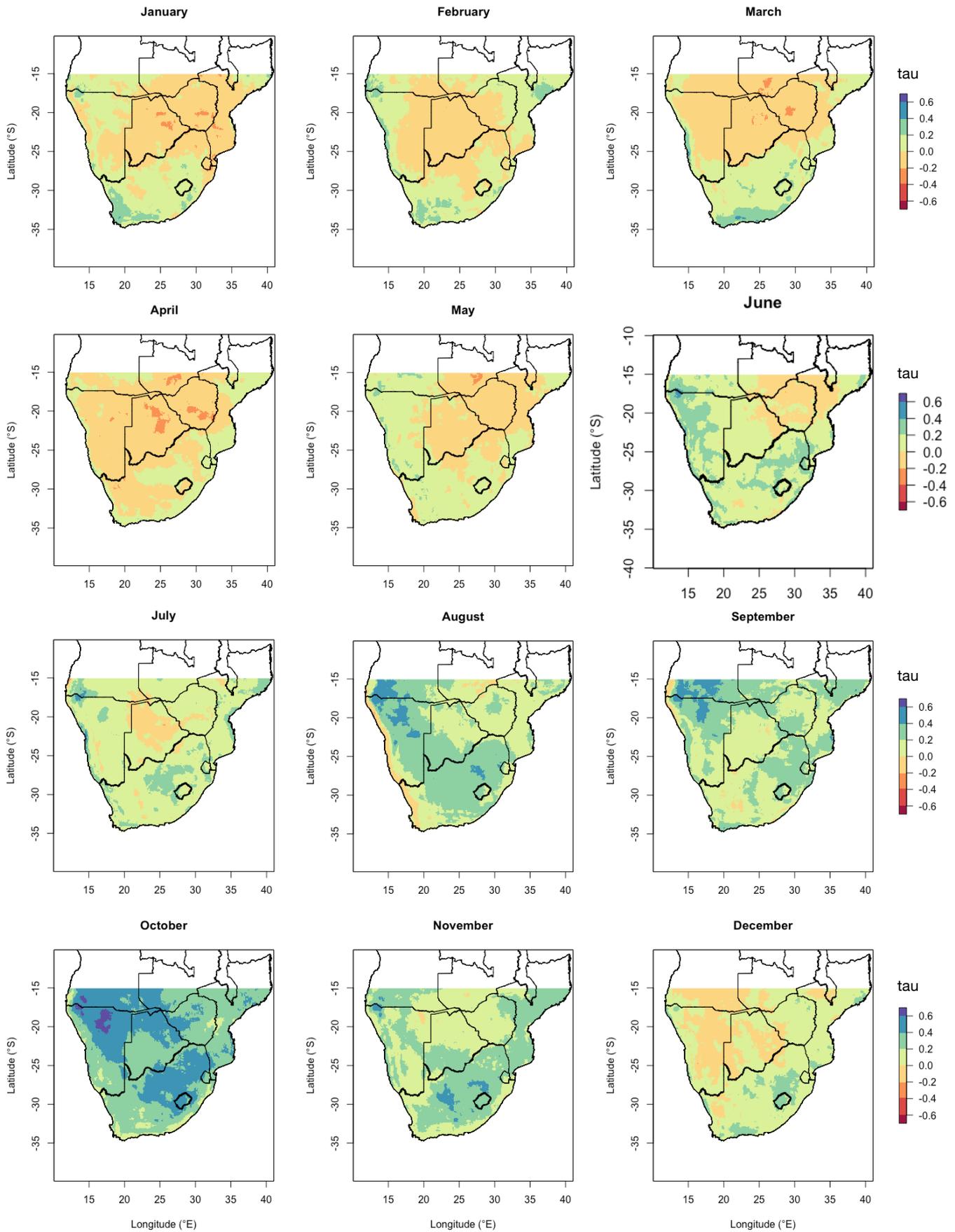Figure B-3. Monthly values of Z-value for precipitation in Mann-Kendall Test.

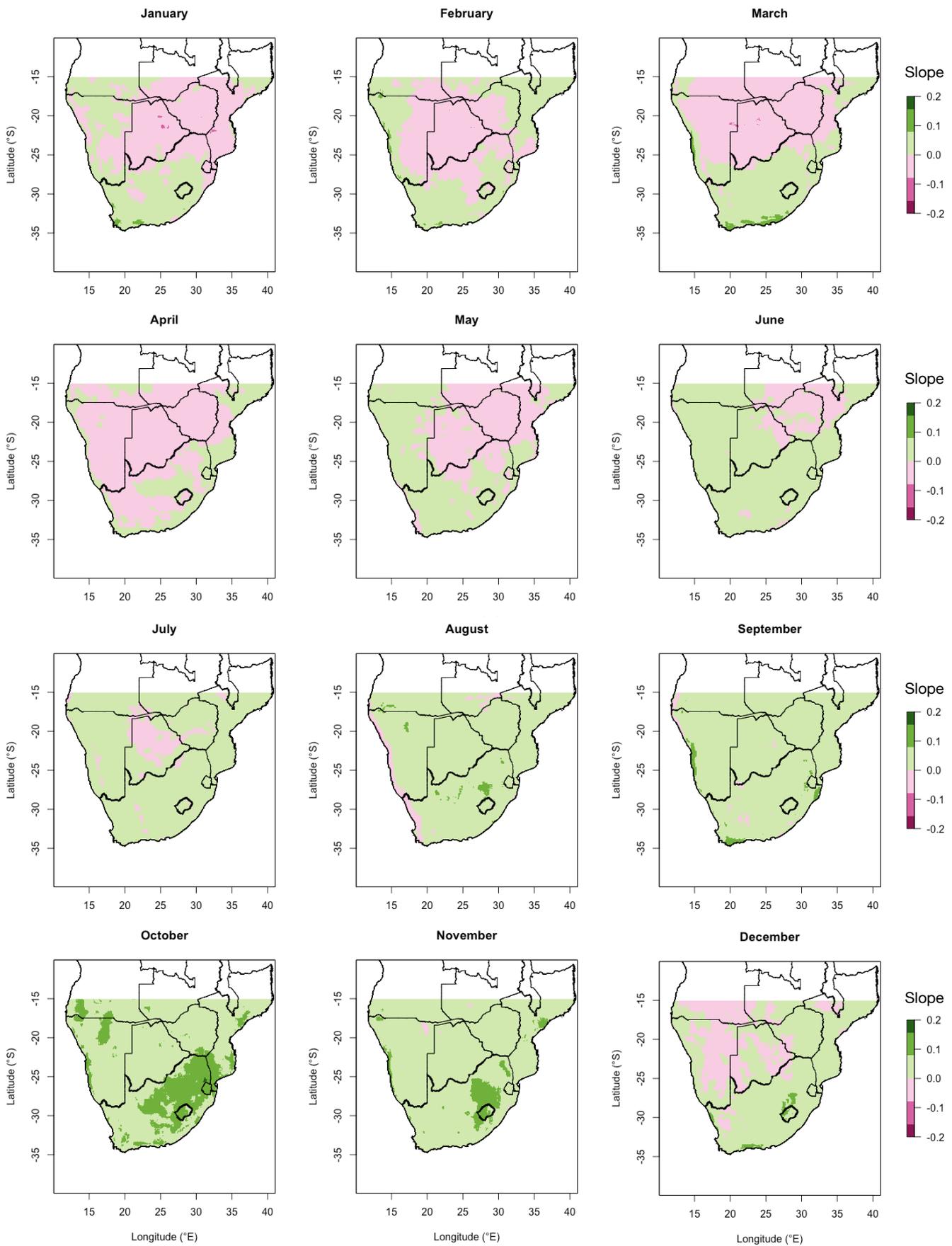Figure B-4. Monthly values of tau for maximum temperature in Mann-Kendall Test.

Figure B-5. Monthly values of Sen's slope for maximum temperature in Mann-Kendall Test.
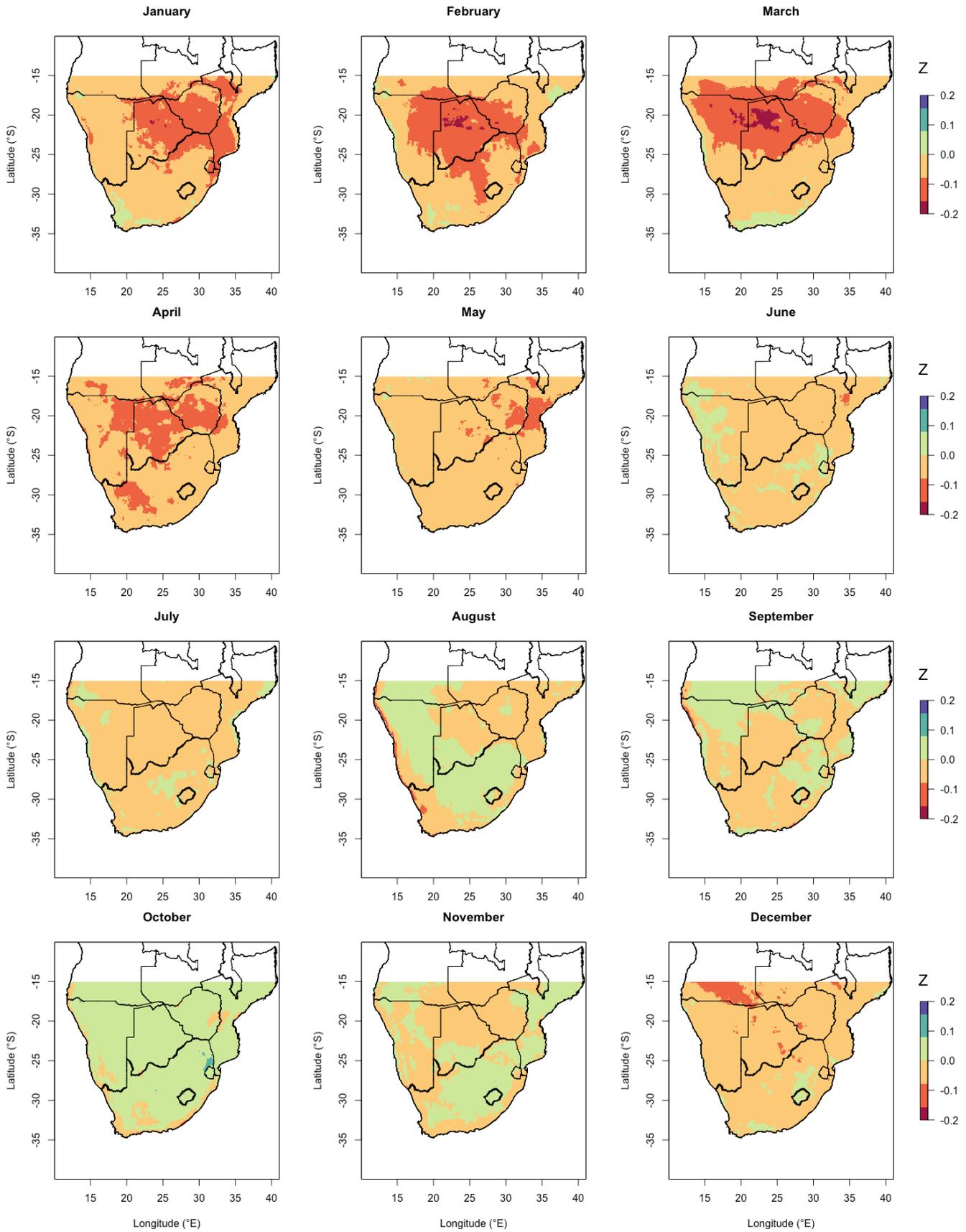
Figure B-6. Monthly values of Z-value for maximum temperature in Mann-Kendall Test.
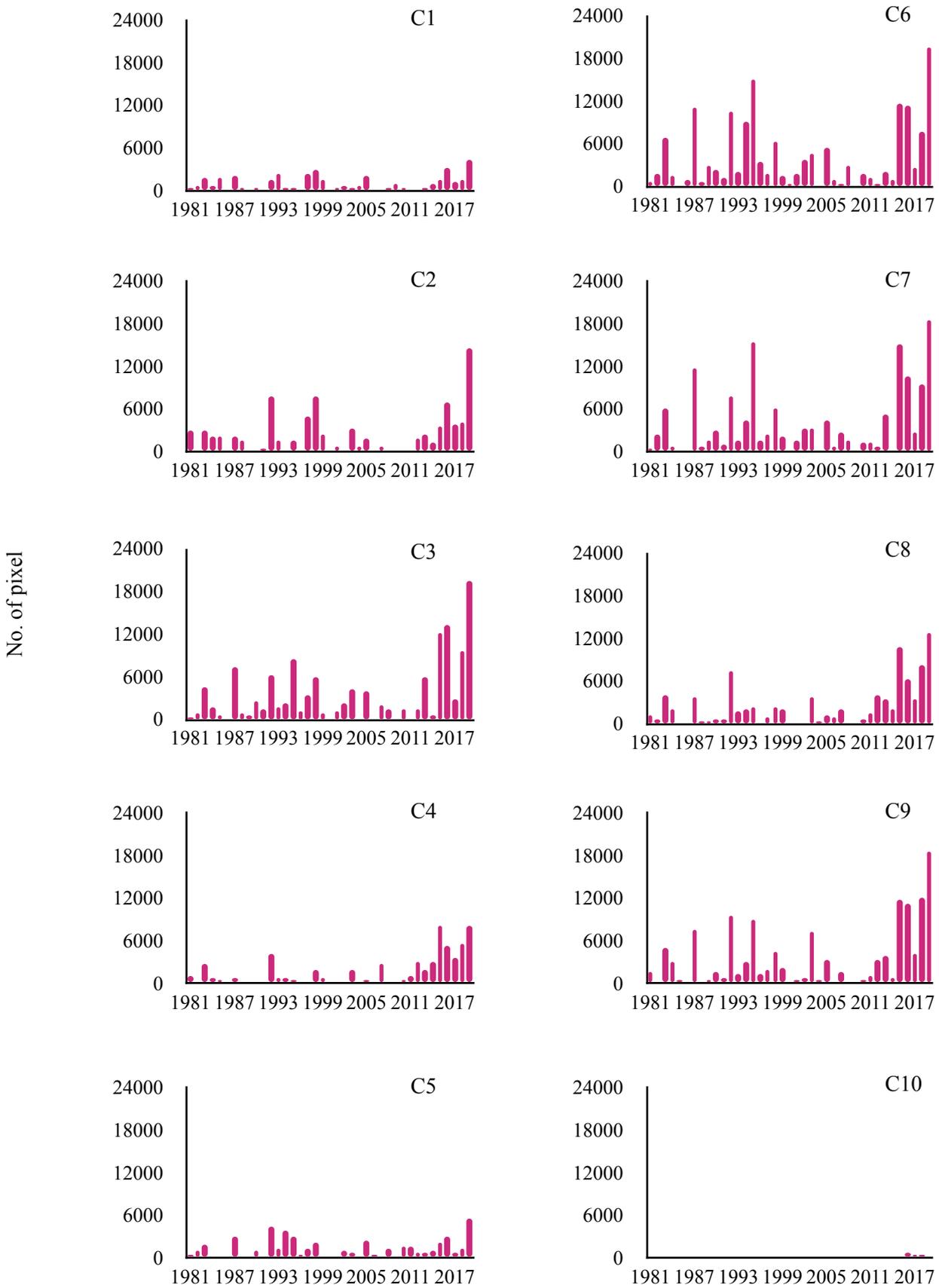
Figure C-1. Numbers of pixel with detected HWEs in 10 sub-region over 1981-2019.
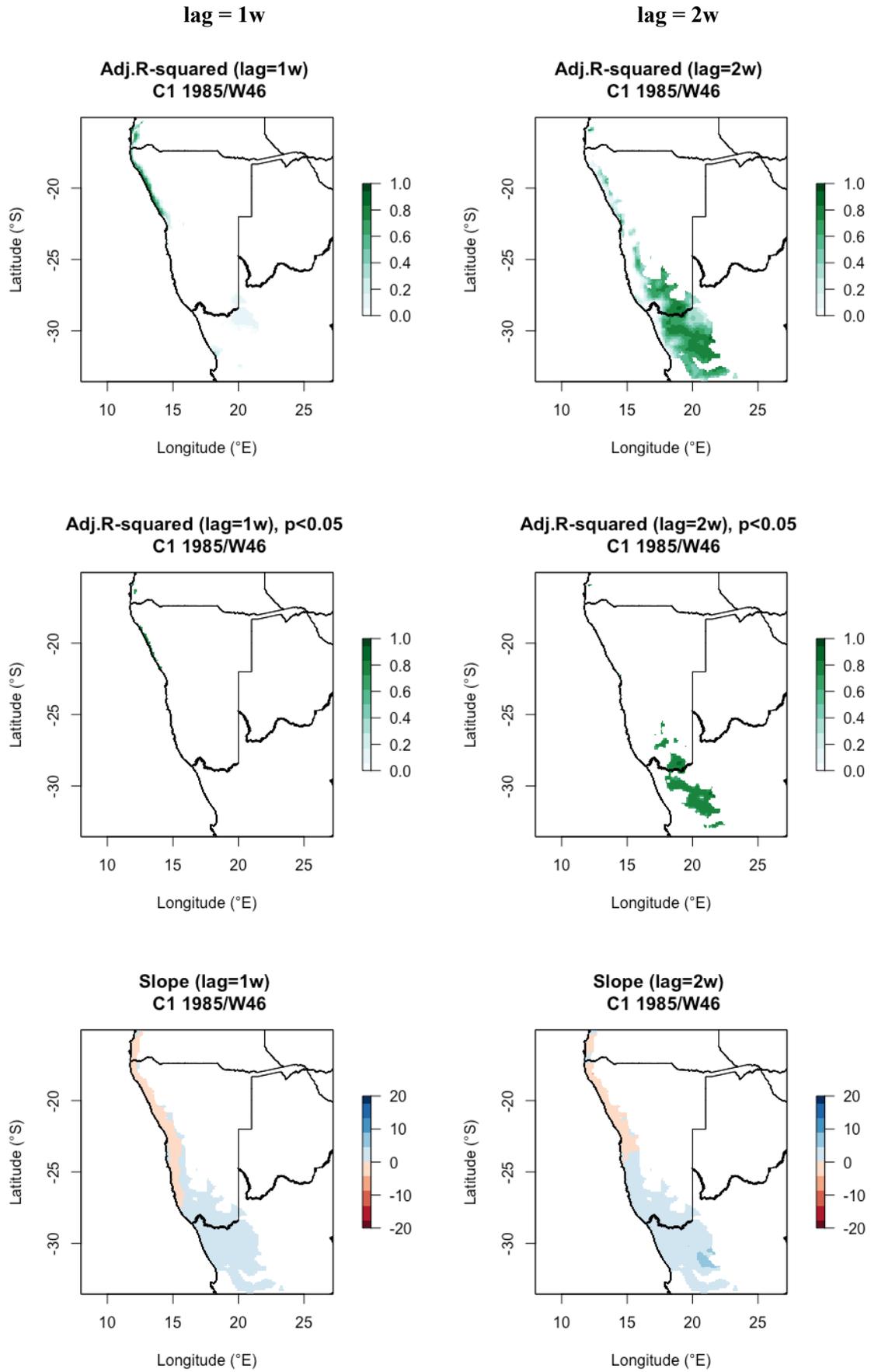
Appendix D.

C1 1985/W46   **lag = 1w**   **lag = 2w**

Figure D-1. The results of lag regression models of 1 and 2weeks in C1 sub-region.

C2 1987/W53   **lag = 1w**   **lag = 2w**
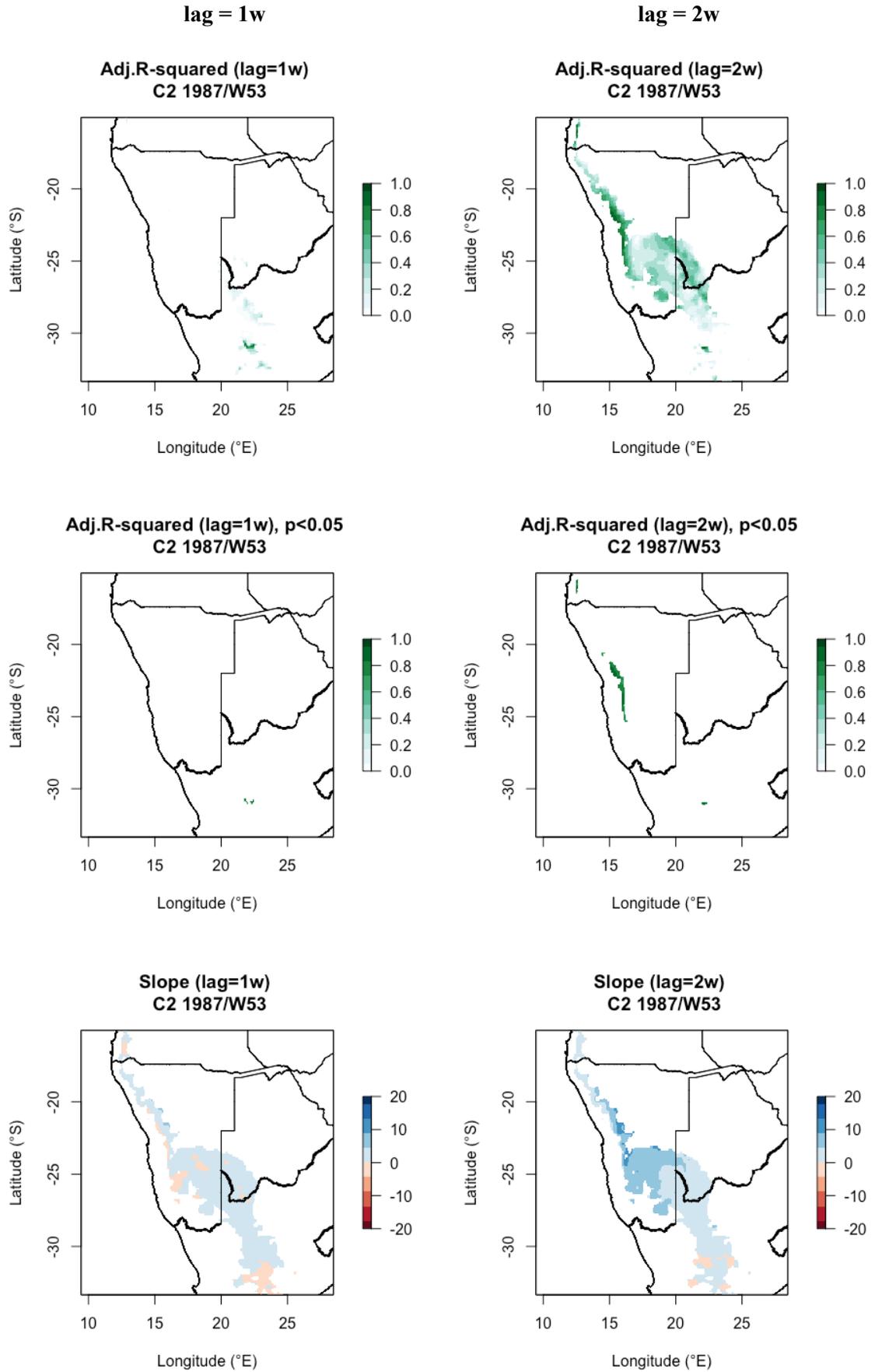
Figure D-2. The results of lag regression models of 1 and 2weeks in C2 sub-region.

C3 2015/W46 **lag = 1w** **lag = 2w**
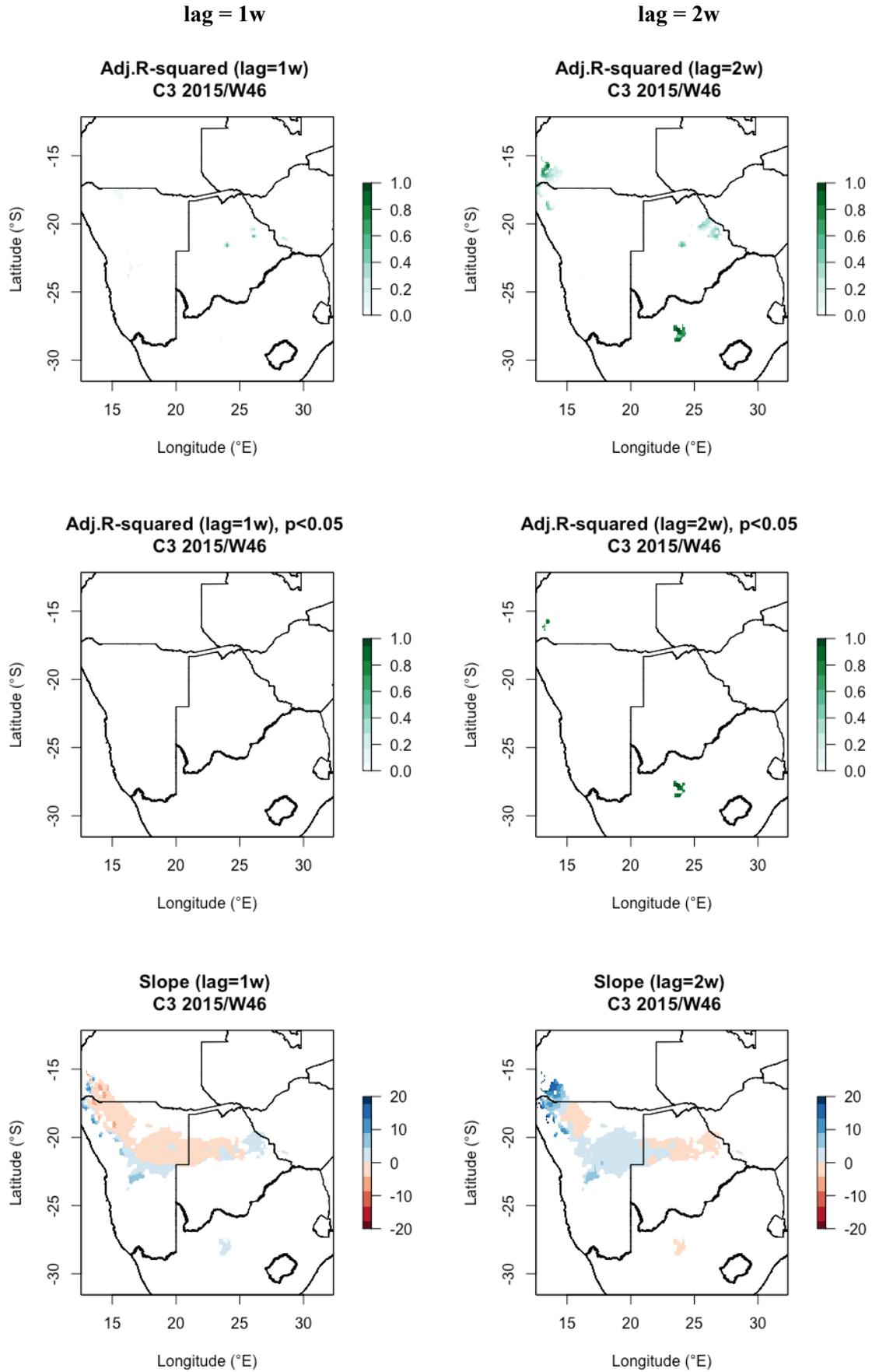

Figure D-3. The results of lag regression models of 1 and 2weeks in C3 sub-region.

C4 2016/W43   **lag = 1w**   **lag = 2w**
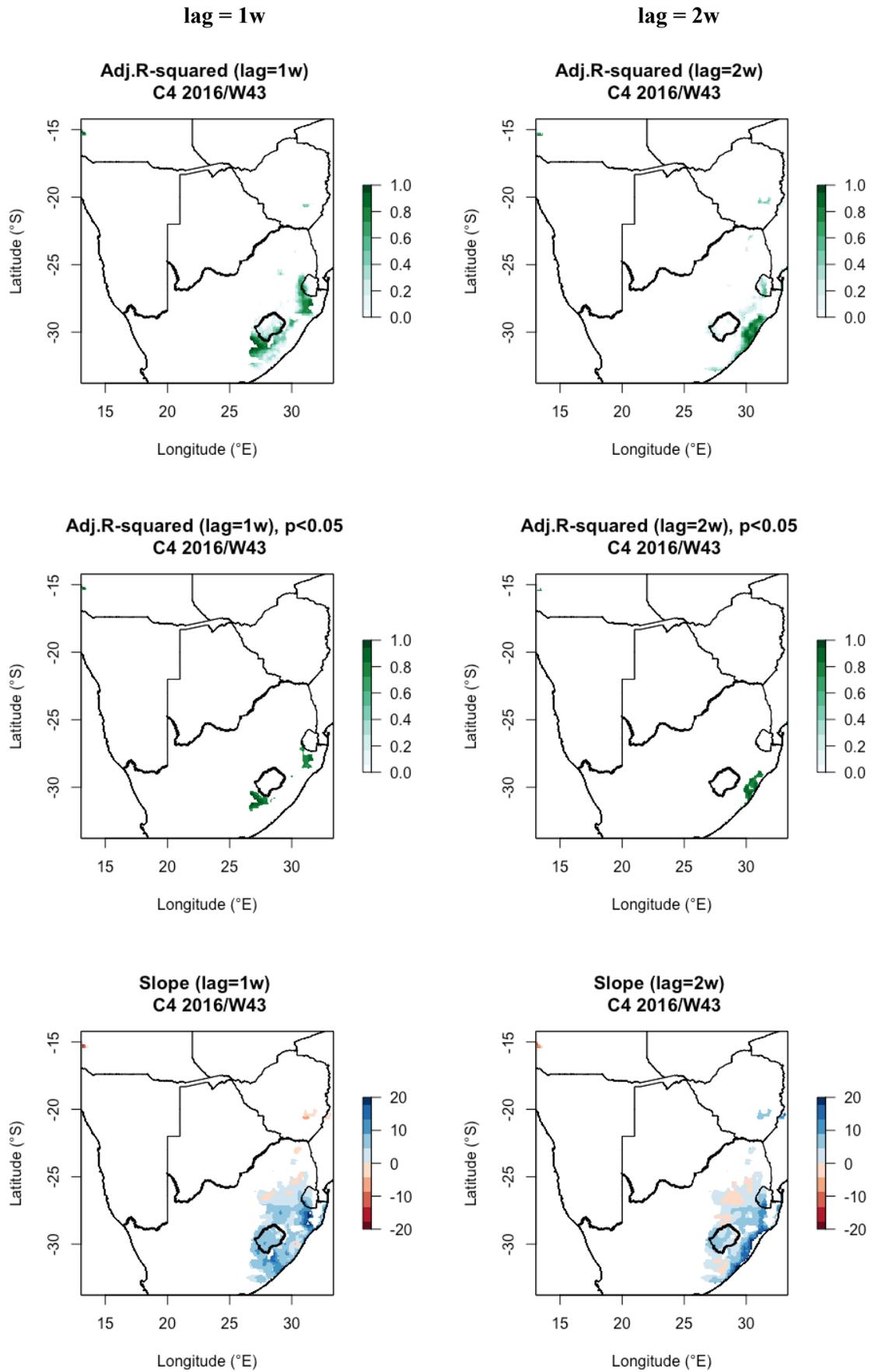
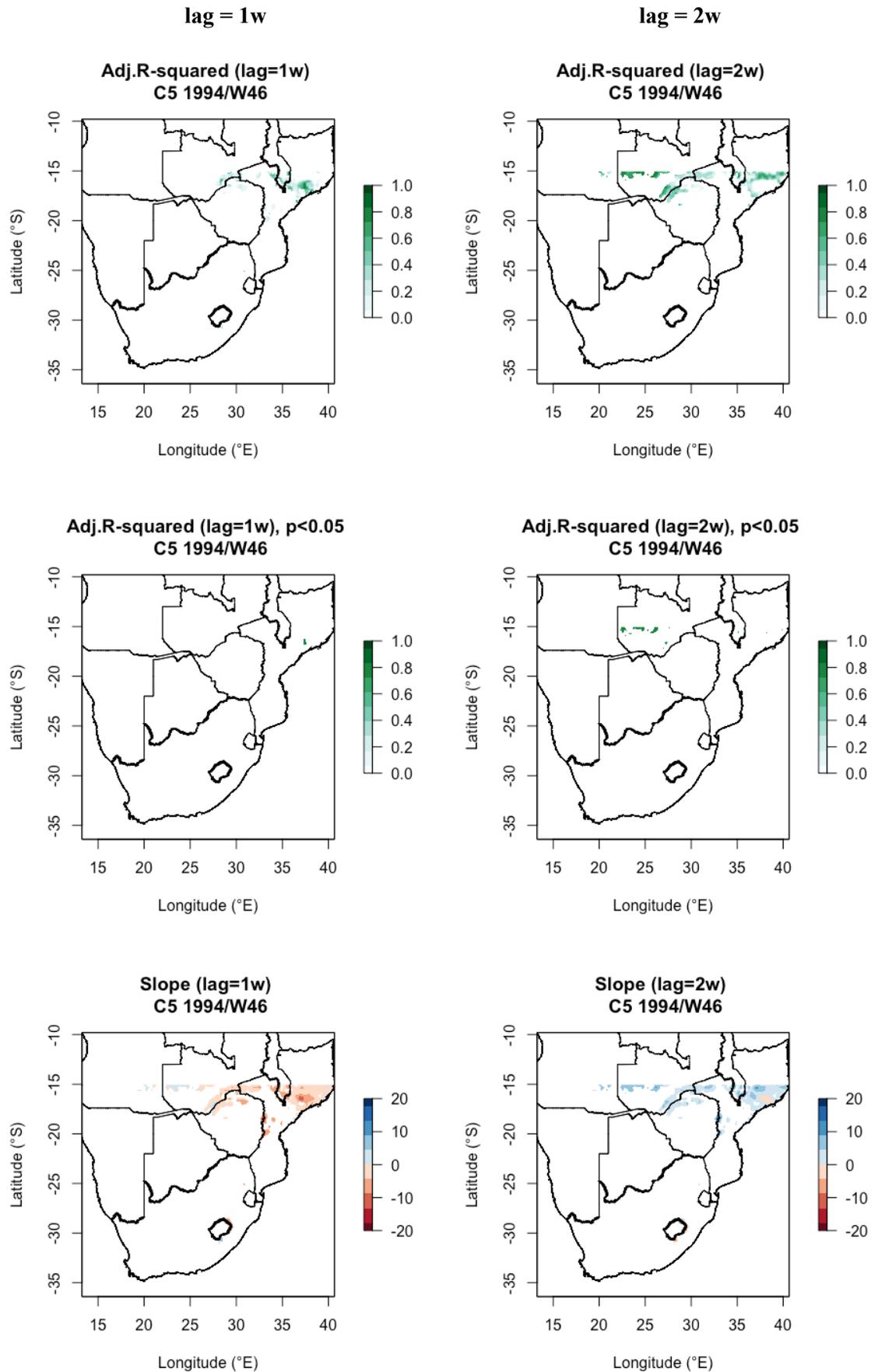Figure D-4. The results of lag regression models of 1 and 2weeks in C4 sub-region.

C5 1994/W46   **lag = 1w**   **lag = 2w**

Figure D-5. The results of lag regression models of 1 and 2weeks in C5 sub-region.

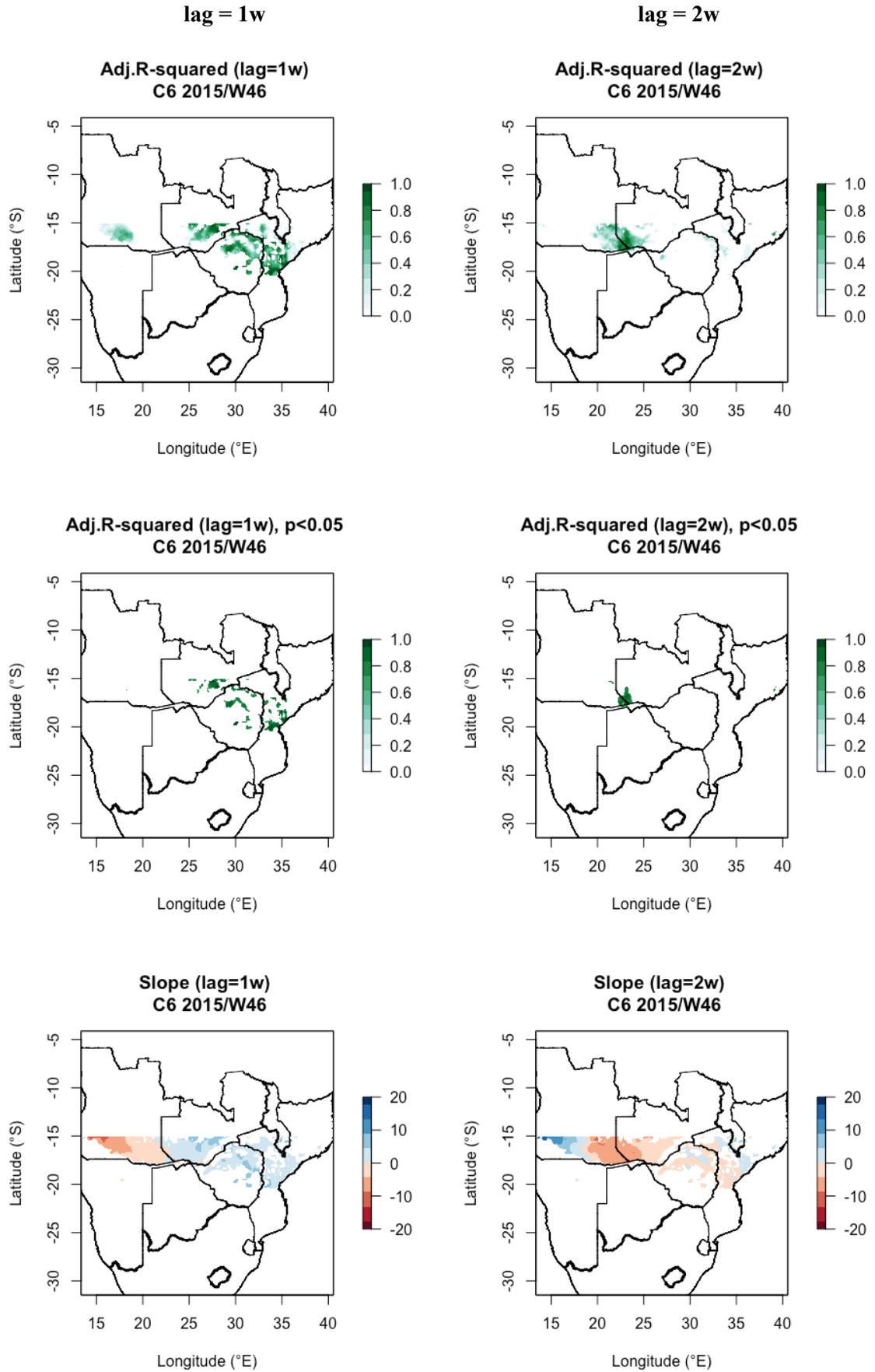**C6 2015/W46**   **lag = 1w**   **lag = 2w**

Figure D-6. The results of lag regression models of 1 and 2weeks in C6 sub-region.
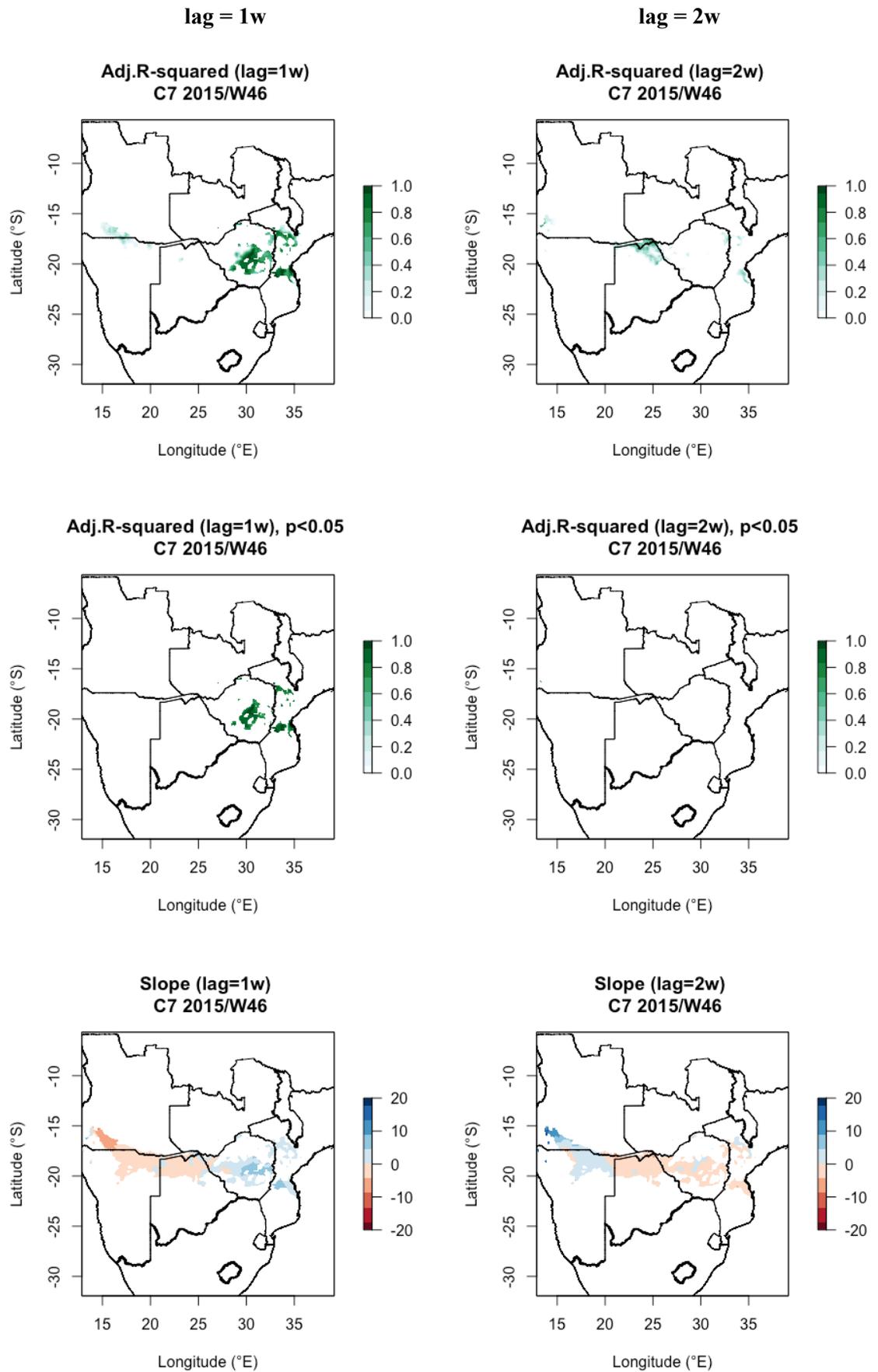
C7 2015/W46   **lag = 1w**   **lag = 2w**

Figure D-7. The results of lag regression models of 1 and 2weeks in C7 sub-region.

C8 2019/W48 | **lag = 1w** | **lag = 2w**
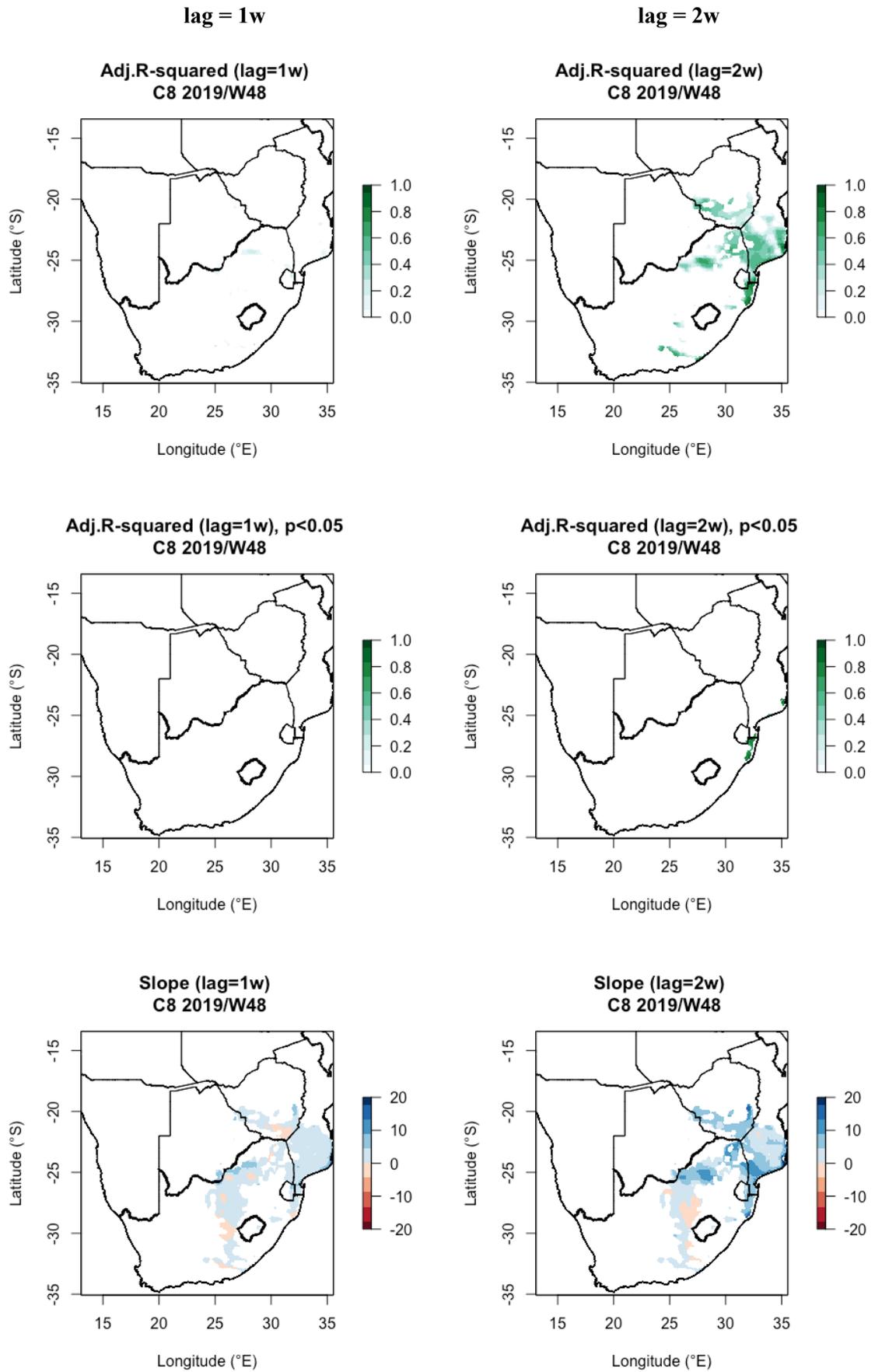
Figure D-8. The results of lag regression models of 1 and 2weeks in C8 sub-region.

C9 2016/W43   **lag = 1w**   **lag = 2w**
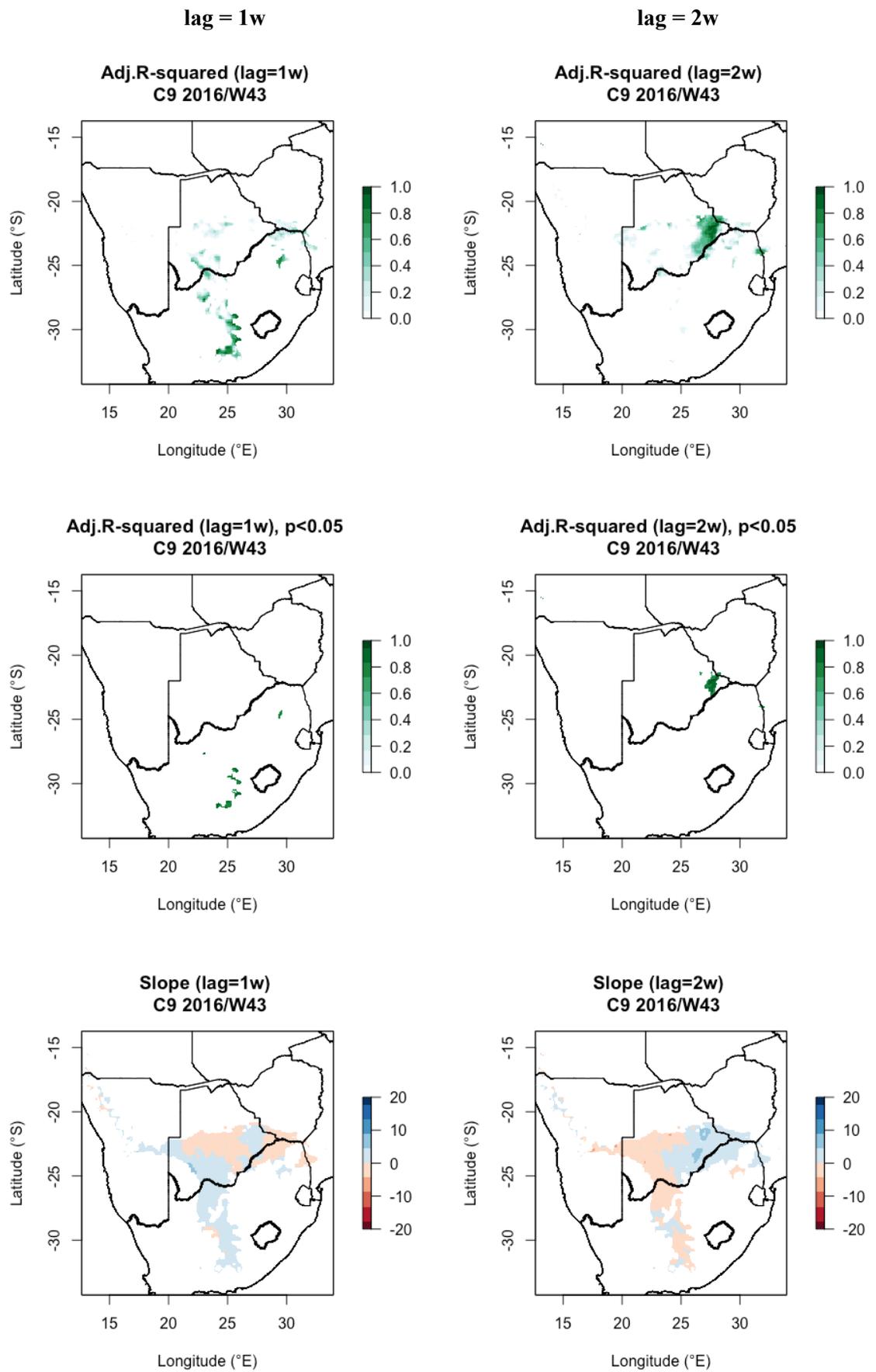
Figure D-9. The results of lag regression models of 1 and 2weeks in C9 sub-region.

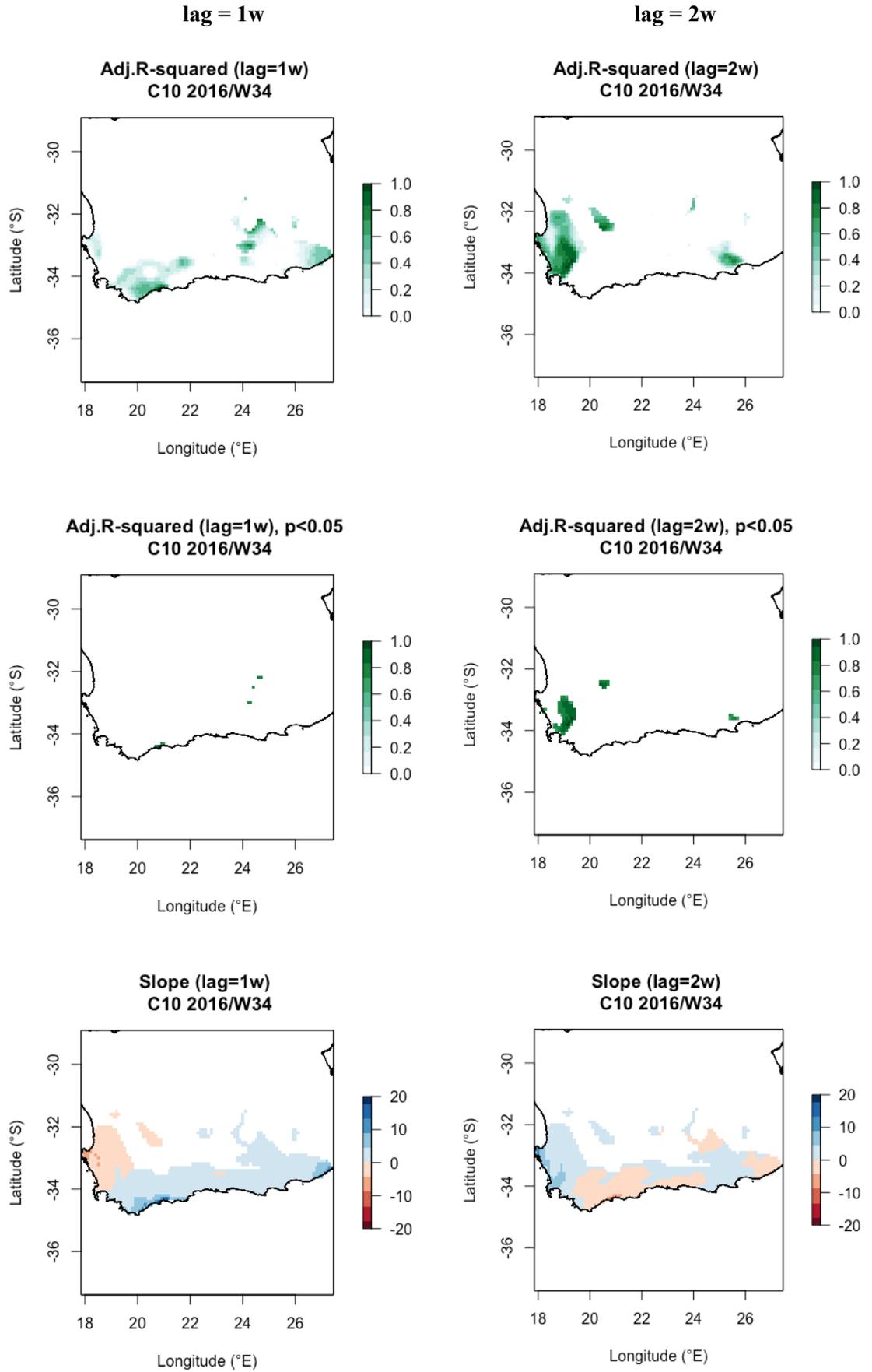**C10 2016/W34**   **lag = 1w**   **lag = 2w**

Figure D-10. The results of lag regression models of 1 and 2weeks in C10 sub-region.

Appendix E.

Supplementary Information

ERA-5 Land dataset

- The raw dataset provided in format GRIB and NetCDF (experimental) can be applied and accessed after the selection of variable as well as time scales via the below link:
  https://cds.climate.copernicus.eu/cdsapp#!/dataset/reanalysis-era5-land?tab=form

GeoTIFF data

- Precipitation
  - Daily (file: *prec_daily_1981_2019_ce.tif*)
  - Monthly (file: *prec_monthly_1981_2019_All.tif*)
  - Annual (file: *prec_annual_1981_2019.tif*)
- Temperature
  - Daily (file: *temp_daily_max_C_1981_2019.tif*)
  - Monthly (file: *temp_monthly_mmax_1981_2019.tif*)
  - Annual (file: *temp_maxmax_annual_1981_2019.tif*)
- Cluster regions (file: *prec_clara.tif*)

R codes

- Transformation of dataset format: NetCDF to GeoTIFF (file: *Grib_ERA5-Land.R*)
- Clustering analysis of precipitation patterns (file: *Cluster_ERA5-Land.R*)
- Trend analysis (file: *Trend.R*)
- Detection of heat waves (file: *Heat_wave.R*)
- Lag regression models (file: *Lag_regression_model.R*)

Results

- Visualisation of all other results of the rest selected lag regression models in 10 sub-regions with severe HWEs (files: *Lag regression models.pdf*)